SUBCELLULAR DISTRIBUTION OF PLATINUM COMPLEXES

Dissertation zur Erlangung des akademischen Grades des

Doktors der Naturwissenschaften (Dr. rer. nat.)

eingereicht im Fachbereich Biologie, Chemie, Pharmazie

der Freien Universität Berlin

vorgelegt in englischer Sprache von

EWELINA REBECKA FOGELSTRÖM

aus Torslunda, Schweden

Berlin, 2013

Die vorliegende Arbeit ist in der Zeit von Februar 2007 bis März 2011 am Institut für Pharmazie der Freien Universität Berlin unter Anleitung von Herren Prof. Dr. Ronald Gust entstanden.

1. Gutachter: Prof. Dr. Ronald Gust
2. Gutachter: Prof. Dr. Gerhard Wolber

Disputation am 14.02.2013

Acknowledgements

I would like to show gratitude to my supervisor Professor Ronald Gust for giving me the opportunity to work in his group, for the creative scientific environment and for his trust in my capabilities and the present work. It is a pleasure to thank Professor Gerhard Multhaup for providing me generous access to his lab for over a year. Moreover, I am truly thankful to his group members (Institute of Biochemistry, Freie Universität Berlin) for showing their support and creating a pleasant atmosphere, especially to Susanne Fehse for spending her time introducing me to western blot and agarose gel electrophoresis and to Andrea Senge for her eagerness to help out. I am truly thankful to Dr. Jens Peter Fürste (Institute of Biochemistry, Freie Universität Berlin) for spending his time for encouraging and fruitful discussions. My gratefulness goes to Deutsche Forschungsgemeinschaft and Sonderforschungsbereich 765 (Multivalenz in Chemie und Biochemie) for the financial support of this work.

I owe sincere and earnest thankfulness to the Microscopy Group at the Max Planck Institute for Molecular Genetics for sharing with me, their resources, competence and time. Many thanks go to Dr. Rudi Lurz and to Beatrix Fauler for preparing and analyzing the negative stain samples. I want to thank Dr. Thorsten Mielke for the opportunity to analyze the samples with cryo-electron microscopy and the long discussions concerning the interpretation. I also want to thank Jörg Bürger for the skillful preparation of the samples. Additional help in interpreting the cryo-electron micrographs was provided by Dr. Dmytro Puchkov (Laboratory for Membrane Biochemistry and Molecular Cell Biology, Institute of Chemistry and Biochemistry, Freie Universität Berlin). I would also like to thank Professor Ingo Ott (Institute of Pharmaceutical Chemistry, Technische Universität Braunschweig) for contributing with discussions and ideas. Very special thanks go to Magnus Krüger with whom I shared lab. I would like to thank him for sharing his enthusiasm, time, competence, creativity and for providing the substances that I used in the present study. Also I would like to thank Anja Schäfer for the numerous and long discussions and for the proofreading, Silke Bergeman for taking care of the cell cultures when I was away. I would like to give a warm thank you to Veronique vom Bauer for assisting with administrative issues and for her helpfulness. I would also like to thank the other members of the group for their friendship and support.

In dear memory of

Karl Svante Lindquist

1970-2003

Du är saknad

Table of contents

List of abbreviations

ADP, adenosine diphosphate

ATCC, American Type Culture Collection

ATP, adenosine triphosphate

BSA, bovine serum albumin

CVS, crystal violet staining

DAB, diamino benzidine

DMF, dimethylformamide

DMSO, dimethyl sulfoxide

DNA, deoxyribonucleic acid

EBSS, Earle's balanced salt solution

EDTA, ethylenediaminetetraacetic acid

EIPA, 5-(N-Ethyl-N-isopropyl)-amiloride

EM, electron microscopy

ER, endoplasmic reticulum

FAAS, flameless atomic absorption spectrometry

FBS, fetal bovine serum

g, relative centrifugal force where $g_{max,}$ g_{min} and g_{av} represent the force that the centrifuge tube experiences at its bottom, at the top and in the middle respectively.

gDNA, genomic deoxyribonucleic acid

GPN, glycyl-L-phenylalanine 2-naphthylamide

HeLa, (Henrietta Lacks) a cervical cancer cell line

HEPES, 4-(2-hydroxyethyl)-1-piperazineethanesulfonic acid

HRP, horseradish peroxidase

HSA, human serum albumin

IC_{50}, half maximal inhibitory concentration

kb, kilo base pair

LDL, low density lipoprotein

LMF, light mitochondrial fraction

MCF-7, (Michigan Cancer Foundation -7) a breast cancer cell line

MLV, multi-lamellar vesicle

MOM, methionine *O*-methyl ester

mtDNA, mitochondrial deoxyribonucleic acid

nq, not quantifiable

ns, not shown

o/w, octanol/water

PBS, phosphate buffer saline

PNF, post-nuclear fraction

POPC, palmitoyl-oleyl(1,9-10cis)-phosphatidylcholine

RER, rough endoplasmic reticulum

RF, resistance factor

RNA, ribonucleic acid

RCF, relative centrifugal force

RSB, reticulocyte suspension buffer

RT, room temperature

SD (σ), standard deviation

SDS-PAGE, sodium dodecyl sulfate polyacrylamide gel electrophoresis

SER, smooth endoplasmic reticulum

T, tesla (magnetic flux density)

$T/C_{corr.}$, treated-to-control, corrected (corr.) for initial biomass

Tris, tris(hydroxymethyl)aminomethane

USA, United States of America

UV, ultra violet

1 Introduction

1.1 Playful science, the discovery of biological activity of Peyrone's salt

Without knowing it, Barnett Rosenberg did the first in vitro test of cisplatin (fig. 1.1) in the year of 1961 (*1*). He wanted to study the effects of an electric field on *E-coli* bacteria. After noticing that the electric field ceased cell division, he started looking for the responsible agent in the incubation buffer. Eventually two electrolysis products were found to be the active species, the platinum salts cis-$[Pt^{II}(NH_3)_2Cl_2]$ (cisplatin) and cis-$[Pt^{IV}(NH_3)_2Cl_4]$ (*2*). The platinum source was the electrodes used in the experiments. The platinum(II) complex, also called as cisplatin, or cis-diamminedichloroplatinum(II), had already been discovered by Peyrone (*3*) and is called as "Peyrones salt". The chemical structure was elucidated by Alfred Werner (*4*) long time before but Barnett Rosenberg was first to investigate the interaction of this coordination compound with living cells. This experiment and following experiments using animal tumor models (*5*) turned out to contribute significantly to cancer therapy (*2*) and to science.

1.2 Cisplatin, the first platinum-containing anticancer drug

Cisplatin is active against several cancers such as testicular cancer, ovarian cancer, cancer of the lung such as small-cell and non-small-cell lung carcinoma, cancer of the head and neck and bladder (reviewed in (*6*)). Success has been achieved after introducing cisplatin in the treatment regimen (not as single agent) of testicular cancer and high numbers of complete remissions (*7*) were achieved. However, cisplatin treatment is accompanied by side effects like nephrotoxicity (kidney toxicity) (*8*), nausea and vomiting. Fortunately, these side effects can be kept under acceptable control with hydration, dialysis (*9-10*) and antiemetic treatment. Many of the treated malignancies eventually develop resistance (reviewed in (*11*)).

Platinum complexes with new properties can be obtained without compromising cytotoxicity by introducing new structural elements. It has long been hoped to discover complexes that are more effective in their antitumor action, lacking in cross-resistance to cisplatin and display fewer side effects and/or side effects with lower severity.

1.3 Other platinum complexes

Since its discovery as a potent anticancer drug, the innumerable chemical modifications including leaving group[1] and ligand[1] modifications of the cisplatin structure led to the clinical use and global approval of two other platinum(II) drugs, namely carboplatin and oxaliplatin, (fig. 1.1) as reviewed in (*12*). ***Carboplatin*** and cisplatin display comparable activity against several cancers (*13-15*) but have different dose limiting side effects which are myelosupression (bone marrow suppression) for carboplatin (*16*) and nephrotoxicity for cisplatin. This motivates cisplatin substitution with carboplatin in those cases when cisplatin is considered effective but contraindicated (*17*).

Oxaliplatin (fig. 1.1) is a result of modifying both the leaving groups and the ligand of cisplatin. Oxaliplatin has proven useful in combination therapy with 5-FU/leukovorin to treat metastatic colorectal cancer (*18-20*). The outcome of several phase II trials proved oxaliplatin superior to the other platinum complexes in the treatment of colorectal cancer (*21*). Moreover, oxaliplatin displays a different toxicity profile compared to cisplatin and carboplatin (*22-23*). Cisplatin analogues are justified in a world of tumor diversities and it is of great value having alternative agents ready that exhibit different dose limiting toxicities. Oxaliplatin has been shown to display low cross resistance to cisplatin in some tumors and tumor cell lines (reviewed in (*24*)) (*25*). Some locally clinically approved platinum compounds are ***Nedaplatin*** (approved in Japan, fig 1.1) and ***Lobaplatin*** (approved in China, fig. 1.1).

Satraplatin (fig. 1.1) is a platinum (IV) complex that can be absorbed from the gastrointestinal system. A phase III study reported no gain in overall survival in the treatment of hormone refractory prostate cancer with satraplatin and prednisone (*26*). The in vitro promising tetranuclear platinum complex ***BBR 3464*** produced unacceptably high toxicity in phase I studies. This together with the outcome from phase II studies did not motivate the developers to move on to phase III trials, as reviewed in (*12*).

---

[1] In coordination chemistry, the molecules and ions that are bound to the metal ion are called as "ligands" and cisplatin has got four ligands. The chloride ligands in cisplatin and similar platinum (II) complexes are more easily replaced than the ammine ligands and are therefore called as "leaving groups".

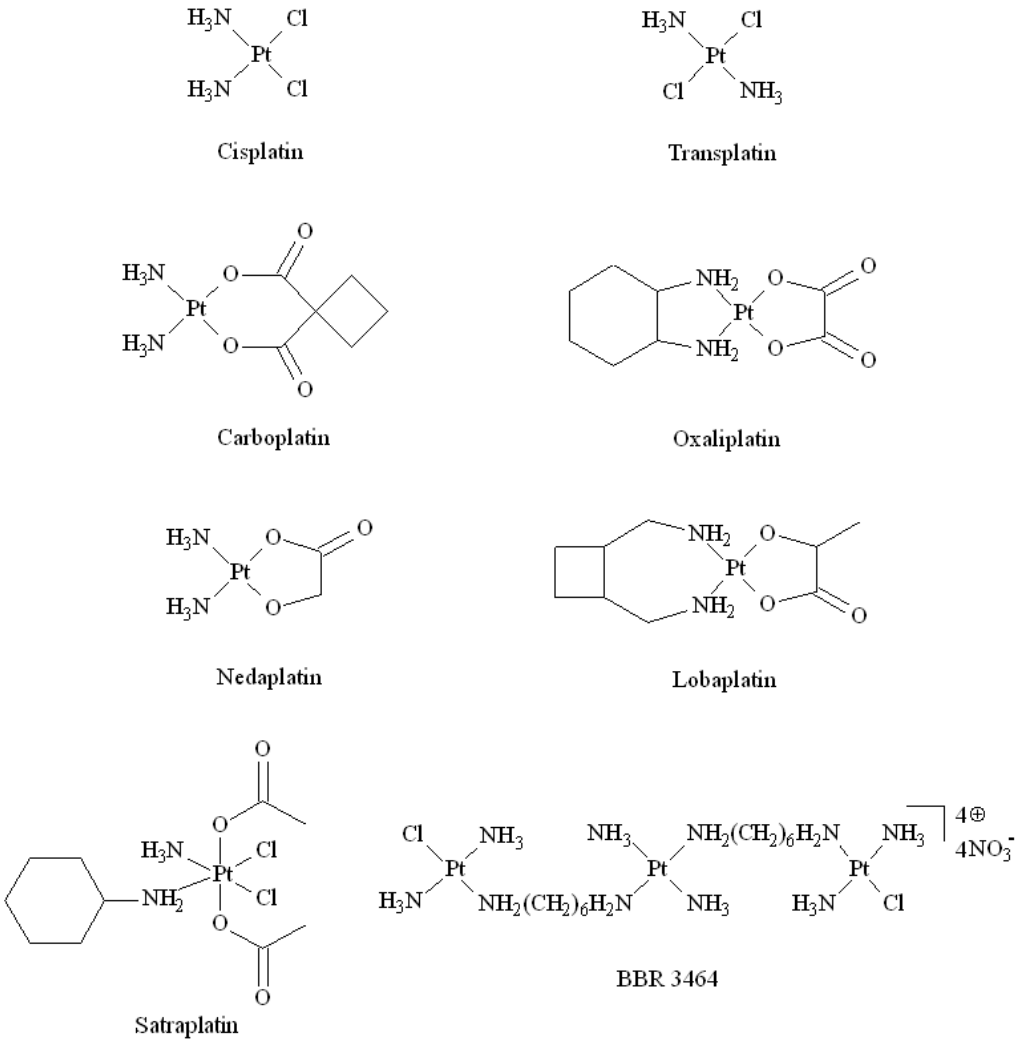

Figure 1.1. Cisplatin and other Pt complexes.

1.4 Cisplatin hydrolysis, prerequisite for sufficient reactivity

Conveniently, the high chloride ion concentration in the blood keeps cisplatin chlorinated. However, after entering the cell, the complex is hydrolysed because of the lower chlorine concentration (*27-28*). Water acts as a nucleophile and replaces the chloride ion(s) in an S_N2 reaction (fig. 1.2) (*29*). The substitution scheme is shown in fig. 1.3. Although the chloride ions in cisplatin can be replaced directly by other nucleophiles, the neutral species is too unreactive to cause enough damage and it is the platinum complexes carrying a water molecule (mainly the monochloro species) that are believed to interact with the DNA nucleobases (fig. 1.3) (*30*).

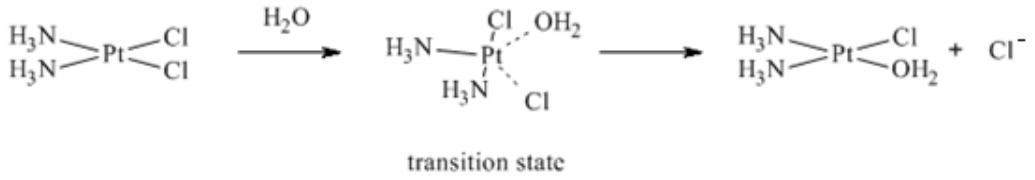

Figure 1.2. Hydrolysis of cisplatin (*29*)**.**

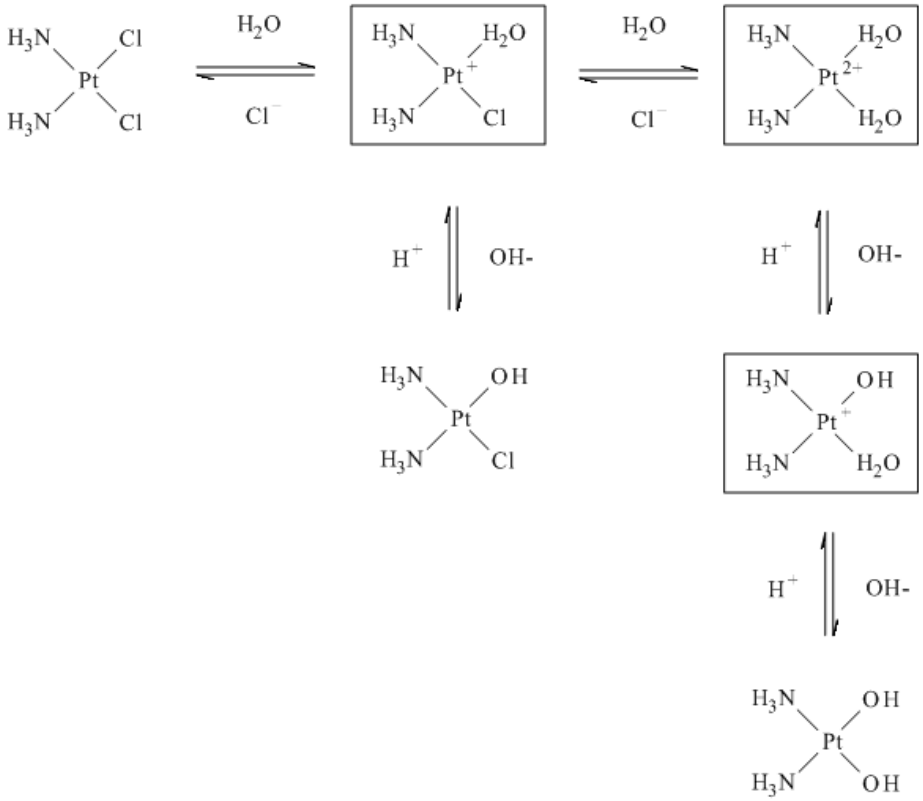

Figure 1.3. Hydrolysis of cisplatin in the cell. The complexes carrying a water molecule (shown in squares) are the species that show the highest reactivity towards nucleophiles.

1.5 Cisplatin action

Cisplatin exerts its antitumor activity through covalently binding to amino groups, thioethers and sulphate groups of bionucleophiles such as amino acids, nucleic acid nucleobases (*31-32*) and antioxidants (fig. 1.4). It is the initiation of the programmed cell death (apoptosis) that is believed to hold the main responsibility for tumor cell death after cisplatin exposure (*33-37*).

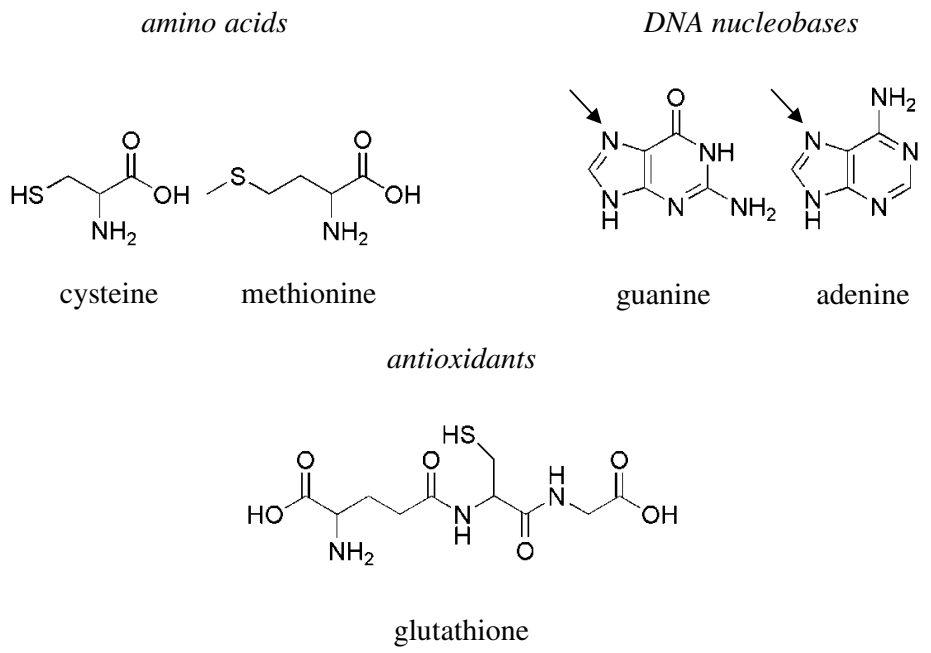

Figure 1.4. Bionucleophiles capable of replacing the leaving groups, such as chloride, in cisplatin and in other platinum(II) complexes. In the amino acids cysteine and methionine and also in the tripeptide glutathione, the sulfur atom is the attacking species whereas in the DNA bases guanine and adenine, the nitrogen in position 7 (indicated by arrows) in the purine is responsible for the reaction (*38*).

Cisplatin has been shown to be capable of initiating apoptosis in enucleated cells (*39*). However, it is the binding to genomic DNA that is considered to be the most important feature of cisplatin cytotoxicity. For example, cisplatin displayed lower cytotoxicity in wild type CHO cells than the DNA repair deficient UV-20 mutant (*40-41*).

Fruitful binding, such as the cross-linking of two guanines (*38, 42*) in the same DNA strand, will force the double-helix to bend (*43*) in a way that causes the responsible proteins to recognize the unusual spatial arrangement of the nucleobases in the DNA helix with compromised three-dimensional structure (*44*). Very simplified, attempts are made by the cell to remove the cisplatin bound nucleotides but if the damage is too extensive, the cell initiates apoptosis.

1.6 Why cis?

Transplatin (fig. 1.1), the trans-isomer of cisplatin, was inefficient in inhibiting bacterial division in the early experiments conducted by Rosenberg and colleagues (*45*) and later on it was shown to display very low cytotoxicity on Sarcoma 180 implanted in mice (*46*) and myeloid and lymphatic leukemia of the rat (*47*). The observed differences between cisplatin and transplatin have highlighted the relationship between structural orientation and antitumor activity. Transplatin cannot form 1,2-d(GpG) (connecting two guanosines) intrastrand (fig. 1.5) crosslinks, which is the major crosslink seen after cisplatin administration (*48*). Transplatin-DNA adducts are removed faster than cisplatin-DNA adducts and cisplatin is more cytotoxic at similar DNA/platinum concentrations (*49*). Transplatin has been shown to cause more DNA-protein crosslinking than its isomer (*50*) and display little mutagenic potency compared to cisplatin (*51*), probably because of faster removal of DNA-bound transplatin (*51*).

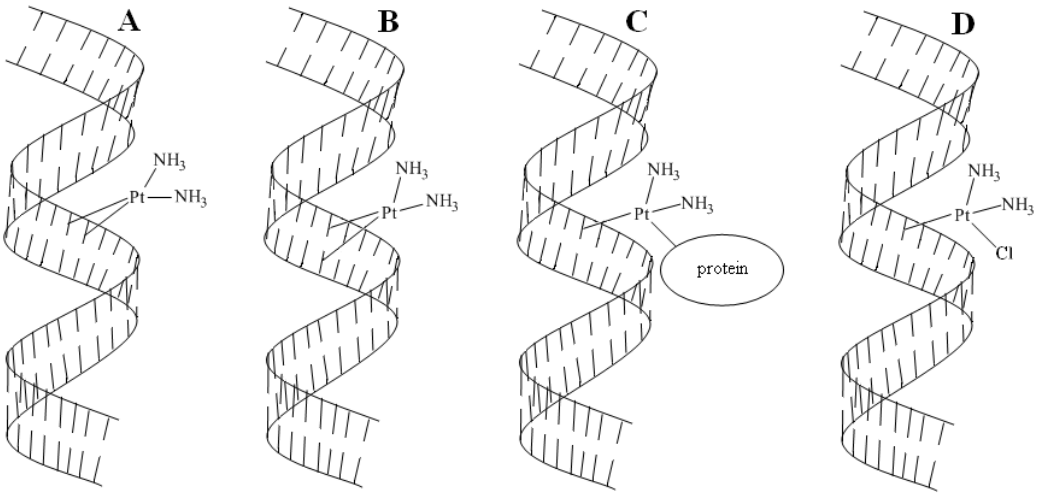

Figure 1.5. Schematic picture of cisplatin-DNA adducts found in the DNA of cells exposed to cisplatin (*48, 52-53*)**.** A: Intrastrand cisplatin-DNA adduct, B: Interstrand cisplatin-DNA adduct, C: cisplatin-DNA-protein adduct. D: Monofunctional cisplatin-DNA adduct (the non-ammine ligand in monofunctionally bound cisplatin is not necessarily chloride).

1.7 Glutathione and metallothionein

Cisplatin is not only selectively attacking DNA but also reacts readily with other bionucleophiles such as glutathione, amino acids and proteins such as metallothionein, a protein rich in cysteine residues. Some authors have failed to correlate the cytotoxicity of cisplatin with glutathione levels in several cancer cell lines (*54-55*). However, some human ovarian cancer cell lines originating from tumors refractory to cisplatin treatment (OVCAR) and a cell line with in vitro induced cisplatin resistance (A2780) displayed increased glutathione levels (*56*) and intracellular levels of glutathione increased in a leukemia cell line (L1210) after incubation with cisplatin (*57*). Regarding metallothionein, the 5-year survival rate was lower for cisplatin treated patients with esophageal cancer having metallothionein overexpressing tumors (*58*). Resistant ovarian carcinoma cells (A2780RCIS) treated with different cisplatin concentrations in vitro answered by increasing the nuclear metallothionein expression (*59*). Another ovarian carcinoma cell line (2008/DDP) with induced cisplatin resistance in vitro did not display increased levels of this protein (*60*). Thus, cisplatin has many interacting partners in the cell besides DNA nucleobases although their individual role in the cytotoxic activity of the complex needs more investigation.

1.8 Cisplatin cell entry

Investigations of cisplatin uptake, subcellular distribution and efflux have been the subjects of extensive research which have been thoroughly reviewed by Hall et al. (*61*). The compiled results of studies investigating the involvement of several transport proteins, e.g. the copper influx and efflux transporter, organic cation transporter and glutathione conjugate efflux transporter, do not allow the interpretation that only a single mechanism is responsible for cisplatin cell entry and its disposal. It is believed that the net accumulation might be a result of the action of several active mechanisms together with passive diffusion (*61*). There are evidences supporting both passive diffusion, such as lack of saturability up to high concentrations of cisplatin (0.1-5 mM) (*62-66*) and active processes where a lower cell accumulation of cisplatin has been observed after incubation with metabolic inhibitors (*62*).

1.9 History of the complexes tested in the present work

1.9.1 Idea of drug targeting to estrogen receptor expressing tissues

Despite of its success in the treatment of some cancers (mentioned above), cisplatin and its analogue carboplatin have been considered insufficient regarding the treatment of metastatic breast cancer as extensively reviewed by Smith and Talbot (*67*). Breast cancer cells exhibiting estrogen dependent proliferation have been shown to express the estrogen receptor (*68-69*). Moreover, it has been discovered that estrogens preferentially accumulate in estrogen receptor expressing healthy tissues (*70*) and tumor metastases that respond to endocrine therapy (*71*). This has tempted many researchers to combine cytotoxic groups together with moieties having affinity to the estrogen receptor (*72-73*). A successful compound possessing a cytotoxic group and an estrogen receptor affine moiety would accumulate and be retained (*74*) in the estrogen receptor expressing tumor tissue and so other organs with lower or no expression of this receptor would experience less or be spared from toxicity (*75-77*). Another idea was that the estrogen receptor would re-localize to the cell nucleus after binding to the cytotoxic compound in the cytosol. This was believed to increase the exposition of the chromatin to the cytotoxic substance (*69, 78*).

1.9.2 Ring-substituted [1,2-bis(4-hydroxyphenyl) ethylenediamine] dichloroplatinum (II) complexes, attempts of drug targeting

At the University of Regensburg, Professor Schöneberger and co-workers had the drug targeting concept in mind (section 1.9.1) when combining diamine hexestrol derivatives owing affinity to the estrogen receptor with a cytotoxic platinum moiety (*79*). One platinum compound, [meso-1,2-bis (2,6-dichloro-4-hydroxyphenyl) ethylenediamine] dichloroplatinum(II) (fig. 1.6A) and its more water soluble analogue (water as leaving groups), the diaquaplatinum(II) complex (fig. 1.6B), proved to be estrogens in vivo because of their uterotropic (increase in uteri weight) effect (*80*).

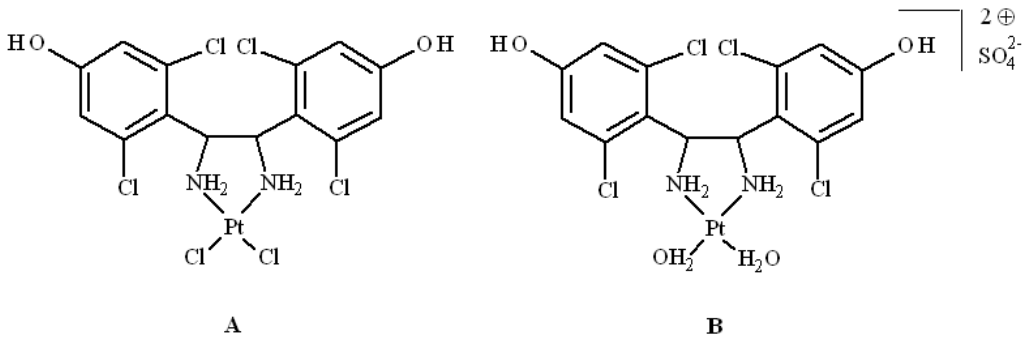

Figure 1.6. Platinum complexes displaying uterotropic effects in vitro (*80*)**.** A: [Meso-1,2-bis(2,6-dichloro-4-hydroxyphenyl)ethylenediamine]dichloroplatinum(II), B: Diaqua[meso-1,2-bis(2,6-dichloro-4-hydroxyphenyl) ethylenediamine]platinum(II) sulfate.

Also, their cytotoxic effects were only seen in the hormone dependent MXT mammary carcinoma of the mouse and not in the tumor lacking the estrogen receptor (*80*). Moreover, the diaquaplatinum(II) complex (fig. 1.6B) was more active than cisplatin on the hormone dependent DMBA-MC mammary carcinoma of the Sprague Dawley rat. Unfortunately, its cytotoxicity towards cultured cells such as MCF-7 (*81*) and MDA-MB-231 proved to be lower than that of cisplatin. However, the diaquaplatinum(II) complex selectively inhibited growth of the MCF-7 cell line compared to the estrogen receptor lacking MDA-MB-231 cell line (*80*).

1.9.3 Complexes of the ring-substituted [1,2-diarylethylenediamine] dichloroplatinum(II)-type carrying non-estrogenic ligands

Many modifications have been carried out in the search for substances with high cytotoxicity also towards tumors lacking the estrogen receptor. Therefore, also non-estrogenic ligands were complexed with platinum. When various substituents were introduced in 4-position of both phenyl rings (e.g. H, F, OH, Cl, CN, Br), two substances displayed the highest cytotoxicity, namely m4FPtCl_2 (fig. 1.7) and dl4FPtCl_2 (fig. 1.7) (named differentially in the publications). They were active towards the 388 leukemia of the CD_2F_1 mouse (*82*). Complexes carrying the 4-F ligand are not estrogens (*83*). However, they accumulate fast in both estrogen-dependent (*81, 84*) and estrogen-independent cell lines (*85*) and dl4FPtCl_2 exerted toxicities similar to cisplatin in both estrogen receptor expressing (*81*) and deficient (*83*) cell lines. Also, dl4FPtCl_2 displayed 7-fold resistance in a 100-fold cisplatin resistant L1210 leukemia cell line (*86*).

By changing the leaving group from chloride to water in complexes carrying a 4-F ring-substituted 1,2-diaryl-ethylenediamine ligand with sulphate or nitrate as counter ions, a higher toxicity towards estrogen-dependent (estrogen receptor expressing) MXT-M 3.2 mammary carcinoma of the BD62F1 mouse than towards the estrogen-independent (no expression of estrogen receptor) MXT-Ovex mammary carcinoma of the BD62F1 mouse was obtained. In the case of the dichloroplatinum(II) complexes, tumor toxicities were generally lower but higher tumor inhibiting properties were seen in the estrogen receptor lacking carcinoma than in the estrogen-dependent carcinoma (*83*). The observed host toxicities were considerably higher for the aquated complexes than for their dichloroplatinum(II) analogues (*87-88*). Cisplatin displayed the highest potency (*87-88*). Unfortunately, the platinum complexes carrying the 4-F phenyl substituted 1,2-diarylethylenediamine ligand did not qualify for cancer treatment because of their low water solubilities (*88*) and despite many leaving group modifications (*89-90*) i.e. groups with higher hydrophilicity, the solubility never reached to desired levels (*90*).

1.9.4 Introducing bivalency

In recent works, the interesting properties of the complexes m4FPtCl$_2$ and dl4FPtCl$_2$ (fig. 1.7) were sought to be retained and improved in bivalent[2] form (*91*) i.e. two complexes linked together (fig. 1.7). Those complexes were thought to bind to the DNA in a different way than do the monovalent complexes (fig. 1.7) and cisplatin. Thus, cross-resistance to cisplatin and to other complexes mainly causing DNA intrastrand crosslinks was hoped to be avoided. Depending on the charge of their leaving groups the bivalent complexes are bearing at least two positive charges which were believed to bring higher water solubilities. However, the results of the in vitro tests of the bivalent complexes were disappointing (*85*). Although one of the complexes (m4FPtDAHCl, see fig. 1.7) did solve well in water and showed fast cell accumulation, all bivalent complexes displayed low cytotoxicity in the MCF-7 cell line. It was shown that they are inactivated through binding to proteins in the (FBS-supplemented) culture medium (*85*). Some of the divalent complexes showed higher

[2]In the present work the terms “bivalent” and “monovalent” refers to complexes containing two linked platinum complexes and complexes containing one platinum atom respectively. Other commonly used terms for platinum complexes are “dinuclear” and “mononuclear” platinum complexes which refers to platinum complexes containing one or two platinum atoms respectively.

DNA-associated platinum amounts than cisplatin (*85*) but during the incubation of the cells with substances, culture medium not supplemented with FBS was used.

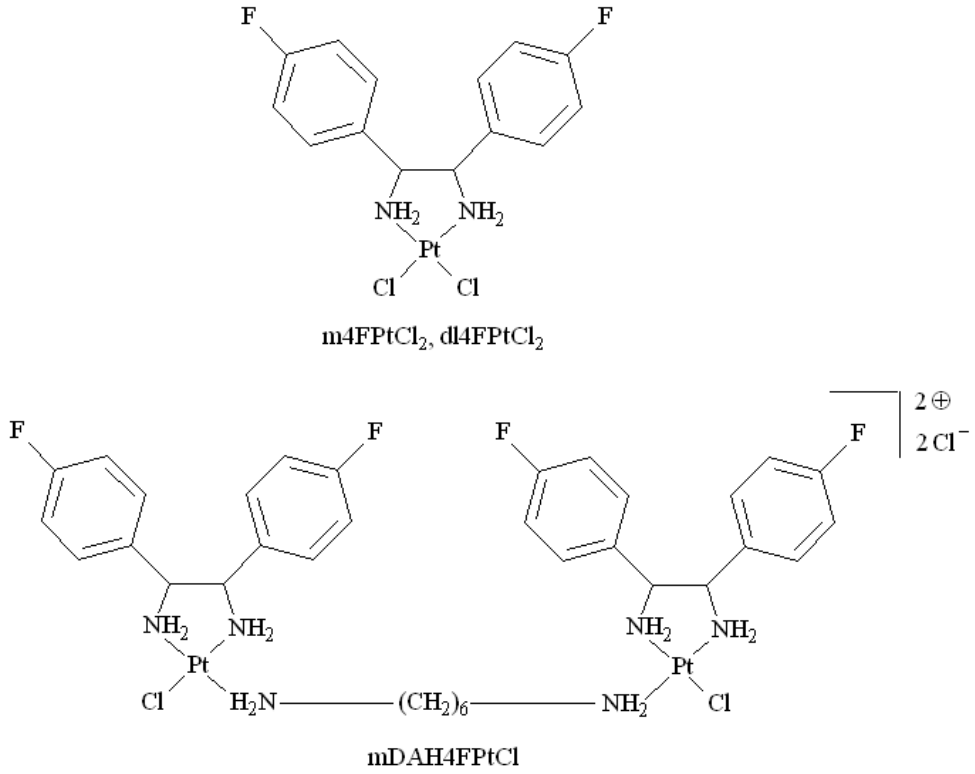

Figure 1.7. Structure and names of three platinum (II) complexes tested in the present work. m and dl stands for meso and racemate respectively and denote the configuration of the diamine ligand (meso = (R,S)/(S,R), racemate = (R,R)/(S,S)).

1.10 Investigating the subcellular distribution of platinum complexes

Number of platinum complexes exerts their functions through covalently binding to their targets and being close to the target spatially is a prerequisite for binding. Since one of the mechanisms of resistance of cancer cells towards cisplatin and other administered platinum complexes is decreased uptake and/or increased efflux, the desire of knowing more about those mechanisms is increasing. If the entry of the platinum complexes into the cancer cells can be increased, therapy efficacy might be enhanced. Collecting information about cisplatin uptake in the cancer cells inevitably includes knowledge about the path of the drug inside of the cell, i.e. the intracellular distribution, since the mechanism of uptake will influence the downstream distribution. It is aspired to obtain data that correlates an action of platinum complexes with their intracellular distribution and cell processing. Also, it is of interest to be able

to compare different platinum complexes. Cytotoxicity, whole cell-, cell nuclei- and DNA-associated platinum of cisplatin, m4FPtCl$_2$, dl4FPtCl$_2$ and mDAH4FPtCl in MCF-7 cells have been investigated in previous works (*85, 91*). However, subcellular distribution is a parameter that can be used to further compare the behavior of those complexes in their encounters with cells.

1.11 Methods for determining the subcellular distribution of platinum complexes

Static visual methods

There are several techniques capable of visualizing platinum atoms in biological material such as electron microscopy (*92-93*) and synchrotron radiation-induced X-ray emission (*94*). Unlike fluorescence detection methods (see below), the benefit of these methods is that no chemical modification of the complex is needed for detection. Both methods require excessive sample preparation including dehydration and embedding prior to sectioning[3] which might explain the sparse use of incubation times, concentrations used and measurements of one or few platinum complexes only.

Dynamic visual methods

Methods using fluorescence microscopy for the mapping of platinum complexes in cells enable visualization of complexes equipped with a fluorescent tag (*95-100*). Some of these methods enable monitoring in living cells and one can follow the intracellular path of the fluorophore for several hours. A possible drawback of fluorescence microscopy methods is that the complex one wishes to study is not the species subjected for detection. However, the integrity of the intracellular environment is not compromised.

Non-visual static methods

The detection of platinum in biological materials can be done using atomic absorption spectrometry (AAS). This method requires that the samples are introduced as homogenized solutions into the instrument. To study platinum content in one population of organelles after treating the cells with the complex of interest, the cells

[3]Preparation of ultra-thin slices in the nm scale

content need to be separated into the respective organelle fractions using subcellular fractionation methods. Differences in organelle size and density between organelle populations allow them to be separated in a centrifugal field using different centrifugation techniques and the help of density media. Quantifying platinum in subcellular fractions using AAS require relative large amounts of cell material and thus, these measurements are not confined to few single cells but to a population of cells from which the material is pooled. The success of the subcellular fractionation method in keeping the heterogeneity of organelles in the resulting fractions as low as possible will determine the significance of the results.

None of the presented detection/quantification methods are taking into account the different substitution reactions that can follow either before or after the platinum complex enter the cells i.e. free complex cannot be discerned from complexes bound to biomolecules.

1.12 The choice of platinum complexes for cell uptake measurements

From a methodological point of view, it is important to choose complexes that accumulate in the cells sufficiently fast. However, there are other factors that need to be considered. The complexes should not display very high cytotoxicity so that the cells are still vital after the chosen incubation times and that test concentrations that enable quantification can be used. Moreover, solubility at those concentrations has to be assured. The complexes tested in the present work (except cisplatin that display comparatively slow accumulation) (fig. 1.7) fulfill all the above stated requirements with little modification.

2 Objective

The present work aimed to develop methods to measure and compare the subcellular distribution of four platinum complexes, cisplatin (fig. 1.1), m4FPtCl$_2$, dl4FPtCl$_2$ and mDAH4FPtCl (fig. 1.7) in cancer cell monolayer cultures. These complexes have been shown in previous works (*85*) to differ in properties such as cytotoxicity, accumulation in whole cells and cell nuclei and DNA binding. It is of interest to investigate if those differences are mirrored also in their subcellular distribution. The present work focused on the development of subcellular fractionation methods capable of enriching organelles such as plasma membrane and mitochondria. These methods were intended to complement the already existing methods (*85*) for measuring the subcellular distribution of platinum complexes. In the process of method development, it is important to put emphasis on assuring oneself about the validity of the methods. In the present work, importance has been put on questioning the used methods and discussing their strengths and weaknesses in the light of platinum quantification in subcellular fractions.

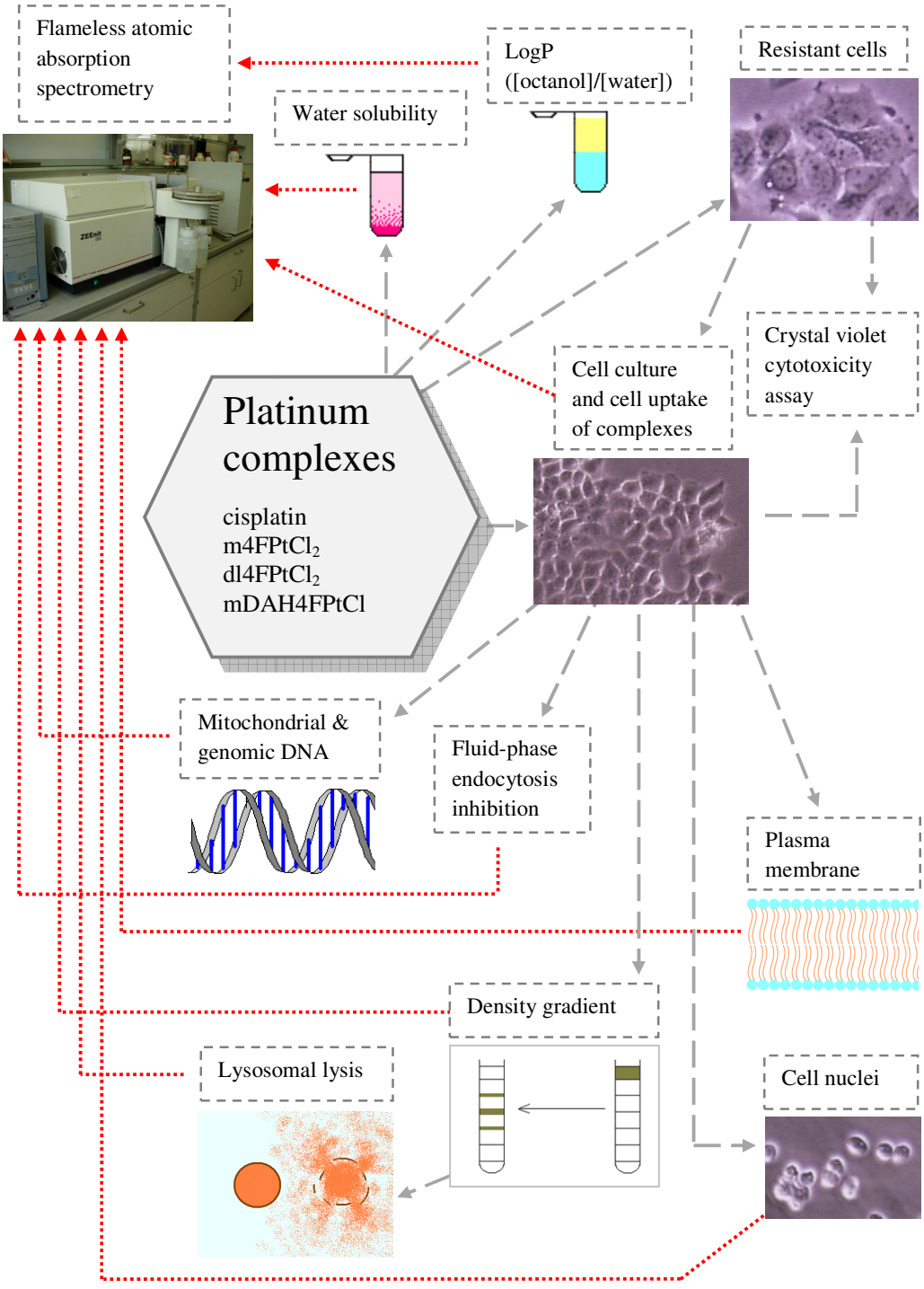

Chart 1. Overview of test methods used in the present work where platinum was quantified. Grey dashed arrows, originating from the platinum complexes, are pointing towards experiments in which the complexes were tested. Experiments where platinum was quantified are connected to FAAS with red dotted arrows.

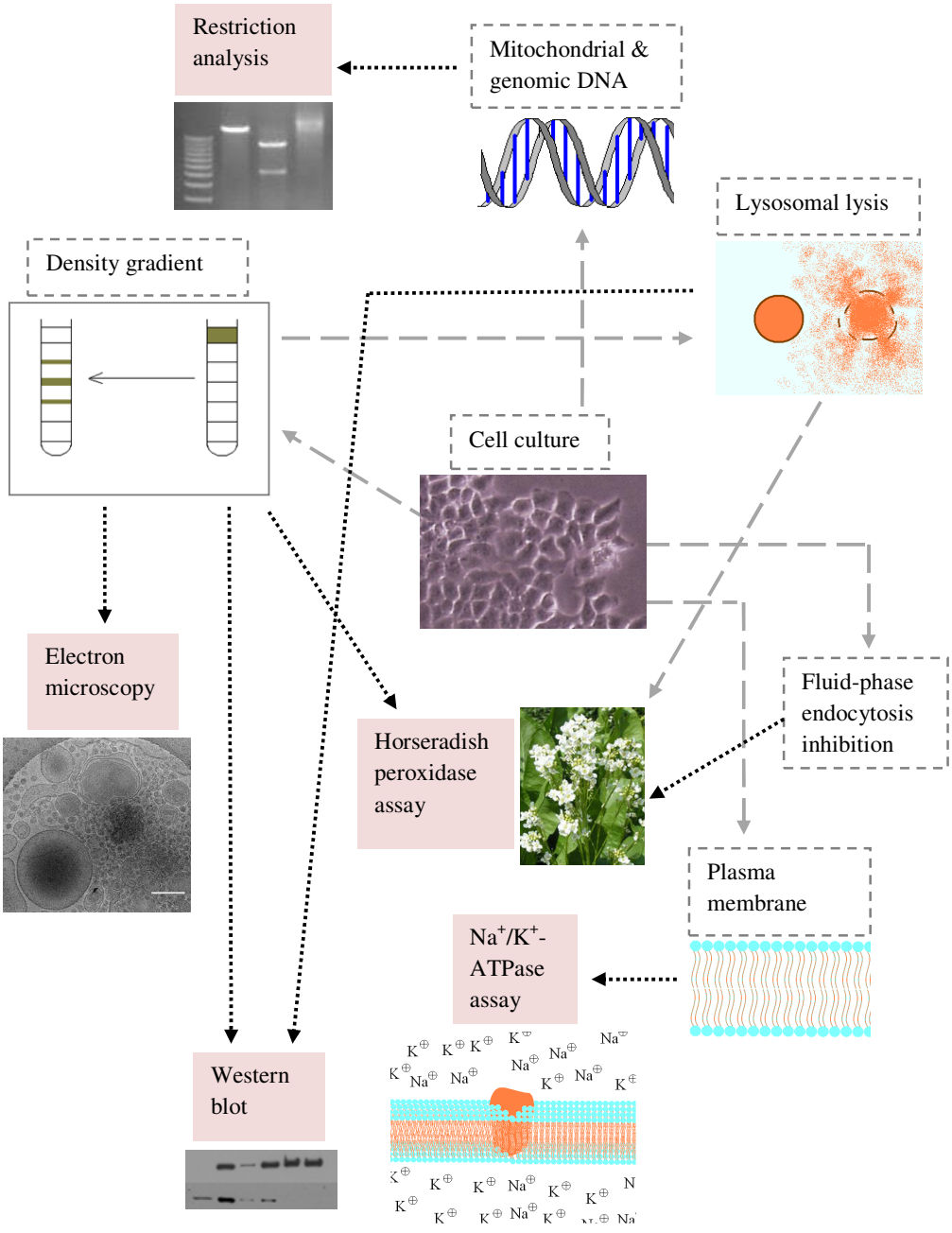

Chart 2. Overview of methods employed to validate the methods used in the present work. Grey dashed arrows show connection between experiments and black dotted arrows are methods used for validation of those experiments.

3 Method optimization for quantification of platinum complexes in cell matrix

3.1 Quantification of platinum in cell matrix using flameless atomic absorption spectrometry (FAAS)

Substances containing platinum can be quantified directly in biological material matrixes[4] such as digested tumor tissue (*101*), body fluids (*102-104*) and tissue culture cells (*90, 105-106*) using atomic absorption spectrometry. The sample is introduced into a graphite tube in a graphite oven and subjected to a temperature program that serves to gradually remove the solvent and as much material, except analyte, as possible prior to atomization. These two steps are termed as "drying" and "ashing". At this stage, in a step called as "atomization", the analyte is given enough thermal energy to appear in its elemental state and thus can absorb light from the hollow cathode lamp.

(F)AAS is a relative method and requires the set up of a calibration curve prior to sample measurements. Absorption is plotted against the known concentration of a platinum standard (hexachloroplatinic acid) and so the platinum in the samples can be quantified. In the present work, the platinum complexes cisplatin, m4FPtCl$_2$, dl4FPtCl$_2$ and mDAH4FPtCl were quantified in cell lysates, cell nuclei fractions, plasma membrane fractions and density gradient fractions.

3.2 Oven program, atomization and ashing temperature optimization

The atomization and ashing temperatures were optimized (fig. 3.1). For the optimization of the atomization temperature, the ashing temperature was kept constant at 1600 °C while the atomization temperature was varied. The sample matrix[4] consisted of MCF-7 cell lysate stabilized with Triton X-100 and HCl and the concentration of the platinum standard was 125 µg/L. For the ashing temperature optimization, the chosen atomization temperature (2400 °C) was kept constant and the specific (analyte) as well as the unspecific (background) absorption was monitored

[4]The sample matrix refers to the components of a sample except analyte i.e. in the case of platinum quantification in cells, the matrix is the cell homogenate (also called as lysate) and platinum is the analyte.

while the ashing temperature was varied. During ashing temperature optimization, the sample matrix consisted of cell lysate without additives. Time integration of the atomization signal (peak area) resulted in lower sensitivity than when the height of the signal (peak height) was used and so the latter was chosen for the quantifications. The absorption (peak height) reached a plateau at 2300 °C and an atomization temperature of 2400 °C, safely residing on the plateau, was chosen (fig. 3.1A). The gain of increase in absorption is too small to justify higher atomization temperatures as the lifeline of the graphite tube is shortened faster. According to the decline in unspecific absorption, an ashing temperature of 1300 °C was sufficient (fig. 3.1B) in this matrix but an ashing temperature of 1600 °C was chosen to increase the flexibility of measurable matrixes. Higher temperatures will lead to decline in analyte during the ashing phase (fig. 3.1C). The resulting temperature program is shown in table 3.1.

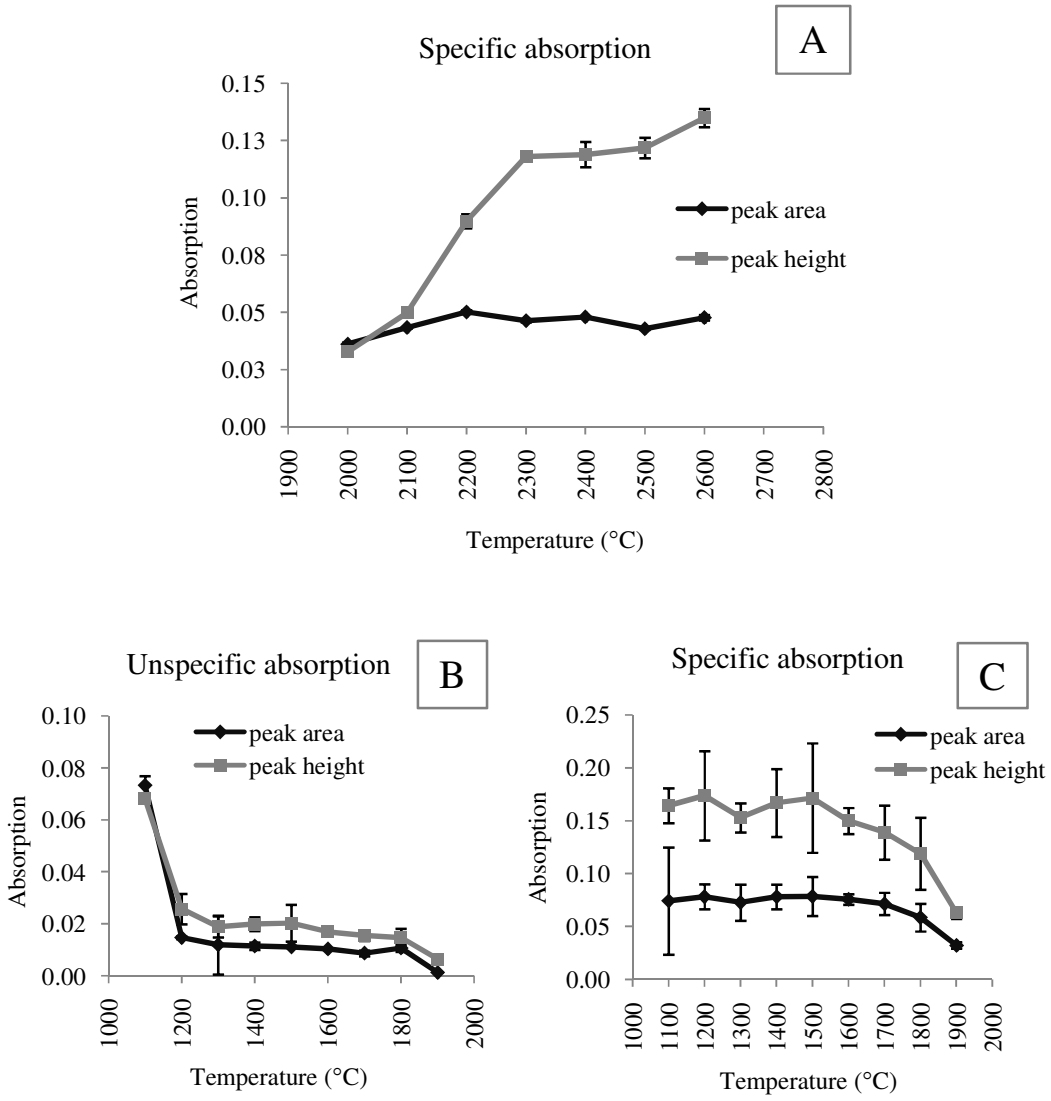

Figure 3.1. Optimization of temperature program parameters. A: Atomization temperature optimization. B: Ashing temperature optimization. C: Specific absorption during ashing temperature optimization. "Specific absorption" refers to the absorption arising from the interaction of the analyte with the light from the hollow cathode lamp and "unspecific absorption" (background absorption) results from interactions of the light with the sample matrix. Values are expressed as mean ± range (two serial measurements of one sample).

Stage No.	Stage type	Temp [ºC]	Ramp [ºC/s]	Hold [s]	Time [s]	Gas flow
1	Dry.	90	5	20	34	Max
2	Dry.	105	5	20	23	Max
3	Dry.	120	5	10	13	Max
4	Ash.	500	45	20	28.4	Max
5	Ash.	1600	250	10	14.4	Max
7	AZ	1600	0	5	5	Stop
8	Atom.	2400	FP	4	4.5	Stop
9	Clean.	2450	500	4	4.1	Middle

Table 3.1. Temperature program used for quantification of platinum in cell matrix. Every sample is injected twice with a total measuring time of about 4.5 min. One measurement takes about five minutes if the cooling phase (not shown in the table) after tube cleaning is considered. The drying procedure was adopted from a temperature program for platinum in the software WinAAS (Analytik Jena). Dry. = Drying, Ash. = Ashing, AZ = Autozero, Atom. = Atomization, Clean. = Cleaning, FP = Full Power (maximal heating rate with the power available).

3.3 Sample stabilization with Triton X-100

The surfactant Triton X-100 was added to some of the samples containing cell material to avoid aggregation and sedimentation. In the present work, sample protein concentration could be high, such as 5 mg/ml in the undiluted sample. Cell lysates, for example, were not stable during the measurements if Triton X-100 was omitted and aggregated material collected on the bottom of the sample vial if left to stand for a few minutes.

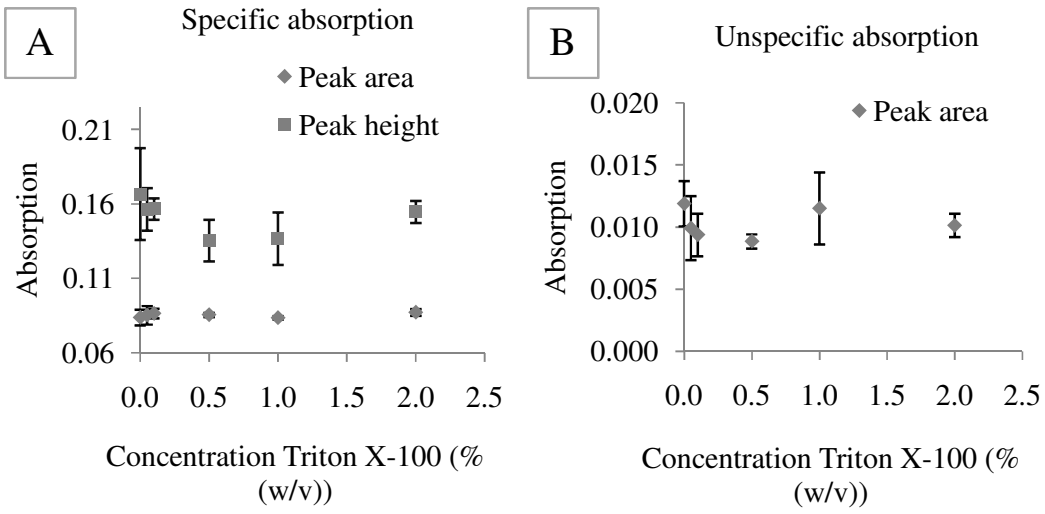

Figure 3.2. Effect of Triton X-100 concentration on specific and unspecific absorption signals. A: Effects of different concentrations of Triton X-100 on the specific absorption, expressed as peak height and peak area. B: Background absorption, expressed as peak area. Values are expressed as mean ± range (two serial measurements of one sample).

To investigate the effect of the concentration of Triton X-100 on the platinum measurements, cell lysate with a protein concentration of 2.5 mg/ml and 125 µg/l of platinum standard with different concentrations of Triton X-100 was measured. No obvious changes in absorption were observed (fig. 3.2A). A decrease in sensitivity was noticed when comparing standard calibration curves made with and without 0.67 % (v/v) Triton X-100 in the sample vial (data not shown) and therefore, the same amount of Triton X-100 was used in the calibration solutions as in the measured samples. Increasing concentrations of surfactant did not lead to higher background absorption (fig. 3.2B) with the used oven program (table 3.1).

3.4 Effect of HNO_3 and HCl

The quantification of platinum in the cell material used in the present work did not benefit from the addition of acid prior to the measurements. It is assumed that the platinum present in the sample is bound to bionucleophiles. When Triton X-100 stabilized cell lysate containing 325 µg/l platinum standard was measured, different acid concentrations of hydrochloric and nitric acid did not affect the absorption signal (fig. 3.3). On the other hand, addition of acid was necessary for obtaining acceptable calibration graphs ($R^2 > 0.99$) if the matrix consisted of only water and Triton X-100.

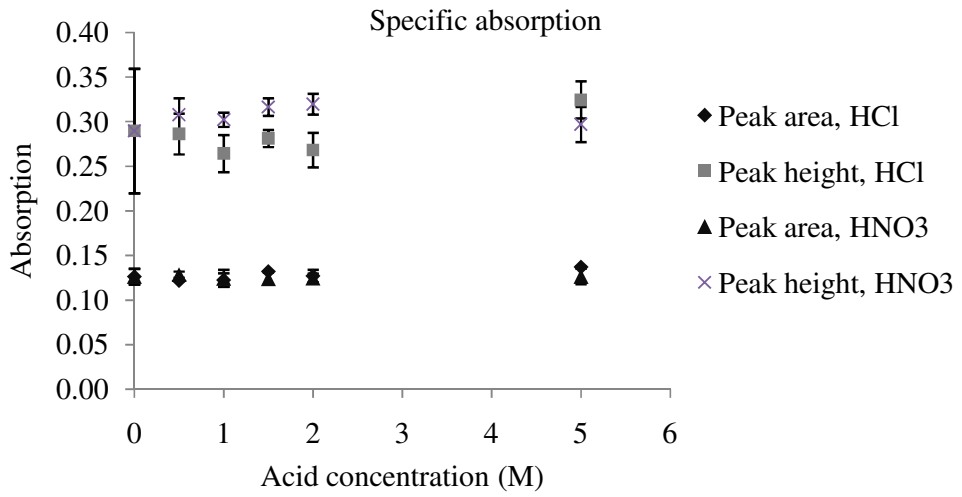

Figure 3.3. Significance of hydrochloric and nitric acid concentration on the specific absorption. Sample solution contained 325 µg/l platinum standard in whole cell lysate containing 1.25 mg/ml protein and was stabilized with 0.6 % (v/v) Triton X-100. Values are expressed as mean ± range (two serial measurements of one sample).

3.5 Matrix effects

The effect of cell matrix components on the atomization behavior of platinum was studied by preparing standard solutions containing different amounts of cell lysate, as determined by the protein concentration. The result shows that for the quantification of platinum in cell material, the calibration can be made without concerns about the amount of cell material present in the solutions, at least for the tested protein concentrations (fig. 3.4).

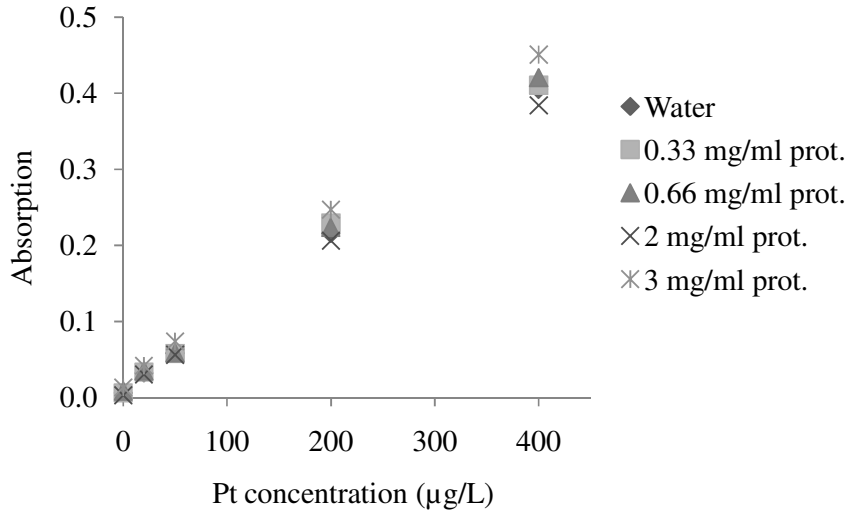

Figure 3.4. Effect of protein concentration on the sensitivity of the platinum quantification method. Samples were stabilized with Triton X-100 and HCl as described under materials and methods (section 15.3). The mean from two serial measurements of one sample is shown. Pt = platinum, prot. = protein.

3.6 Detection and quantification limit of platinum using FAAS

The detection limit of the method was determined by repeatedly measuring a *blank* (about 10 times) and was 0.0056 ± 0.0001 absorbance units (determined on a 3 σ basis, values are expressed as mean ± range from two independent measurements). The blank consisted of Triton X-100 (0.67 % (v/v)) and HCl (3 % (v/v)) stabilized cell lysate with a protein concentration of 2 mg/ml. The quantification limit, (calculated as 5 x detection limit) was 0.0280 ± 0.0007 absorbance units, which corresponds to 32 ± 4 µg/L. However, concentrations of 25 µM never deviated from the calibration graphs and measurements of samples with concentrations below 25 µg/L platinum were avoided if possible. The quantification limit is lower for the bivalent platinum complex, a consequence of lower sensitivity (fig. 3.5).

3.7 Comparison of atomization signal between platinum complexes and the AAS platinum standard

The analyte standard can only be useful as calibration agent if the measured platinum complexes give rise to the same signal at the same concentration. Otherwise, the substances have to be employed for calibration. All the substances tested in this work behaved as the standard (fig. 3.5A) except mDAH4FPtCl, which displayed a sigmoid curve when absorption was plotted against concentration (fig. 3.5B). This was

prevented by the addition of the solvent DMF (dimethylformamide) and the calibration curve was linearized. The slopes of calibration curves prepared with mDAH4FPtCl were lower than calibration curves prepared with the platinum standard and consequently, mDAH4FPtCl had to be employed for calibration prior to the quantification of this complex.

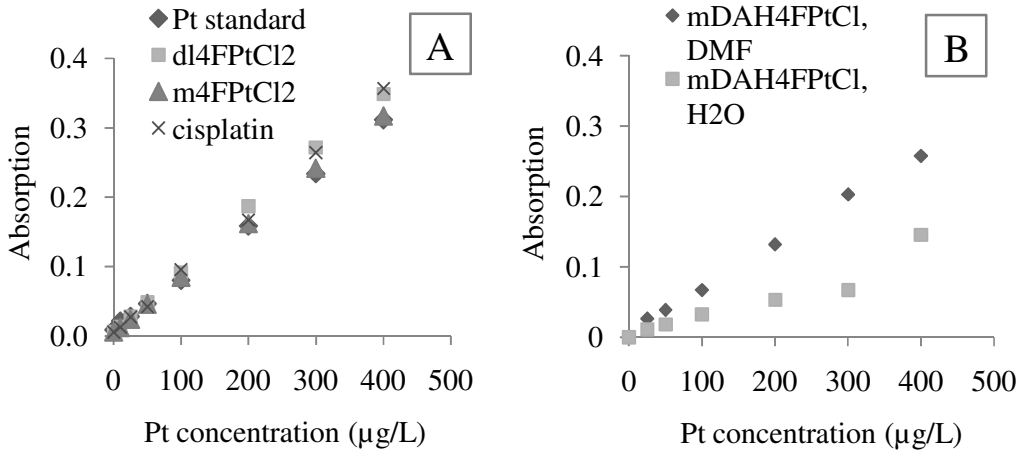

Figure 3.5. Calibration curves for the platinum complexes tested in the present work. A: Calibration curves of three platinum complexes (and platinum standard) diluted in water from stock solutions in DMF, stabilized with HCl. B: Calibration curves of mDAH4FPtCl prepared in water and DMF. The mean from two serial measurements of one sample is shown. Pt = platinum.

The effect of DMF could be explained by hindering the adsorption of mDAH4FPtCl to the walls of the teflon autosampler tube. Manual transfer of the sample to the graphite tube using a micro pipette had the same effect as automatic transfer of the sample with DMF (fig. 3.6). The optimal amount of solvent was shown to be 1/3 (v/v). Since DMF has a solving effect on the sample vial plastic material, the lowest possible concentration was sought.

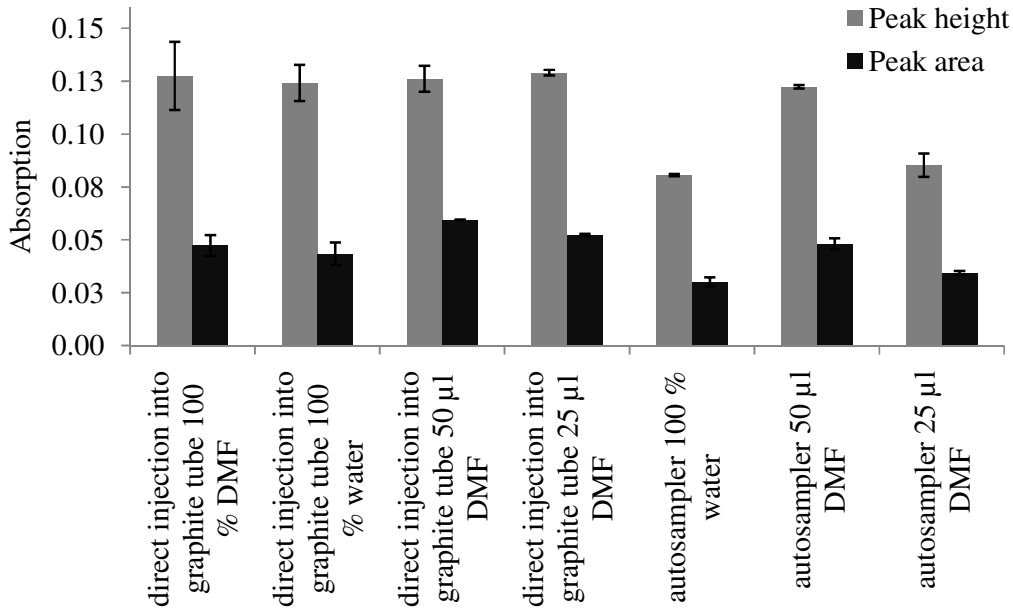

Figure 3.6. Influence of DMF on the atomization signal of mDAH4FPtCl. Measurement of a solution containing mDAH4FPtCl (100 µg/L) stabilized with different amounts of DMF (total volume of sample is 150 µl) where the sample was either introduced in the graphite tube manually, using a micro pipette, or automatically, by the autosampler. Values are expressed as mean ± range (two serial measurements of one sample).

4 Characterization of the platinum complexes

4.1 Water solubility determination of cisplatin, m4FPtCl$_2$, dl4FPtCl$_2$ and mDAH4FPtCl

If solubility is not guaranteed at the concentrations used in the tests, the effective concentration is unknown. To determine the solubility of the platinum complexes, they were suspended in cell culture medium without FBS and ultra-centrifuged after 30 min in an ultrasonic bath. Substance aggregates were sometimes seen on the surface and the pipette tip had to be carefully wiped off before the supernatant was transferred to a clean tube to reduce false positive results. Also, the supernatant had to be collected slowly to avoid disrupting the pellet. The solubilities for the substances were 125 ± 11, 10 ± 0 and 121 ± 81 µM (range of two independent determinations) for m4FPtCl$_2$, dl4FPtCl$_2$ and mDAH4FPtCl respectively. The deviations for the values obtained for mDAH4FPtCl are unacceptably high but the lowest value (40 µM) is still higher than the concentrations used for all tests except for the concentration dependence on cellular accumulation (fig. 10.1D). The linear relationship between concentration (10-60 µM) and whole cell associated platinum for this complex indicates that the solubility limit is probably higher than 40 µM.

4.2 Determination of water/octanol partition and LogP$_{o/w}$

Drug transport, in the sense of passage through the cell membrane and/or distribution in different compartments of the body, is often being correlated with the LogP$_{o/w}$ value which is the $\log_{10}$ value of the partition coefficient, P:

$$P = [\text{octanol}]/[\text{water}],\ \text{LogP}_{o/w} = \log_{10}(P)$$

The octanol/water partition coefficient is expressed as the ratio of the concentration of a solute in the octanol and the water phase after mixing of the two phases. This way of experimentally determining partition coefficients is called as the “shake flask” method. LogP$_{o/w}$ for some organic substances and solvents are listed in table 4.1. It was desired to see if the LogP$_{o/w}$ values correlate with cellular uptake and or the intracellular distribution for the complexes tested in the present work.

Substance	$logP_{o/w}$
Fluoranthene	5.16
Benzophenone	3.18
Diethylstilbestrol	2.48
Fluorobenzene	2.27
Benzene	2.13
Phenol	1.46
Benzamide	0.64
Ethylamine	-0.13
Ethanol	-0.30

Table 4.1. List of experimentally determined $logP_{o/w}$ values for some common substances and solvents (*107-108*)**.**

To determine the $logP_{o/w}$ value, the substances (10 µM) were added to the aqueous phase which consisted either of serum-free cell culture medium or water (pH 7.4). Before vigorously mixing of the two solvents for 30 s, an aliquot was taken out from the aqueous phase for the determination of the initial concentration. An equal volume of octanol was added and the tube vigorously shaken (vortex) to mix the phases. After 2 h of incubation at room temperature, the tubes were centrifuged and platinum quantified in the aqueous phase. Thus, the platinum concentration in the organic phase was determined indirectly by measuring the concentrations in the aqueous phase before and after octanol extraction. This is because of incompatibility of octanol with the AAS sample vial. The solubility of water in octanol is 2.3 M whereas 4.5 mM of octanol can be found in water after equilibrium (*109*). Accordingly, the water that enters the octanol phase when the two phases are mixed corresponds to 41 µl if the volume of the respective phase is 1 ml. In the present work, the volume of the water phase was measured gravimetrically, before and after mixing of the solvents. It should be noted that the data obtained in the present study are not necessarily equilibrium partition coefficients because of the relatively short incubation time.

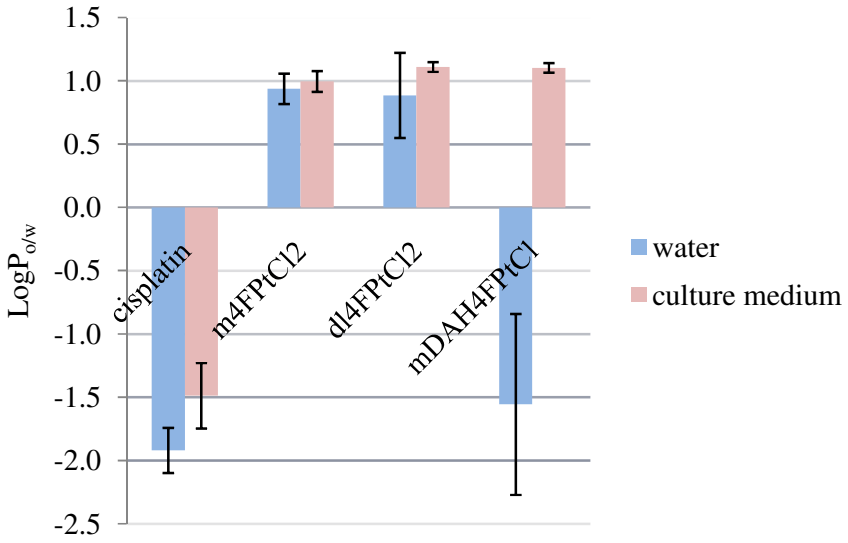

Figure 4.1. $LogP_{o/w}$ values determined through a shake flask method using octanol with water or cell culture medium. Values are presented as mean ± standard deviation (SD) from at least three independent experiments.

$LogP_{o/w}$ values for cisplatin presented in the literature are -2.36 (*110*) (theoretical method), -2.53 ± 0.28 (*111*) and -2.28 ± 0.05 (*112*). A small but significant ($p = 0.0268$) difference is seen between the $LogP_{o/w}$ values of cisplatin in culture medium and water (student's t-test, two-tailed with a significance level of 0.05, unpaired with unequal variance. It is not known if the samples are normally distributed) (fig. 4.1). One explanation to the lower hydrophobicity with water as aqueous phase might be the aquation of cisplatin. Methods using the shake flask method with aqueous phases containing salt solutions with chloride for the determination of $LogP_{o/w}$ of cisplatin (*111-113*) found about one log unit lower value for cisplatin than was found in the present work (-1.49 ± 0.26, fig. 4.1). The explanation for this discrepancy is not known but might be different concentrations of platinum complex, different incubation times used and how the concentrations were determined. Hall et al. (*112*) used 100 µM cisplatin in the aqueous phase and concentrations were determined in both phases after 24 h of shaking. Screnci et al. (*111*) used 300 µM cisplatin in the aqueous phase and platinum quantification was done in both phases after 30 min of vigorous mixing. Also, both authors have used 0.15 M NaCl or 0.15 M KCl as aqueous phases, however, in the present work, culture medium was used. One may speculate, components of the culture medium might partition into the octanol phase and alter the partition conditions of cisplatin.

The $logP_{o/w}$ for the bivalent platinum complex (mDAH4FPtCl) differed between experiments employing water as aqueous phase and experiments using cell culture medium (fig. 4.1). When 150 mM NaCl was used, the complex behaved similarly as when culture medium was used (data not shown). A possible explanation for the drop in hydrophobicity using water as aqueous phase might be the exchange of the chloride leaving groups with water. If both platinum moieties are carrying water molecules, the total charge will be +4 which increases the polarity of the complex. For aquated cisplatin at pH 7.4, one proton can leave the water resulting in species carrying one or two hydroxyl groups (*114-115*). It is possible that this is true also for the bivalent platinum complex. For the complexes $m4FPtCl_2$ and $dl4FPtCl_2$, on the other hand, changing the aqueous phase had no significant influence on the $LogP_{o/w}$ values (fig. 4.1). The differences seen for the bivalent platinum complex and cisplatin, highlights the importance of using as similar conditions as possible for the octanol/water distribution experiments as used in the in vitro accumulation experiments if the results are to be correlated.

4.2.1 Investigations of $logP_{o/w}$ values for platinum complexes, presentation of studies from the literature

Robillard et al. (*116*) determined cytotoxicity in a large cell lung carcinoma (LXFL 529) and a melanoma (MEXF 989) cell line and $LogP_{o/w}$ for three complexes, structurally similar to cisplatin. The cytotoxicity, expressed as the IC_{70} value, did not correlate with the $LogP_{o/w}$ values. Martelli et al. (*117*) found a linear relationship (R^2 = 0.9962) between the uptake in cisplatin resistant U2-OS cells and their $LogP_{o/w}$, as determined by the shake flask method (*118*). For cisplatin, oxaliplatin and JM216, $LogP_{o/w}$ values of -2.53 ± 0.28, -1.65 ± 0.21 and -0.16 ± 0.16 respectively were used (*111*). Hall et al. (*112*) investigated the relationship between $LogP_{o/w}$ values and cell-associated platinum for simple platinum (IV) complexes in the ovarian carcinoma cell line A2780 and found no clear relationship between lipophilicity and uptake but argue that a broader range of values (higher number of platinum complexes with larger differences in lipophilicity) might give better correlations. Platts et al. (*110*) evaluated a theoretical model for calculation of $logP_{o/w}$ values for several platinum (IV) ammine/cyclohexylamine dicarboxylate complexes, with small structural variations, and used the uptake data from Loh et al. (*119*) for correlations and found that both parabolic and exponential fits displayed R^2 values of 0.994 and 0.930 respectively.

4.3 Chemosensitivity assay

The ability of a substance to kill cancer cells is determined in chemosensitivity assays where the cells are subjected to varying concentrations of the test substance for different time periods. The higher the proportion of dead cells and/or the higher the growth inhibition, the more cytotoxic a substance is. To compare the cytotoxicity of substances in a given system (such as a cell culture), the concentrations needed to cause 50 % reduction of either viable cells and/or biomass relative to solvent treated cells, are calculated. This concentration is called as IC_{50} value. Several tests are available that measure the sensitivity of cells to substances through determining cell viability or cell survival, such as the neutral red assay (*120*), the MTT (3-(4,5-dimethylthiazol-2-yl)-2,5-diphenyltetrazolium bromide) assay (*121-122*), the crystal violet staining (CVS) assay (*123*) and the [^{3}H]-thymidine incorporation assay (*124*). In the present work, the CVS assay was used. In brief, the cells are seeded out in 96-well culture plates and left to grow until they reach logarithmic growth, usually after three days. The test substance is added to the cells after dilution in serum-containing culture medium. After four days (96 h), the medium is removed and cells still attached to the plate surface are fixed with glutardialdehyde and stained with a crystal violet solution which stains nuclear proteins (*125*). The quantification of cell-bound dye is done spectrophotometrically after alcohol extraction. The quantity of surviving cells is expressed as T/C_{corr}:

$$T/C_{corr.} = [(T-C_0)/C-C_0)] \times 100$$

Where T = absorption from substance-treated cells, C_0 = absorption from cells fixed at the time of substance addition, C = absorption from cells treated with solvent. T/C_{corr} is plotted against the initial culture medium concentrations (logarithmic scale) and a sigmoid trend is fitted using a Boltzmann function. The IC_{50}-value obtained from the resulting graph is the concentration giving rise to a T/C_{corr} of 50. T/C = "treated to control" and corr. (= corrected) means that the values are corrected for initial biomass. It is important that the cells subjected to either test substance or solvent (control) are experiencing logarithmic growth throughout the experiment (*126*). If this is not the case, the values obtained will lead to an underestimation of substance toxicity. Another prerequisite for this type of chemosensitivity assay is that the cells detach

from the culture-plate surface when they die, attached cells will be considered alive and vital.

Substance	IC_{50} value
cisplatin	0.57 ± 0.26
$m4FPtCl_2$	3.54 ± 1.04
$dl4FPtCl_2$	0.38 ± 0.1
mDAH4FPtCl	24 ± 6, > 50[a]

Table 4.2. Effects of four platinum complexes in a crystal violet assay. The data was obtained from at least three independent experiments and results are presented as mean ± SD. [a]Sometimes the growth inhibition was not strong enough to result in T/C_{corr} values ≤ 50.

The cytotoxicity of $dl4FPtCl_2$ is comparable to that of cisplatin but higher than for $m4FPtCl_2$ (table 4.2). The bivalent complex only displayed weak antiproliferative activity and for some tests, the remaining cell mass exceeded 50 % for all concentrations used and no mean could be calculated. In previous works, similar results were obtained for these substances in MCF-7 cells (*91*).

5 Subcellular fractionation, method development

5.1 Subcellular fractionation

The separation and collection of the intracellular content is called as "subcellular fractionation" where the cells are lysed and the released cell content separated according to differences in size and density. Depending on the refinement of the method, organelle populations can be separated and purified which is done in a series of centrifugation steps. The velocity (v) of sedimentation of a particle in a centrifugal field can be described:

$$v = (d^2 (\rho_p - \rho_l)/18\ \mu)\ g$$

Where d = diameter of the sedimenting particle (assuming spherical geometry), ρ_p = density of the particle, ρ_l = density of the surrounding liquid, g = gravitational field (expressed as Relative Centrifugal Force, RCF) and μ = the viscosity of the surrounding liquid. The particles, or organelles in the case of subcellular fractionation, will move in different speeds depending on their size and density and if they reach to a point in the surrounding liquid having the same density they will stop and together form a band. Thus, this density of the gradient medium is called as the "banding density" of the organelle in that particular gradient medium. The protocol used in the present work is described in detail in section 15.8 and the centrifugation scheme shown in figure 5.1.

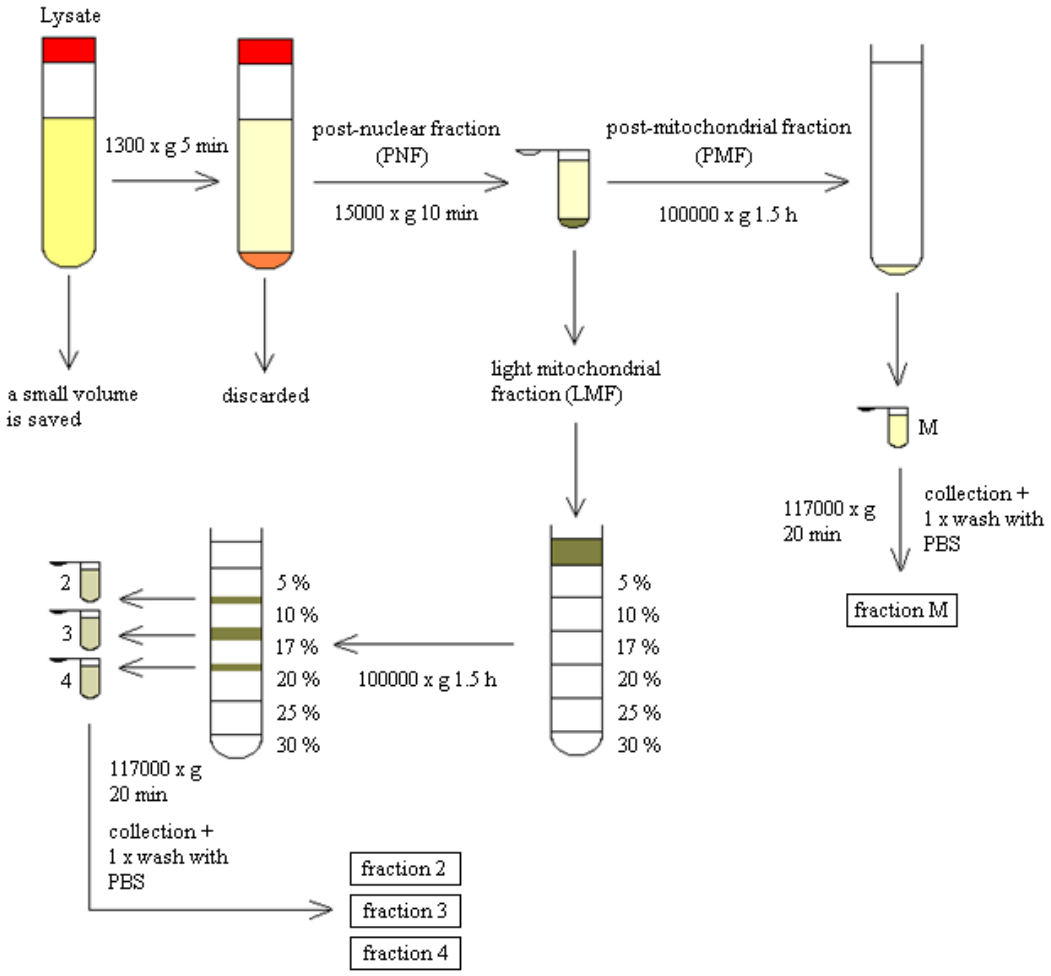

Figure 5.1. Centrifugation scheme of the subcellular fractionation method used in the present study.

5.2 Density media

There are several available density media that differ in properties such as osmotic pressure, viscosity, ability of self-forming gradients at conventional speeds and the influence on assays and/or downstream sample manipulations (*127*). In the present study, the dimer of the iodinated density medium Nycodenz®, iodixanol (OptiPrep™) was chosen because of its low viscosity (relative short centrifugation times are needed), compatibility with enzymatic assays and the Coomassie Brilliant blue dye present in the Bradford protein reagent (see section 5.4) and low osmotic pressure (*128*).

5.3 Homogenization

An efficient cell lysis is a prerequisite for a successful subcellular fractionation protocol. An ideal cell lysis should release as many intracellular components as possible with low compromises regarding organelle integrity. In the present work, > 90 % cell breakage was achieved by subjecting cells to the hypo-osmotic reticulocyte suspension buffer (RSB) and liquid shear using a Dounce glass homogenizer. To preserve organelle integrity, isotonic buffers should be used as homogenization media. However, in the present study, the HeLa cells were resistant to homogenization if isotonic sucrose was employed. Attempts were therefore made to homogenize the cells with isotonic sucrose containing 0.1 % digitonin (mild non-ionic tenside). Western blot analysis revealed that the peroxisomal membrane marker protein PMP70 was absent in the mitochondrial fraction (LMF) (fig. 5.1) but instead found in the low-density fraction M (fig. 5.1) (results not shown). Postulated peroxisomal lysis led to abandonment of this strategy. Buffers with higher salt concentrations than RSB were also not successful (e.g. 150 mM $MgCl_2$, 10 mM KCl and 10 mM Tris-HCl). They required more number of strokes in the homogenizer resulting in aggregation of cell material, maybe a consequence of DNA release from damaged nuclei (*129*).

5.4 Bradford protein quantification

To account for deviations in the amount of cells used in different experiments or different quantities of cell material in one fraction compared to another, the values have to be normalized to a common component. If the platinum amount in whole cells is measured, it is easy to normalize to cell count. If platinum is measured in subcellular fractions, on the other hand, it would be ideal if this could be normalized to bio mass. A more convenient approach is to normalize to protein content. One of the most frequently used methods, the Bradford method (*130*) has in its linearized and more sensitive form (*131*) been ubiquitously used in the present study. The HSA (human serum albumin) standard solutions ranged between 0 and 0.75 mg/ml (increment: 0.025 mg/ml) in the solutions being mixed with the Bradford reagent (1/11 dilution). In most cases, the R^2 value of the standard curve was never below 0.990 (data not shown).

When comparing the protein normalized platinum amount in different subcellular fractions, it is worth to consider that the protein to mass ratio might be different in

different compartments of the cell. For example, the plasma membrane contains less protein per dry weight (60 % (w/w)) than does whole cell homogenate (85 % (w/w)) (*132*). The same amount of platinum per weight in the homogenate and the plasma membrane fraction will result in a higher calculated protein normalized platinum amount in the plasma membrane than in the homogenate.

5.5 Western blot

Western blot is used for the detection of specific proteins in a sample. Briefly described, the proteins in a sample are separated according to size using SDS-PAGE (SDS-polyacrylamide gel electrophoresis) where denatured proteins, covered with negative charges from SDS molecules, are migrating in the gel towards the anode (positive electrode) in an electric field. Subsequently to separation, the proteins are again subjected to an electric field, allowing them to migrate out from the gel and on to a membrane (e.g. a nitrocellulose membrane). The membrane is incubated with an antibody (primary antibody), specifically recognizing one protein in the gel. Thereafter, the gel is subjected to a second antibody (secondary antibody), with affinity to the first primary antibody. The secondary antibody commonly carries horseradish peroxidase (HRP) and can be detected by a HRP catalyzed chemoluminescence reaction. The light is captured e.g. on an X-ray film and the resulting bands represent the target protein.

5.5.1 Western blot analysis of the subcellular fractionation method

To find out the organelle distribution between the bands in the density gradient and the post-mitochondrial fraction (fraction M) (fig. 5.1), western blot analysis of the collected material was done with antibodies owing affinity to organelle specific proteins (marker proteins) (fig. 5.2). The protein normalized distribution of marker proteins amongst the collected fractions is shown in fig. 5.3.

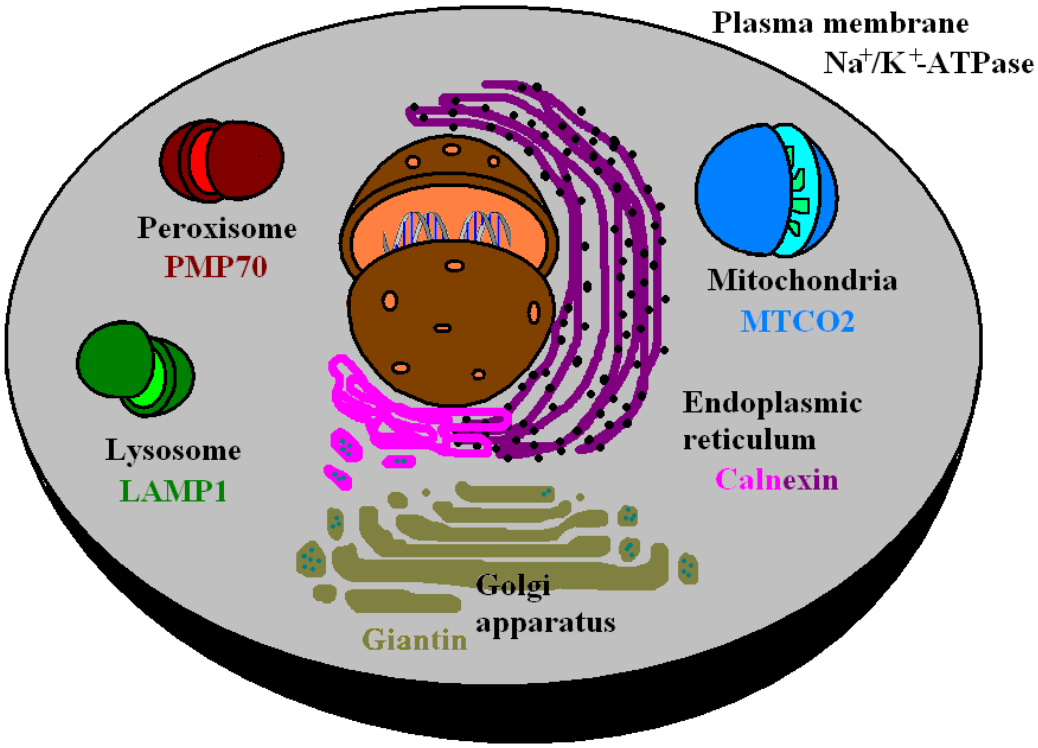

Figure 5.2. Schematic picture of a cell with organelles whose marker proteins were used in the present work. Na^+/K^+-ATPase for the plasma membrane, MTCO2 (cytochrome c oxidase subunit) for the mitochondrial inner membrane, Calnexin for the endoplasmic reticulum, Giantin for the Golgi complex, PMP70 for the peroxisomal membrane and LAMP1 for the lysosomal membrane. Other cellular components except cell nuclei, which were not considered, are intentionally left out from the picture.

In the present work, the peroxisomal marker was found co-localized with the mitochondrial marker and in fractions with lower density. Using MCF-7 cells, Li et al. (*133*) found the peroxisomes not to co-localize with the mitochondria but on the bottom of the 24 %/20 %/32 % gradient (sample in 32 %, bottom loaded). The cells were lysed with a tissue grinder in a buffer containing 0.25 M sucrose (*133*).

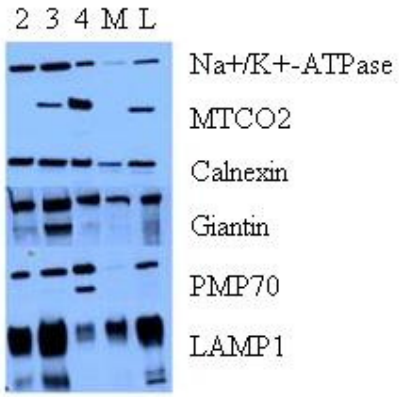

Figure 5.3. Western blot analysis of fractions from the density gradient centrifugation. Lysate (L) was used as positive control with a 5 times higher applied protein amount. The numbers 2, 3 and 4 represent the fractions in the density gradient and M is the collected LMF supernatant (see fig. 5.1). A sample volume corresponding to ~ 4 µg of protein was loaded on the gel (SDS-PAGE) from each fraction.

In protocols separating organelles from rat- and mouse liver cells, the peroxisomal markers are found in fractions with higher density than the mitochondrial markers. In these works (*127, 134-135*), 0.25 M sucrose was used during cell homogenization. Peroxisomes are osmotically sensitive organelles (*136*) and the lysis method used in the present study might have caused disruption of peroxisomes which contributes to the different banding pattern of peroxisomes when compared to that in the above mentioned literature.

5.6 Purification of cell nuclei

The nuclei purification method used in the present work is based on a protocol employing hypotonic swelling of the cells with subsequent addition of Triton X-100 and citric acid (*137*). The surfactant causes cell lysis and releases the nuclei from the outer nuclear membrane (*138*) which is continuous with membranes of the endoplasmic reticulum (*139*). Citric acid helps removing remaining adhering cytoplasmic material (*140*). The method is fast and efficient, but harsh. Knowler et al. (*138*) showed that nuclei treated with citric acid lost acidic high molecular weight histones. Electron micrographs of nuclei purified with citric acid indicate loss of nuclear material, probably proteins (*140-141*). Rosenberger et al. (*142*) found that this effect is not exclusively due to the lost integrity of the nuclear membrane. Including $MgCl_2$ in the citric acid solution has been reported to have a protective effect on the nuclei and thereby milden the damage caused by citric acid, at least visually, as seen in

electron micrographs (*138*) and was therefore added to the citric acid solution used in the present work. The method in the present study was first used for the purification of MCF-7 cell nuclei but is applicable to HeLa cells without the requirement of modifications. The nuclei were examined under the phase contrast microscope revealing relatively few visible contaminants and little material adhering to the nuclei (fig. 5.4). Nuclei from HeLa cells will give an intact impression under the light microscope despite suffering the loss of both membranes after detergent treatment (*143*). Thus, the level of intactness of the nuclei purified in the present work is not known.

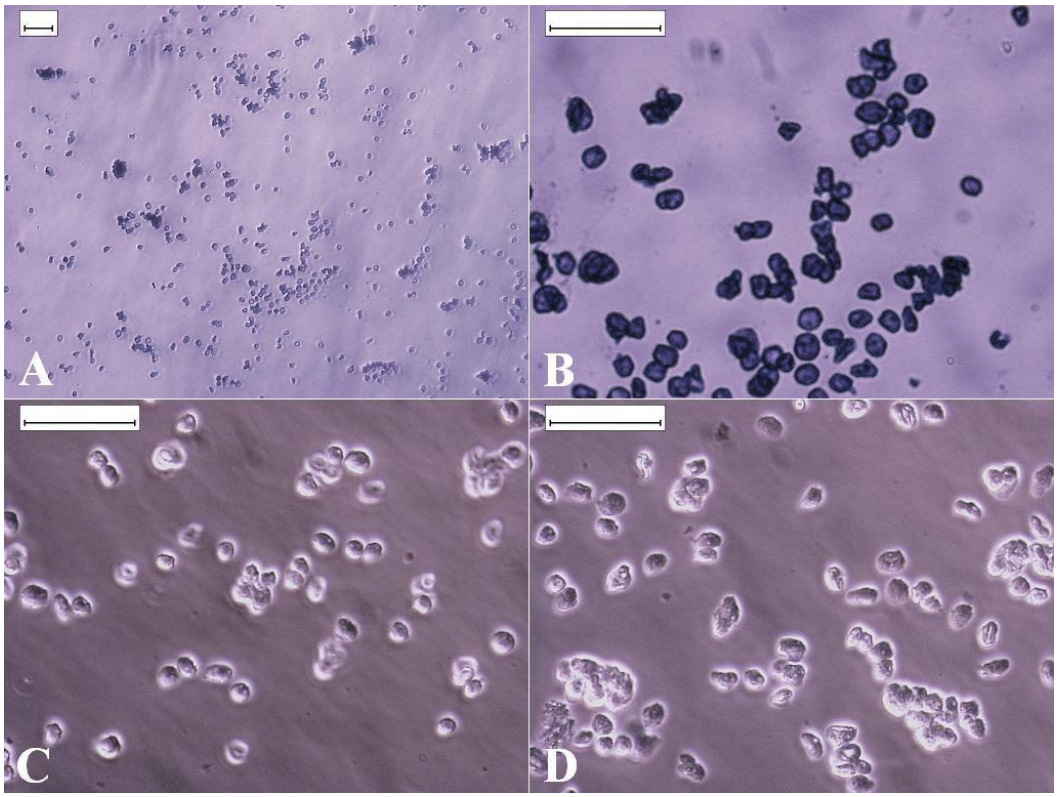

Figure 5.4. MCF-7 cell nuclei purified using a citric acid detergent method. A and B: Different magnifications of purified nuclei stained with methylene blue. C: Unstained nuclei prepared directly from freshly harvested cells. D: Unstained nuclei prepared from cells previously frozen (-20 °C). Scale bar = 100 µM.

5.7 Purification of HeLa cell membrane sheets (ghosts)

HeLa cells can be disrupted in a fashion that leaves large portions of the plasma membranes intact (*144-145*). These large membrane sheet fragments (ghosts) are typical in shape and can easily be identified under the phase contrast microscope. The plasma membranes can be collected at low centrifugal forces because of their size and no ultra centrifugation is necessary. In the present study, a modified method of Atkinson (*144*) was employed. It includes several steps of differential centrifugation and the method was validated by assaying the ouabain-sensitive Mg^{2+}-dependent Na^{+}/K^{+}-ATPase activity and by western blot (fig. 5.5). An enrichment of enzyme activity in the plasma membrane fraction normalized to protein content was 4.85 ± 1.7-fold compared to the protein normalized activity in the whole cell homogenate.

The nuclei should be stabilized by the addition of bivalent cations as soon as possible after cell lysis. Otherwise nuclei will not sediment to the same extent in the first centrifugation step and be present in the membrane ghost preparation. Prior to cell lysis, the cells were washed with Eagle's Balanced Salt Solution (EBSS) as described in the original protocol (*144*). Substitution of EBSS with PBS resulted in lower amounts of ghosts, as seen under the phase contrast microscope. As mentioned in the original method (*144*), cells in multi-layers or cultures that had reached a high (~ 80 %) or low (~ 40-50 %) confluence did not provide good yields of ghosts. The plasma membrane ghosts were layered on an iodixanol density gradient (fig. 5.1) and the bands analyzed using western blot (fig. 5.5). The gradient centrifugation resulted in a purification of the plasma membranes compared to using differential centrifugation only. However, the material loss in the gradient and the long purification time (~ 8 h) led to abandonment of the density gradient centrifugation.

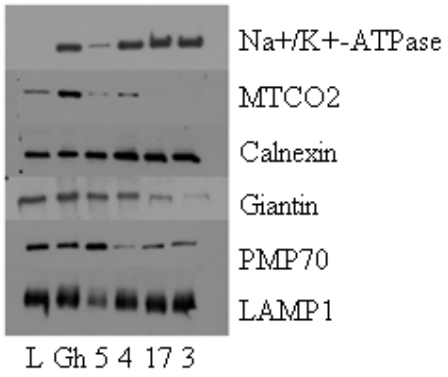

Figure 5.5. Western blot analysis of fractions from the plasma membrane ghost purification. The HeLa cell membrane ghosts (Gh), resulting after a series of differential centrifugation steps, were layered on an iodixanol density gradient (fig. 5.1) and several fractions analyzed with western blot. L = lysate (positive control). Fraction 5 represents the material collected at the interface of 20/25 % iodixanol. See fig. 5.1 for description of fraction 4 and 3. Fraction 17 is the sample collected from the 17 % density layer. The amount of protein loaded on the gel was ~ 5 µg. For whole cell lysate, the plasma membrane marker seems absent but is rather very weak, 1/5 less protein was loaded on the gel for Na^+/K^+-ATPase from the lysate than on the other gels.

5.7.1 Purification of HeLa cell membrane ghosts, presentation of results from the literature

Costantino-Cerccarini et al. (*146*) used similar discontinuous sucrose gradients as reported by Atkinson et al. (*145*) for the purification of HeLa cell plasma membranes. The protein-normalized activity of the ouabain-sensitive Mg^{2+}-dependent Na^+/K^+-ATPase was ~ 9 times higher in the plasma membrane fraction compared to whole cell homogenate. Atkinson et al. (*144*) labeled the cell membrane with tritiated fucose. One discontinuous sucrose gradient and subsequent washes in Tris-HCl buffer resulted in ~ 5 times protein-normalized enrichment of sugar in the plasma membrane fraction compared to whole cell homogenate. The enrichment was doubled when the plasma membrane fraction was run on a second gradient (*144*). Boone et al. (*147*) incubated the cells with radio-labeled antibodies prior to purification. After one discontinuous sucrose gradient, the plasma membrane fraction was ~ 10 times enriched in protein-normalized radioactivity, as compared to whole cells. When employing density gradient centrifugation of a continuous sucrose gradient subsequently to the discontinuous gradient, the enrichment was additionally five times higher (*147*). However, this density gradient required long centrifugation times (~ 16 h) (*147*).

5.8 Activity assay of the Mg^{2+}-dependent, ouabain-sensitive Na^+/K^+-ATPase

This ion transporting protein is used as marker for the plasma membrane (*146-148*). The activity can be determined by measuring the release of orthophosphate ions (PO_4^{3-}) accordingly:

$$ATP + H_2O \xrightarrow[Mg^{2+}]{Na^+ \ K^+} ADP + PO_4^{3-} + H^+ + energy$$

ATP = adenosine triphosphate, ADP = adenosine diphosphate

The Na^+/K^+-ATPase specific release of PO_4^{3-} is calculated as the difference between total PO_4^{3-} and the PO_4^{3-} released in the presence of the Na^+/K^+-ATPase inhibitor ouabain. The present work employed the method described by Cariani et al. (*149*) for the quantification of PO_4^{3-} and a combination of two methods for the preparation of cell material (*146, 149*). In brief, after incubation of cell material with ATP containing buffer (with or without ouabain), the released PO_4^{3-} was complexed with ammonium molybdate. This complex is reduced in the presence of ascorbic acid to form a blue colored complex, "molybdenum blue". The remaining ammonium molybdate was complexed with bismuth citrate. The molybdenum blue species was quantified spectrophotometrically at 590 nm (A_{max}= 710 nm) with K_2HPO_4 as standard. The time-dependent release of PO_4^{3-} was linear for at least 50 min and the ratio between the purified plasma membrane fraction and the lysate was unchanged during this time interval (fig. 5.6). An incubation time of 30 min was sufficient for protein concentrations of 0.3 mg/ml of membrane fraction and 1 mg/ml of whole cell lysate to produce signals within the linear range of the standard curve (data not shown).

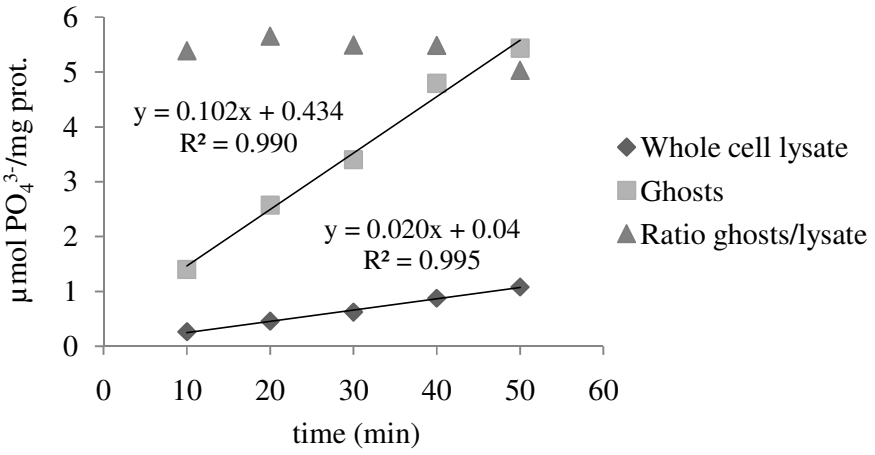

Figure 5.6. Time-dependent PO_4^{3-} release in an assay of the ouabain sensitive Mg^{2+}-dependent Na^+/K^+-ATPase in the ghost membrane fraction and in the whole cell lysate of HeLa cells. prot. = protein. Values are presented as mean of two independent experiments.

5.9 Purification of mitochondrial DNA

Mitochondrial DNA (mtDNA) can be purified in several ways. Depending on the purpose of the purification, different methods will render useful. The "alkaline lysis" method, developed for the purification of plasmid DNA from bacterial cells (*150*) selectively purifies CCC-DNA (covalently closed circular DNA). This method has been used for the purification of mtDNA from *Drosophila* (*151*) and from head and neck squamous cell carcinoma cell lines (*152*). A drawback of this method is the loss of non covalently closed circular mitochondrial DNA (*153*). Therefore, another method was employed in the present study. In brief, the method is based on differential centrifugation of the whole cell lysate for complete removal of cell nuclei. The LMF is thereafter collected and subjected to lysis with sodium dodecyl sulphate (solubilizing membranes and stripping proteins off the DNA) and proteinase K. The lysed LMF is extracted once with Tris-equilibrated phenol (deproteinization), several times with an equal volume of a mixture of phenol, chloroform and 3-methylbutanol (anti-foaming agent) (ratio of solvents = 25(phenol):24(chloroform):1(3-methylbutanol)) followed by two extractions with chloroform (phenol removal) (*154*). The aqueous phase is extracted twice with diethyl ether (solvent removal). After solvent evaporation, the DNA is precipitated with ethanol and after careful mixing of the phases, left at -20 °C over night. After collecting the DNA from the first extraction round and evaporating most of the solvent (mtDNA was never left completely dry, this

can cause breaks), it was solubilized and incubated with buffer containing RNase A and RNase T_1 followed by another round of deproteinization and extractions. CsCl gradients can be used to purify the mtDNA in the presence of gDNA but only CCC-DNA will be collected (*153*). To recover the other forms, the LMF has to be treated with DNase prior to lysis which can have deleterious effects on the recovery of the mtDNA if the mitochondria are not intact at the time of digestion.

5.9.1 Restriction enzyme analysis of mitochondrial DNA with *Bam* HI and *Hind* III

The mitochondrial DNA contains 16 kb (kilo base pair). A result of subjecting mtDNA to restriction enzymes is bands of distinct sizes. Restriction enzymes recognize short sequences in the DNA where they cut the double strand. In the present work, two restriction enzymes were used, *Hind* III (three-cutter) and *Bam* HI. The former will cut at three places (fig. 5.7) and the latter only at one place. Although having the same size as undigested mtDNA, the linearized molecule will migrate faster in the gel (fig. 5.8A). Restriction analysis of gDNA will not give rise to distinctive bands in the agarose gel because of the high occurrence of restriction sites.

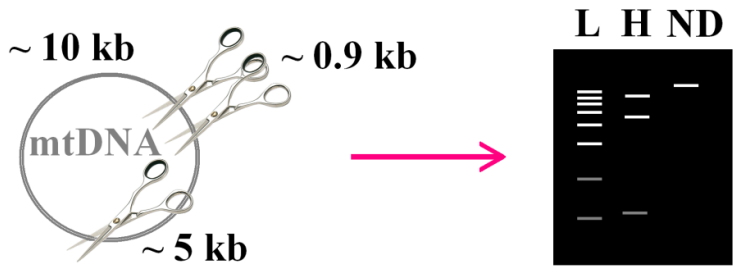

Figure 5.7. Schematic picture of restriction analysis of mitochondrial DNA using *Hind* III. Mitochondrial DNA (mtDNA) is cut at three places when subjected to digestion by the restriction enzyme *Hind* III (~ 10 kb, ~ 5 kb and ~ 0.9 kb). The fragmented DNA is separated according to size on an agarose gel in an applied electric field. The gel contains an intercalating fluorescent dye that emits light after intercalation when subjected to light of suiting wavelengths. kb = kilo base pair, L = DNA ladder, H= *Hind* III digested mtDNA, ND = non digested.

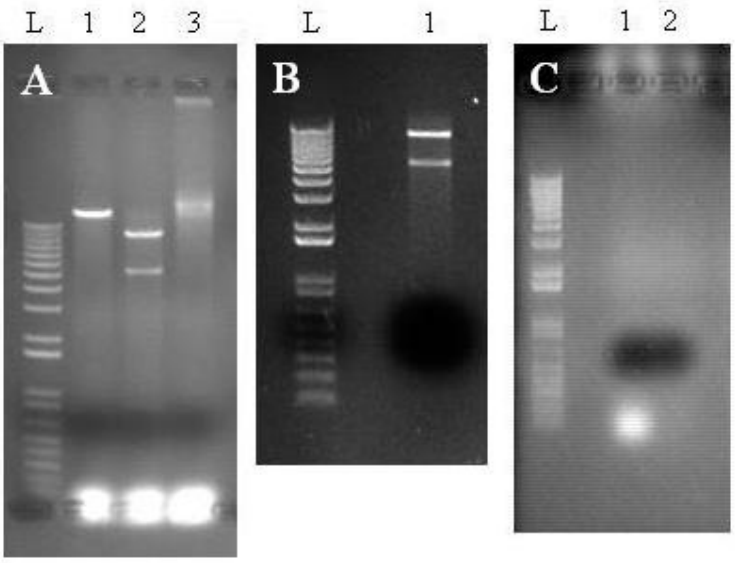

Figure 5.8. Agarose gel electrophoresis of purified HeLa cell mitochondrial DNA and yeast RNA. A: Digested with RNase A. No extra EDTA in washing buffer, no RNase T_1. Lane L: 1 kb DNA ladder, lane 1: mtDNA linearized with *Bam* HI, lane 2: mtDNA digested with *Hind* III and lane 3: undigested mtDNA. A total amount of 11.25 µg DNA (according to UV measurements) was loaded on the gel. B: 20 mM EDTA in washing buffer, digested with RNase A and RNase T_1. Lane L: 1 kB DNA ladder, lane 1: mtDNA digested with *Hind* III, 1.5 µg DNA was loaded on the gel (according to UV measurements). C: Yeast (*Saccharomyces cerevisiae*) RNA, digested with RNase A (lane 1) and RNase A and RNase T_1 (lane 2) followed by deproteinization and precipitation according to protocol (section 15.12), 8 µg RNA was loaded on the gel (according to UV measurements).

5.9.2 Restriction enzyme analysis of the purified mitochondrial DNA

Contamination of the mtDNA with gDNA was considered to be a minor problem in the present work because of low fluorescence between the digested mtDNA bands (fig. 5.8B). In the initial stages of method development, RNase A was used for the digestion of RNA in the mtDNA preparation. The resulting fragments were large enough to co-precipitate with the DNA and to be visible on the agarose gel as a large band migrating at 100 bp (fig. 5.8A). According to absorption at 260 nm, 11 µg of DNA was required for the appearance of clearly visible mtDNA bands (fig. 5.8A). After changes in the protocol such as excessive washing of the LMF with isotonic sucrose containing 20 mM EDTA and the addition of RNase T_1 in the RNA digestion step, the bands at 100 bp were absent and less DNA was required for bright bands (fig. 5.9B). EDTA removes the adhering microsomes and ribosomes from the mitochondria (*155*). Fragments of RNA that are small enough not to stay on the gel will still contribute to absorption at 260 nm. To evaluate the RNA digestion efficiency, yeast RNA was digested either with RNase A only or RNase A and RNase T_1. After deproteinization and subsequent washing of the ethanol precipitate, nucleic acids were still present (absorption at 260 nm) indicating that the ethanol precipitation did not completely remove the digested fragments. The RNase A treated DNA (fig. 5.8C) displayed a thick band migrating at 100 kb but the fraction digested with both enzymes, did not give rise to bands with the same amount of applied DNA, as determined by UV absorption. In the present work, the DNA was left to precipitate over night which might have been the reason for the presence of short fragments since smaller fragments require longer times to precipitate.

5.9.3 DNA purity determination

The purified DNA was checked for protein and phenol residues spectrophotometrically by determining the A_{260}/A_{280} and A_{260}/A_{230} ratio respectively. Common knowledge in this field is that pure DNA display an A_{260}/A_{280} ratio of 1.8 while pure RNA has a ratio of 2. Lower values are said to indicate protein contamination but the usefulness of this method is being discussed. According to calculations done by Glasel (*156*), this is a poor measurement of purity considering protein contamination and these measurements cannot tell the purity of the DNA because of the relative insensitivity to changes in protein concentration. Other ratios

that can be of value are the A_{260}/A_{230} ratio that should be higher than 2 and 2.2-2.5 for phenolate- and protein (*157*) free DNA respectively. A A_{260}/A_{270} ratio of 1.2 indicate that the DNA is free from phenol contamination (*154*). In the present work, ratios of $A_{260}/A_{280} \geq 1.8$ and $A_{260}/A_{230} \geq 2$ were accepted and complete absence of phenolate ions and proteins is therefore not assured.

5.10 Disruption of lysosomes and endosomes using lysotropic peptides

Lysosomes and/or endosomes can be osmotically disrupted using the peptides GPN (glycyl-L-phenylalanine 2-naphthylamide) and MOM (methionine *O*-methyl ester). Hydrolytic enzymes present in the organelle catalyze the hydrolysis of the dipeptides to products with higher polarity that experience difficulties in crossing the lysosomal membrane and accumulate in the organelle. The accumulation of polar compounds eventually leads to osmotic lysis.

GPN (a substrate for cathepsin C (*158*)) was shown to act on lysosomes whereas MOM (a cathepsin G substrate (*159*)) additionally disrupted non-lysosomal compartments, assumingly endosomes (*160*). Berg et al. (*160*) used the release of radiolabeled endocytosed material and a lysosomal enzyme, acid phosphatase, to confirm lysosomal and endosomal disruption. Others (*161-162*) have used chloroquine, a known lysotropic agent, to investigate lysosomal breakage. They found a switch of the lysosomal marker LAMP1 to lower densities after density gradient centrifugation. This was accompanied by reduction in β-glucuronidase, a lysosomal matrix enzyme. The lysosomal marker LAMP1 has also been found in endosomes (*163*). In the present study, the LMF was treated with MOM and GPN according to the method of Berg et al (*160*) prior to gradient loading and the distribution of LAMP1 amongst the fractions was analyzed with western blot (fig. 5.9). Since MOM gave rise to a larger shift of the marker protein to lower densities, this peptide was used in the subsequent tests.

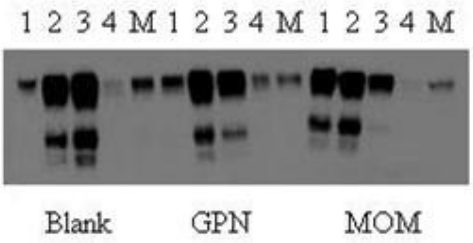

Figure 5.9. LAMP1 banding pattern in subcellular fractions after the subjection of LMF to lysotropic agents. GPN (glycyl-L-phenylalanine 2-naphthylamide) and MOM (methionine *O*-methyl ester) are lysolytic peptides. Blank = untreated LMF. Numbers represent the bands in the density gradient (fig. 5.1) and M is the pellet from the collected LMF supernatant (fig. 5.1). The gel was loaded with 5 µg protein.

5.10.1 Lysosomal disruption, use in subcellular fractionation

The consequence of MOM treatment on the distribution of m4FPtCl_2 in fractions 2-4 and M is shown in fig. 5.10. HRP was used as a control for lysosomal disruption, since it is taken up endocytotically by the cells and found in lysosomes after pinocytosis (see section 8.1). The small gain for m4FPtCl_2 (fig. 5.10C) in fraction 2 might be explained by platinum complexes residing in lysosomal and endosomal structures i.e. lysosomal membranes which are experiencing lighter banding densities after MOM treatment. For HRP (fig. 5.10D), the gain to fraction 2 is believed to be a method artifact. One might postulate that MOM is hindering the lysosomal breakdown of HRP. Protease inhibitors were omitted in this experiment. The investigation of the stability of the enzyme in whole cell lysate was done with ultrasound disrupted HeLa cells in PBS (fig. 7.1). The unfavorable pH for enzymatic breakdown in this suspension, inevitable sedimentation of protein aggregates during incubation and the large excess of other proteins might have a protecting effect on HRP in the lysate. Proteolytic breakdown would make HRP unsuitable as validating agent for lysosomal disruption and as marker in a quantitative manner. Thus, the validity of the results obtained for HRP in this experiment (fig. 5.10) is questioned and it is not ascertained how to interpret the results. If the platinum complex is present in the intralysosomal and intraendosomal matrix and MOM treatment results in complete disruption of these organelles, the matrix is released. Thus, the platinum compound would be lost from the gradient and no gain in any fraction was therefore expected. However, a protease insensitive control for lysosomal disruption is needed.

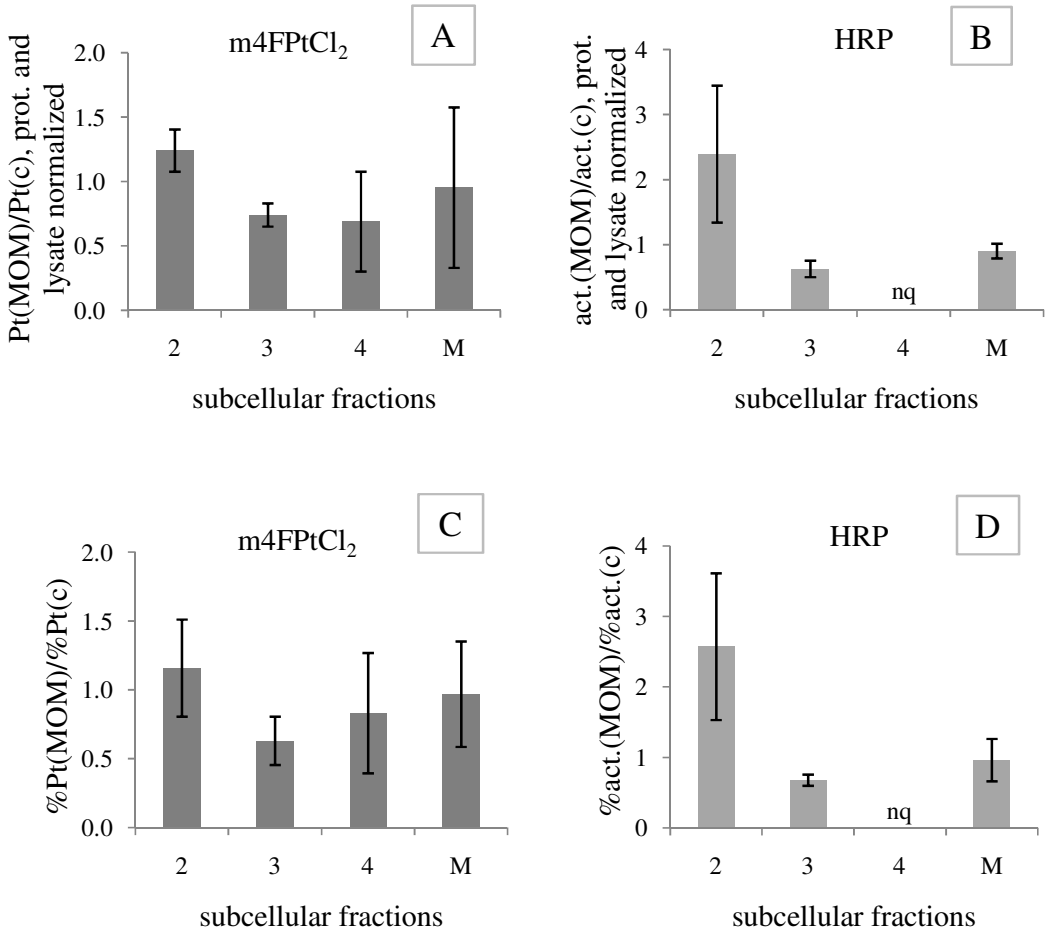

Figure 5.10. Subcellular distribution of $m4FPtCl_2$ and HRP after treatment of the LMF with the lysosomal disruptive agent MOM (methionine *O*-methyl ester). A: Ratio of platinum amount in MOM-treated fractions and platinum amount in control fractions, values are protein normalized and divided by the protein normalized platinum amount in whole-cell lysate. B: Ratio of HRP activity in MOM-treated fractions and HRP activity in control fractions, values are protein normalized and divided by the protein normalized HRP activity in whole cell lysate. C: Ratio of percent (of total amount in the cell lysate prior to fractionation) platinum in MOM-treated fractions and percent platinum in control fractions. D: Ratio of percent HRP activity (of total activity in the cell lysate prior to fractionation) in MOM-treated fractions and percent HRP activity in control fractions. Experiments were performed in triplicate and the values are presented as mean ± SD. Significant difference ($p < 0.05$) was seen between fraction 2 and 3 in all cases (A: $p = 0.000$, B: $p = 0.043$, C: $p = 0.025$, D: $p = 0.0354$) using the student's t-test, two-tailed, with unequal variance and a significance level of 0.05. It is not known if the values are normally distributed.) Pt = platinum, prot. = protein, nq = not quantifiable, act. = activity, c = control.

6 Subcellular fraction associated platinum

6.1 Platinum content in subcellular fractions from HeLa cells

Cells were incubated with the platinum complexes cisplatin (60 µM), m4FPtCl$_2$ (15 µM), dl4FPtCl$_2$ (10 µM) and mDAH4FPtCl (15 µM) for two hours. Thereafter, the cells were collected and washed (sections 15.1 and 15.8) and subjected to homogenization and subcellular fractionation (fig. 5.1, section 15.8). The resulting fractions were analyzed for platinum and protein content and these results together with the results from purified cell nuclei and plasma membrane ghosts are shown in figures 6.1-6.3. The data is presented either as platinum amount normalized to protein amount in each fraction divided by the protein normalized platinum amount in the whole cell homogenate (fig. 6.1) or as platinum amount in each fraction expressed as percent of the amount in the whole cell homogenate (fig. 6.2 and 6.3). For cisplatin, platinum amounts in fraction 4 were too low to be quantified (fig. 6.1-6.3).

The complexes display different abilities to accumulate in the cells over time (fig. 6.4) and as a consequence, different initial medium concentrations were used in the experiments (fig. 6.1-6.3). Cisplatin is accumulating slowly and initial medium concentrations lower than 60 µM will result in difficulties in quantifying platinum amounts in fraction 2 and in the whole cell lysate. For m4FPtCl$_2$, a concentration of 15 µM resulted in quantifiable amounts in all fractions. Concentrations above 10 µM for dl4FPtCl$_2$ could not be used due to limitations in solubility (section 4.1). Because of different initial medium concentrations, the platinum amounts in the fractions (fig. 6.1) are normalized to platinum amounts in the whole cell homogenate.

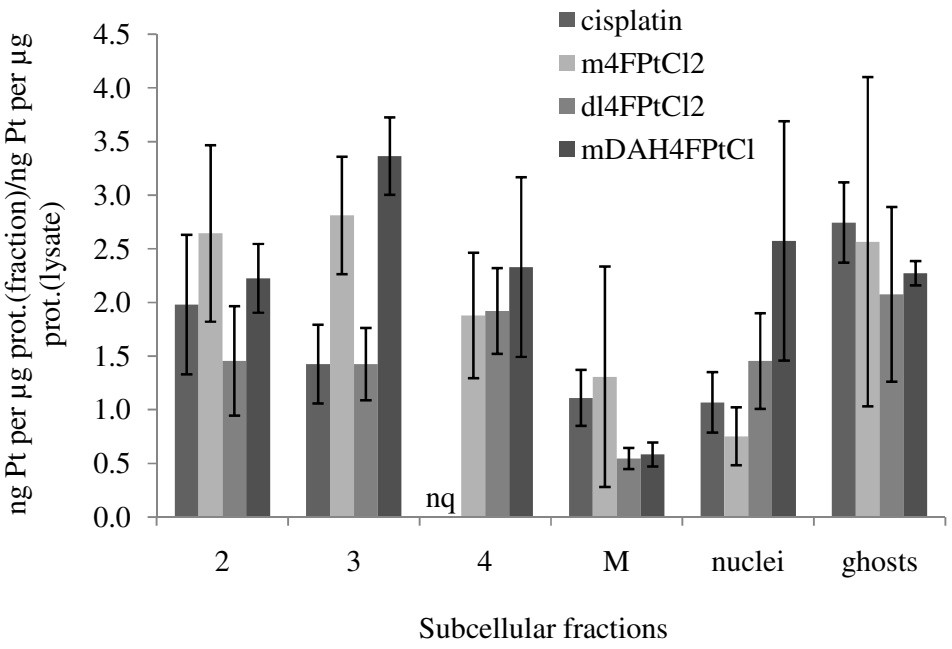

Figure 6.1. Protein normalized platinum amount in fractions 2-4, M, purified HeLa cell nuclei and HeLa plasma membrane ghosts. The cell nuclei and membrane ghosts were purified using separate methods. Results are expressed as ng platinum/µg protein in the fraction divided by ng platinum/µg protein in the lysate. Initial concentrations in culture medium for the respective substances: cisplatin = 60 µM, $m4FPtCl_2$ = 15 µM, $dl4FPtCl_2$ = 10 µM, mDAH4FPtCl = 15 µM. Fractions 2-4 and M represent the fractions shown in fig. 5.1. Experiments were performed in triplicates with exception for data from cisplatin associated with fraction 2 (duplicate). HeLa cell membrane ghost associated platinum was determined twice for all complexes except for $m4FPtCl_2$, which was measured five times. The values are presented as mean ± SD (for all duplicate measurements, the values are expressed as mean ± range). When using the student's t-test (two-tailed, unpaired with unequal variance and a significance level of 0.05. It is not known if the samples are normally distributed), no significant difference was seen between the substances in fraction 2. A significant difference between fraction 2 and 3 was found for mDAH4FPtCl, but not for $m4FPtCl_2$. For the nuclei fraction, significant differences were seen between mDAH4FPtCl and cisplatin and mDAH4FPtCl and $m4FPtCl_2$ respectively. Pt = platinum, prot. = protein, nq = not quantifiable.

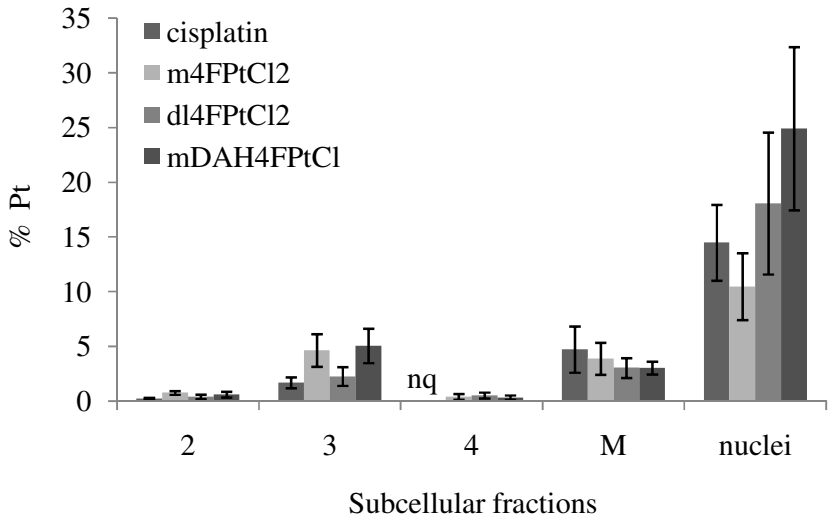

Figure 6.2. Percent platinum in the fractions 2-4, M and cell nuclei of total amount in lysate. Initial concentrations in culture medium for the respective substances: cisplatin = 60 µM, m4FPtCl$_2$ = 15 µM, dl4FPtCl$_2$ = 10 µM, mDAH4FPtCl = 15 µM. Fractions 2-4 and M represent fractions shown in fig. 5.1. Experiments were performed in triplicates (duplicate for cisplatin in fraction 2) and the values are presented as mean ± SD (mean ± range for duplicates). The cell nuclei were purified using a separate method. Pt = platinum, nq = not quantifiable.

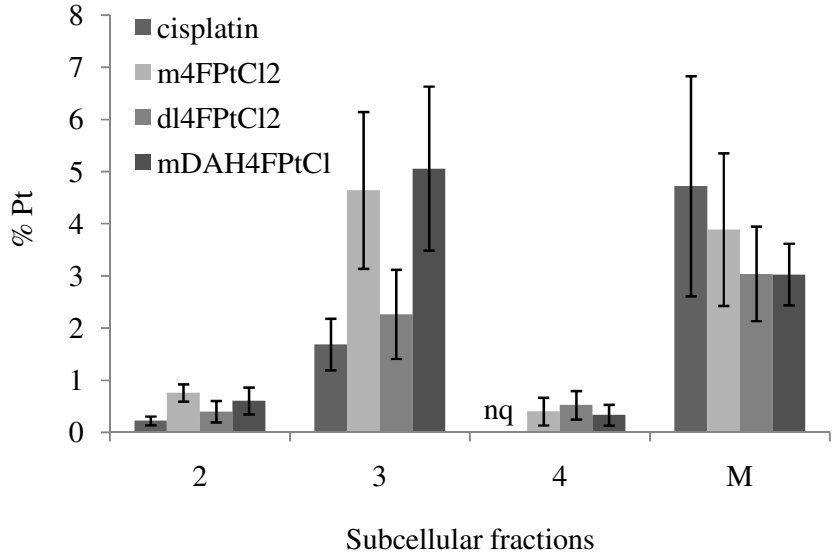

Figure 6.3. Percent platinum in the fractions 2-4 and M of total amount in lysate. Initial concentrations in culture medium for the respective substances: cisplatin = 60 µM, m4FPtCl$_2$ = 15 µM, dl4FPtCl$_2$ = 10 µM, mDAH4FPtCl = 15 µM. Fractions 2-4 and M represent fractions presented in fig. 5.1. Experiments were performed in triplicate (duplicate for cisplatin in fraction 2) and the values are presented as mean ± SD (mean ± range for duplicates). Pt = platinum, nq = not quantifiable.

6.1.1 Quantities of platinum complexes in fractions 2-4, fraction M and nuclei

For mDAH4FPtCl, the difference between fraction 3 and M is about six-fold and is the highest seen amongst the tested platinum complexes (fig. 6.1). The highest percents of platinum for all complexes were found in fractions 3, M and purified nuclei (fig. 6.2-6.3). Those were the fractions containing the highest amount of protein. Even though fully intact, nuclei cannot completely retain molecules, metabolites and medium size macromolecules because of diffusion pores in the nuclear double membrane (*164-165*). Platinum complexes, free or bound to macromolecules, can diffuse out of the nuclei during the purification procedure even if the organelle is relatively undamaged. It is therefore assumed that the platinum content obtained in the nuclei fraction is an underestimation of the content present in the nuclei of whole cells.

6.1.2 Platinum quantification in a HeLa cell plasma membrane fraction

The measurements of platinum bound to plasma membrane ghosts suffered high deviations when m4FPtCl$_2$ or dl4FPtCl$_2$ were tested (fig. 6.1). On the other hand, for cisplatin and mDAH4FPtCl, the deviations were smaller. From the results of the concentration-dependent uptake measurements (fig. 10.1), it is postulated that m4FPtCl$_2$ and dl4FPtCl$_2$ interact more strongly with the plasma membrane lipids than the other complexes. All subsequent steps in the membrane ghost purification after removal of the substance containing culture medium is favoring diffusion out of the membrane for the complexes residing there in a non-covalent manner. Thus, for those complexes whose interaction with (or retention by) the plasma membrane to a greater extent relies on non-covalent incorporation in the lipid bilayer, plasma membrane associated platinum amounts are expected to be more easily influenced by inter-experimental fluctuations (i.e. in overall duration of and temperatures during purification) than for those covalently associated with the membrane e.g. bound to membrane proteins. It is therefore believed that the measured platinum in the ghost preparations of cells incubated with cisplatin and mDAH4FPtCl is mainly protein bound. The platinum measured for m4FPtCl$_2$ and dl4FPtCl$_2$ might be the combined result of covalent interactions with membrane proteins and incorporation in the bilayer which gives rise to the higher inter-experimental deviations seen for those complexes compared to cisplatin and mDAH4FPtCl (fig. 6.1).

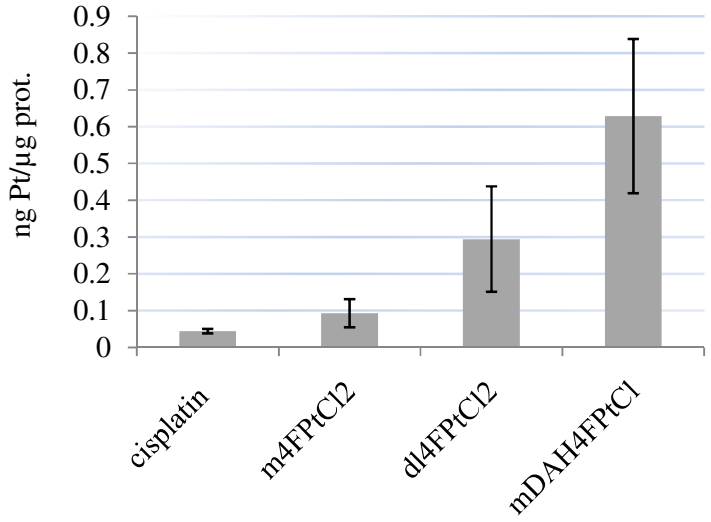

Figure 6.4. Platinum present in HeLa whole cell lysate after 2 h incubation with platinum complexes. Initial concentrations in culture medium for the respective substances: cisplatin = 60 µM, $m4FPtCl_2$ = 15 µM, $dl4FPtCl_2$ = 10 µM, mDAH4FPtCl = 15 µM. Values are presented as mean ± SD from at least three independent experiments. Note that mDAH4FPtCl contains two platinum atoms and that the whole cell accumulated amount is 50 % lower if expressed in moles and not significantly different from $dl4FPtCl_2$. Significant differences are seen between $m4FPtCl_2$ and mDAH4FPtCl, taking into account the two platinum atoms in mDAH4FPtCl ($p = 0.0073$) and between cisplatin and $m4FPtCl_2$ ($p = 0.008$) using the student's t-test (two-tailed, unpaired with unequal variance and a significance level of 0.05. It is not known if the samples are normally distributed). No statistical significance was seen between $m4FPtCl_2$ and $dl4FPtCl_2$ ($p = 0.1315$) and between $dl4FPtCl_2$ and mDAH4FPtCl ($p = 0.8467$). Pt = platinum, prot. = protein.

6.2 Recovery of $m4FPtCl_2$ in the pooled material from the subcellular fractionation procedure

Two independent experiments were made with $m4FPtCl_2$ for which all fractions along the fractionation procedure were saved. These include the intact cells and nuclei that were separated from the whole cell lysate in the first and second centrifugation step and the supernatant of the second wash of the LMF and the material remaining in the density gradient (see fig. 5.1) after collection of the material at the density layer interfaces (fractions 2-4). Because of incompatibility of the platinum measurements with sucrose and the iodixanol gradient medium, the material remaining in the density gradient had to be collected using ultracentrifugation after dilution with PBS. The platinum in the resulting supernatant could not be quantified. Surprisingly, only 54.1 ± 1.4 % were found in all fractions together. The loss of complex might be explained by

the breakage of organelles during cell lysis, i.e. if the released platinum bound components are too light to be collected in the LMF and/or M pellets (fig. 5.1). Another possible explanation might be the binding to cytosolic components. Sharma et al. (*166*) reported that ~ 70 % of platinum found in rat liver- and kidney cells 24 h after intraperitoneal administration of cisplatin was present in the cytosol. Zayed et al (*167*) reported that ~ 70 % of the cell associated platinum was found in the cytosol after 1 h of incubation of the human lung cancer cell line A549 with cisplatin.

6.3 Mitochondrial DNA and platinum complexes

Mitochondria seem to hold an important position in mediating cisplatin toxicity. Qian et al. (*168*) reported a correlation between cisplatin induced toxicity and mitochondrial density in intestinal cells. This toxicity was lowered in cells which were depleted of mtDNA, as was seen in a tryphan blue viability test. Mitochondrial DNA (mtDNA) lacks excision repair mechanisms (*169-170*) and is therefore believed to be more susceptible to the attack of platinum complexes than genomic DNA (gDNA). In the present work, the binding of the platinum complexes to mtDNA and gDNA was investigated to see if they are capable of entering the mitochondria and binding to their DNA.

6.3.1 Platinum associated with mitochondrial and nuclear DNA purified from HeLa cells

HeLa cells were incubated with cisplatin, m4FPtCl$_2$, dl4FPtCl$_2$ and mDAH4FPtCl for 24 h and platinum was measured in the collected mtDNA and gDNA. All complexes were shown to be associated with the mtDNA purified in the present work (fig. 6.5). No obvious difference in binding to mtDNA and/or gDNA was seen between cisplatin and m4FPtCl$_2$ which were added to the cells in the same concentration. Cisplatin is poorly accumulated in the cells compared to m4FPtCl$_2$ but manages to bind to mtDNA to the same extent. No major preferences could be seen for the complexes regarding mtDNA or gDNA. Only a very small preference of m4FPtCl$_2$ and dl4FPtCl$_2$ towards gDNA could be seen (fig. 6.5). In previous works, using MCF-7 cells and an incubation time of 24 h, the complexes m4FPtCl$_2$, dl4FPtCl$_2$ and cisplatin displayed accumulation grades (concentration in cells/concentration in culture medium at incubation start) of ~ 26, ~ 103 and ~ 3.6 respectively (*85*).

The possibility that intact complexes enter broken mitochondria after whole cell lysis cannot be ruled out. Lindauer et al. (*105*) found that even after 24 h of incubation, MCF-7 cells incubated with cisplatin and two other platinum complexes still contained platinum species capable of binding to calf thymus DNA. Cisplatin bound to methionine, as free amino acid or as part of a protein, can still react with DNA as the N7 in guanine (see fig. 1.4) is capable of replacing the platinum thioether bond (*171*). This has not been seen for glutathione or cysteine-bound cisplatin (*172*). Andrews et al. (*62*) found that after 1 h of incubation of cells with cisplatin, 10-11 % of the cell-associated platinum in the human ovarian carcinoma cell line 2008 was intact, non-reacted complex. This is probably an underestimation because of the relatively long time of presence of the complex in the whole cell lysate prior to analysis (*62*).

6.3.2 Comparability of results regarding DNA associated platinum

It is difficult to directly compare the results of the complexes considering their different cell growth inhibiting properties. Because of the low yield of mtDNA obtained with the purification method used in the present work (~ 20-30 µg), cells had to be incubated with substance for 24 h. Cisplatin and m4FPtCl$_2$ were present at 10 µM and after 24 h, some of the cells showed signs of toxicity, such as detachment from the flask surface. Most cells were dead after incubation with 10 µM of dl4FPtCl$_2$. Therefore, a concentration of 2.5 µM was used instead. This concentration also did not leave the cells unaffected but lower concentrations were believed to give rise to quantification problems. This toxicity was not expected for dl4FPtCl$_2$ since it showed comparable toxicity with cisplatin in the CVS assay (table 4.2). This can be explained by the use of culture medium lacking FBS during the uptake measurements and the use of FBS supplemented culture medium in the CVS assay. As investigated in previous works (*85*), dl4FPtCl$_2$ displays higher HSA binding (~ 80 %) than cisplatin does (~ 25 %). The cells incubated with the bivalent complex (mDAH4FPtCl) kept on growing during the 24 h of incubation. This led to a dilution of the complex in the biological material and an underestimation of the DNA-bound platinum.

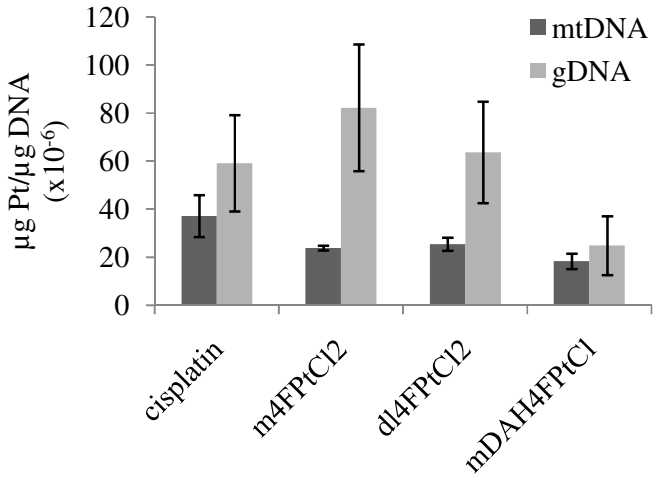

Figure 6.5. Binding of platinum complexes to mitochondrial and genomic DNA. HeLa cells were incubated 24 h with cisplatin (10 µM), m4FPtCl$_2$ (10 µM), dl4FPtCl$_2$ (2.5 µM) and mDAH4FPtCl (10 µM). The mitochondrial DNA (mtDNA) and the genomic DNA (gDNA) were collected, in which platinum and DNA amounts were determined using FAAS and UV-spectrometry respectively. The DNA associated platinum amount is expressed in µg per µg DNA. Pt = platinum.

6.3.3 Association of cisplatin with mtDNA and gDNA: Comparison of the results in the present work with results from the literature

Yang et al. (*152*) measured the platinum content of mtDNA and gDNA after 1 and 2 h of incubation of two head and neck squamous cell carcinoma cell lines (PCI-13 and PCI-15) with 50 µM cisplatin. They found at least 150 times more platinum in mtDNA compared to gDNA which is a strong preference of cisplatin to mtDNA. In the present work, incubations with 60 µM cisplatin for 2 h did not result in quantifiable amounts of platinum, neither for mtDNA nor for gDNA (results not shown). Substantial amounts of mitochondria are probably lost to the pellet during the extensive removal of nuclei. In the present work, cells incubated for 24 h with 10 µM cisplatin resulted in quantifiable amounts of mtDNA bound platinum. Surprisingly for cisplatin, only 0.65 ± 0.07 times more platinum was found in the mtDNA than in the gDNA (fig. 6.5). The quantification of mtDNA and gDNA was performed differently by Yang et al. (*152*). They quantified the gDNA by measuring the absorbance at 260 nm whereas the mtDNA was quantified using a high-sensitive agarose gel. The digested (*Hind* III) fragments of the purified mtDNA were compared with bands of known size and concentration from a DNA marker. The amount of gDNA associated platinum in the present study was about half the value found by Yang et al. (*152*). The

amount of platinum associated mtDNA was about 145 times higher in the work of Yang et al. than in the present work. Other studies investigating the binding of cisplatin to mtDNA and gDNA report somewhat lower preferences towards mtDNA. Giurgiovich et al. (*173*) investigated the binding of cisplatin to mtDNA and gDNA in different organs of fetuses and mothers after intraperitoneal doses of cisplatin in pregnant rats, killed 24 h later. The ratios of platinum bound mtDNA to platinum bound gDNA in the different organs ranged from 0.5 to 18, depending on the tissue. Olivero et al. (*174*) investigated the preference of cisplatin for mtDNA over gDNA in chinese hamster ovary cells where the cells were incubated for 24 h with 50 μM cisplatin and an average ratio of ~ 6 was reported.

In the present work, it was seen that a simple ethanol precipitation is probably not sufficient for separating digested RNA fragments from the DNA (section 5.9.2). Thus, a method detecting the platinum amount from selected bands in the agarose gel would be ideal. The results presented in fig. 6.5 suggest that the complexes tested in the present study are capable of delivering platinum species to the mtDNA. It is not known if the platinum complexes are bound to bionucleophiles when entering the organelle and to what extent these species are capable of reacting with the nucleobases. It is therefore not feasible to use information about the mtDNA associated amounts of these complexes to draw conclusions about their ability to enter mitochondria.

7 Optimization of a horseradish peroxidase activity assay

The enzyme horseradish peroxidase (HRP) is taken up by cells endocytotically (section 8.1). In the present work, the subcellular distributions of HRP and that of the platinum complexes were compared (section 8.1). HRP was also employed as positive control for inhibition of fluid-phase endocytosis (fig. 9.1). HRP can be detected indirectly, in its capacity of a peroxidase, using a substrate (see below). Since the activity of an enzyme is susceptible to its chemical environment, optimization of assay conditions needs to be conducted.

7.1 Quantification of horseradish peroxidase

In the present study, the quantification of HRP was done by determining its activity using a modified method of Steinman et al. (*175*). In the presence of H_2O_2, HRP oxidizes the substrate *o*-dianisidine which forms a dimeric compound through intermediates (*176*). This compound has a different UV-absorption maximum (~453-475 nm (*176*)) than the substrate. The absorption of the product is plotted against time and the slope of the linear part of the curve used as a measure for enzyme activity. The steepness of the slope is proportional to the enzyme concentration. In the present work, the absorption was measured at 460 nm.

7.2 Investigation and optimization of the horseradish peroxidase activity assay

7.2.1 Freezing of samples

Dehydration and up-concentration of solutes and ions at slow freezing rates might have adverse affects on enzyme activity. The fractions resulting from the density gradient centrifugation (see fig. 5.1) differ in protein concentrations and offer protection to different extents to HRP during freezing (*177*). Thus, if the samples are not frozen fast enough, comparability between different fractions might be compromised. In the present work, the suspensions were always frozen in liquid nitrogen before storage at -20 °C if not assayed directly.

7.2.2 Threat of proteolytic enzymes in whole cell lysate

In whole cell lysates and subcellular fractions, there is a threat on HRP by proteases. To test the susceptibility for proteolytic breakdown in whole cell lysate, the enzyme

was incubated with HeLa cells (2 h) that were subsequently collected and lysed in RSB (sonotrode). The HRP activity was assayed after incubation of the lysate on ice or at room temperature and shock frozen after different incubation times. An aliquot of the lysate was directly frozen after lysis (control). No loss in activity could be seen after 24 h of incubation (fig. 7.1). In the literature, only very slow degradation of HRP in living cells has been reported (*178-179*).

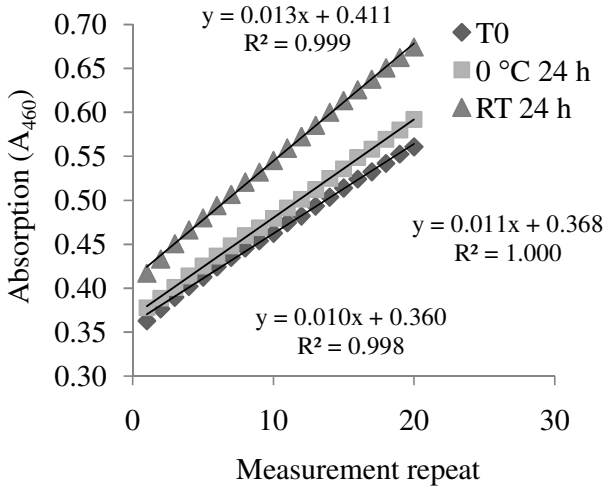

Figure 7.1. Activity of horseradish peroxidase after incubation with HeLa cell homogenate. Cells were lysed after incubation with HRP, subjected to ultrasound lysis (in RSB) and thereafter immediately frozen in liquid nitrogen (T0) or stored for 24 h at either room temperature (RT 24 h) or 0 °C (0 °C 24 h) prior to the enzyme assay. One measurement repeat corresponds to approximately 12 s.

7.2.3 Effect of pH on HRP activity

To test the pH in which the enzyme displays the highest activity, a solution of HRP was added to assay solutions differing in pH and the highest activity was seen for pH 4 (fig. 7.2).

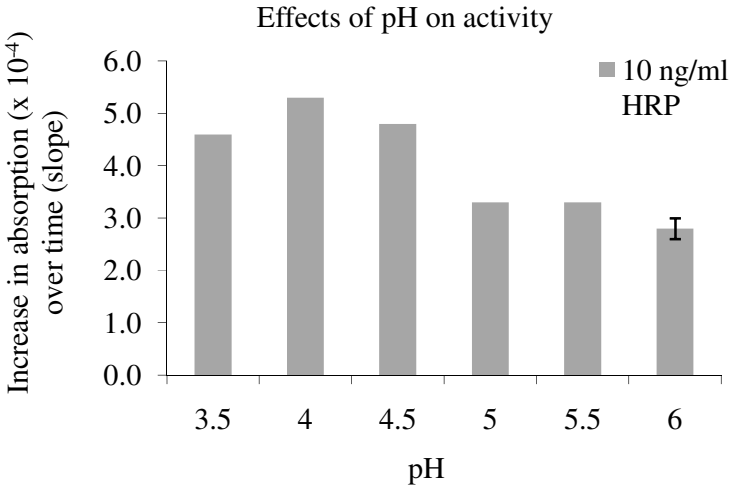

Figure 7.2. Effect of assay solution pH on horseradish peroxidase activity. A solution of 100 ng/ml enzyme was diluted by 1/10 with KH_2PO_4 buffer solutions with different pH. The assay was initiated after a few minutes of incubation at room temperature. Values are from two independent measurements with the same enzyme stock solution but freshly prepared buffer solutions. The enzyme activity is expressed as the (linear) increase in absorption at 460 nm over time. Error bars are seemingly absent where the range is narrow.

7.2.4 Effect of fractionation buffer solutions on HRP activity

The effect of solutions included in the fractionation procedure on HRP activity was investigated (fig. 7.3). HRP was added to the solutions and the activity measured after 6 h of incubation at room temperature. None of the tested solutions altered the activity of HRP.

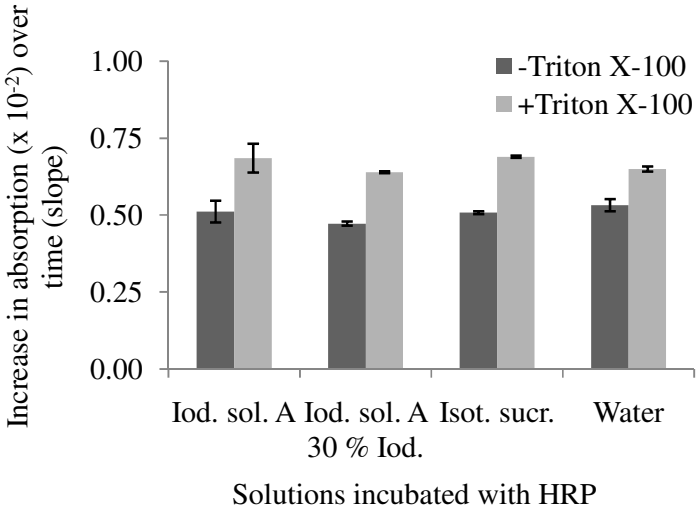

Figure 7.3. Effect of solutions used during the fractionation procedure on HRP activity. HRP (10 ng/ml) was incubated for 6 h with solutions used in the subcellular fractionation and the activity was measured. Values are from two independent experiments with the same enzyme stock solution but freshly prepared test solutions and are expressed as mean ± range. The enzyme activity is expressed as the (linear) increase in absorption at 460 nm over time. Iod. sol. A = Iodixanol solution A (section 16), Iod. sol. A 30 % Iod. = Iodixanol solution A with 30 % Iodixanol, Isot. sucr. = Isotonic sucrose.

7.2.5 Effect of Triton X-100 on HRP activity

In this work, Triton X-100 was shown to increase the linearity and sensitivity of the assay (fig. 7.4). This has also has been reported by Porstmann et al. (*180*) which refer to this as being a consequence of delayed inactivation of HRP by H_2O_2. Gallati et al. report that the higher the H_2O_2 concentration, the shorter the useful reaction time regarding linearity (*181*).

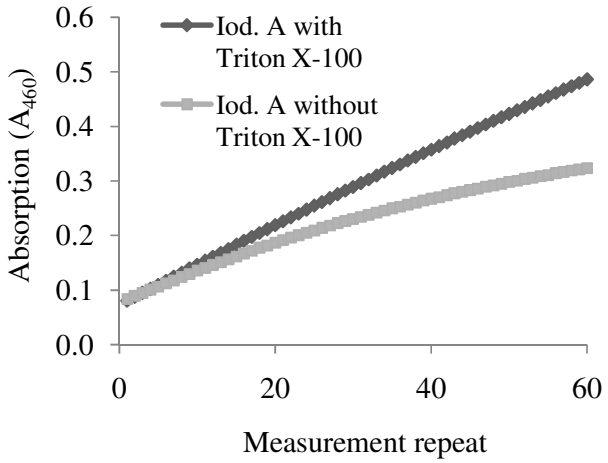

Figure 7.4. Influence of Triton X-100 on the linearity of HRP catalyzed oxidation of *o*-dianisidine. One measurement repeat corresponds to ~ 20 s. Iod. A = Iodixanol solution A (section 16).

Although an increase in linearity is seen for HRP activity in the presence of Triton X-100, this surfactant is affecting the activity of the enzyme negatively so it has to be introduced as late as possible. In the present work, Triton X-100 was present in the buffer that was added to the samples to initialize the assay. If Triton X-100 is added to stabilize the samples some time before starting the assay, the enzyme activity is lowered (fig. 7.5). It is therefore better, not to stabilize the samples and to have their first encounter with the tenside when mixed with the assay solution. Eremin et al. (*182*) report that Triton X-100 alter the secondary structure of HRP.

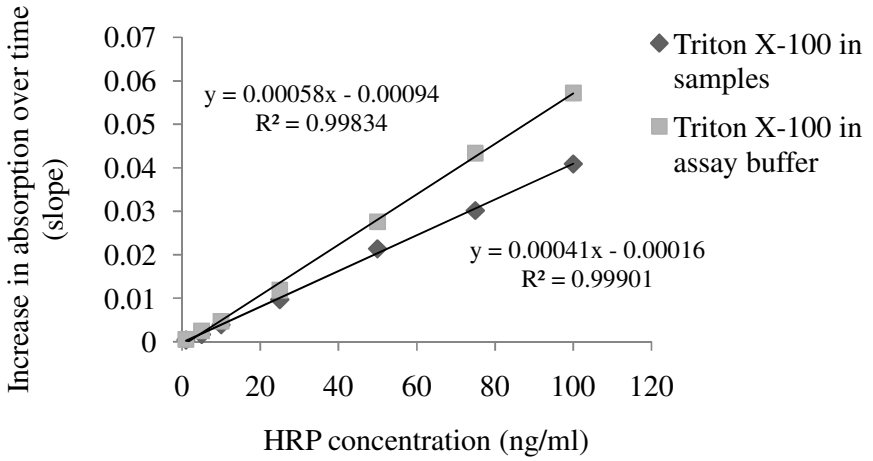

Figure 7.5. Difference in sensitivity of the HRP activity assay if Triton X-100 is added to the samples or to the HRP assay solution prior to assay begin. The enzyme activity is expressed as the (linear) increase in absorption at 460 nm over time.

7.2.6 Linearity of the HRP activity assay

The assay was linear over a wide concentration range (fig. 7.6). The detection limit (calculated on a 3 σ basis) was 0.45 ng/ml and the quantification limit (calculated as 5 x the detection limit) was 2.25 ng/ml.

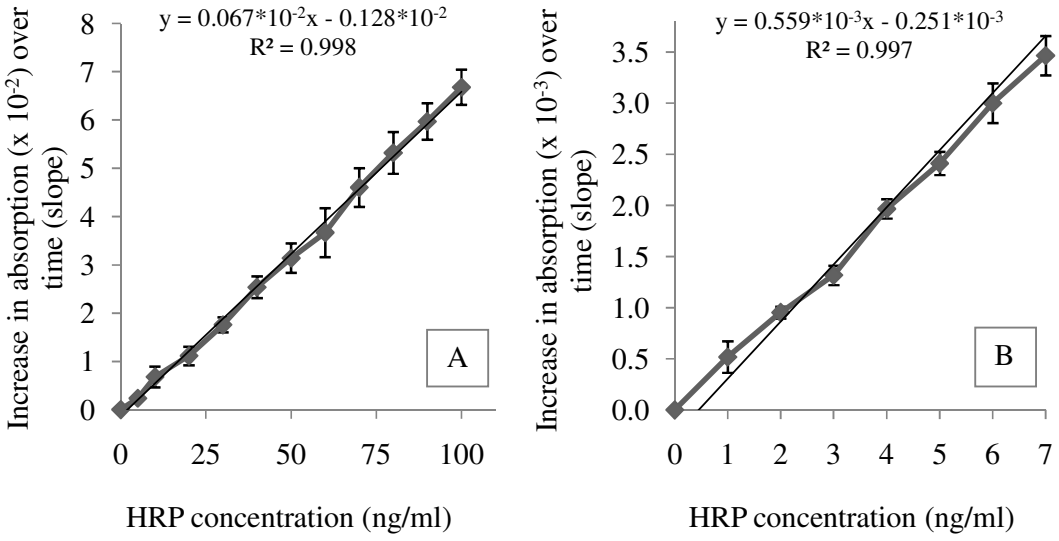

Figure 7.6. Linearity of the HRP activity assay. A: Linearity of concentrations in the range 0-100 ng/ml. B: Linearity of concentrations in the range 0-20 ng/ml. The HRP concentration (x-axis) is the concentration in the sample that is being added to the HRP assay solution. Standard deviations are calculated from three individually diluted and measured standard curves from one stock solution of enzyme and values are expressed as mean ± SD. The enzyme activity is expressed as the (linear) increase in absorption at 460 nm over time.

8 Horseradish peroxidase distribution in subcellular fractions

8.1 Subcellular distribution of HRP

Horseradish peroxidase has long been used as a pinocytotic marker (*179, 183*) and accumulates in endocytotic compartments, (*163*) such as lysosomes (*175, 184-185*). HRP cannot cross the cell membrane by diffusion and has to use fluid-phase endocytosis to enter the cells. In the present work, the subcellular distribution of HRP was investigated using the same fractionation method as employed for the platinum complexes (fig. 5.1). The cells were incubated with the enzyme at a concentration of 0.1 mg/ml and the incubation time was the same as for the platinum complexes, i.e. 2 h. The activity in fraction 4 was below the quantification limit (section 7.2.6) and therefore not shown (fig. 8.1). This fraction contains little lysosomal marker (LAMP1) relative to protein amount (fig. 5.3).

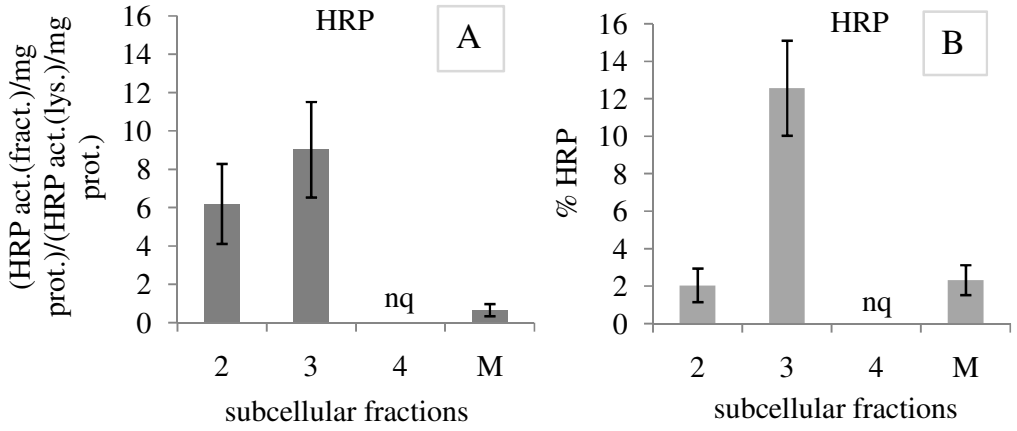

Figure 8.1. Subcellular fractionation of HeLa cells incubated with HRP. A: Protein normalized HRP activity in fractions 2-4 and M (fig. 5.1) divided by protein normalized HRP activity in whole cell lysate. B: HRP activity expressed as percent of the total amount in the whole cell lysate. Values are expressed as mean ± SD of at least four independent tests. No significant difference was seen between fraction 2 and 3 in A ($p = 0.133$) (student's t-test, two-tailed, unpaired with unequal variance and a significance level of 0.05. It is not known if the samples are normally distributed). The data shown is the control from the experiment described in section 5.10.1. act. = activity, fract. = fraction, prot. = protein, lys = lysate, nq = not quantifiable.

Fraction M contains some lysosomal marker (fig. 5.3) which can explain the presence of HRP. Compared to the distribution of the platinum complexes (fig. 6.3), higher percents (about twofold) of the enzyme were found in fractions 2 and 3 but not in fraction M (fig. 8.1B). This is also true for the protein normalized activity (fig. 8.1A) where higher preference for fractions 2 and 3 was found for HRP than for the platinum complexes (fig. 6.1).

The total amount of enzyme in all fractions presented in fig. 8.1 was only about 15-20 % of the amount in the whole cell lysate prior to fractionation. HRP is expected to be primarily located in endocytotic vesicles. Storrie et al. (*184*) mention that HRP is easily released from lysosomes upon mechanical shear and/or hypotonic lysis. Schröter et al. have successfully separated lysosomes from endosomes taking advantage of their different osmotic properties and the lysis of lysosomes upon subjection to osmotic stress (hypotonic conditions) (*186*). Except for damage through osmotic stress, homogenization and frequent re-suspensions, material might also be lost with the nuclei-pellet (fig. 5.1) (co-sedimentation of other organelles with the nuclei). Results from the experiment using the lysotropic dipeptide MOM (see section 5.10.1) indicate that the enzyme might be subjected to digestion.

9 Involvement of endocytosis in whole cell accumulation of platinum complexes

9.1 Fluid-phase endocytosis pathways and inhibitor substances

Endocytosis is part of the complicated membrane vesicle formation and transport system present in more or less all mammalian cells. The endocytotic machinery is responsible for specific- and unspecific uptake of surrounding fluid. Specific uptake is initiated when a ligand, e.g. a protein, binds to a receptor in the plasma membrane. On the other hand, unspecific uptake is not dependent on cargo-receptor interactions for vesicle initiation. In previous works, it was shown that the accumulation of the bivalent platinum complex mDAH4FPtDMSO (similar to mDAH4FPtCl (fig. 1.7) but with DMSO as leaving groups instead of Cl^-) in MCF-7 cells was inhibited by substances inhibiting macropinocytosis (*187*). In the present work, it was investigated if this is true also for the complexes cisplatin, m4FPtCl_2 and mDAH4FPtCl. The same endocytotic pathways (macropinocytosis and clathrin- and caveolae-mediated endocytosis) were tested for uptake involvement, as in the work of Kapp et al. 2006 (*187*). These pathways all occur in HeLa cells (*188-189*) but caveolin-dependent endocytosis has been reported to be low in this cell line (*190*). The mentioned pathways differ in mechanism of initiation, intracellular route and vesicle size (described below).

Macropinocytosis

This endocytotic pathway employs the actin cytoskeleton for the extension of the plasma membrane to the cell exterior followed by fusion to form vesicles. These vesicles, macropinosomes, are filled with fluid from the cell surroundings and any molecule present in the fluid can enter the cell by this manner. Using rat macrophages, visual proof of this phenomenon was first published by Lewis (*191*) already in the Thirties and he also confirmed the occurrence of this process in three cultured rat carcinoma cell lines (*192*) and rat fibroblasts (*191*). The vesicles formed during macropinocytosis are heterogeneous in size but the majority are about 1 µM in diameter (*193*). The formation of vesicles is not receptor mediated but subjected to regulation. Macropinocytosis is stimulated by growth factors such as EGF (*193*), as has been shown in HeLa cells (*188*). For immature dendritic cells, this process is

constitutive (*194-195*). Some known inhibitors of macropinocytosis are cytochalasins such as cytochalasin B and D. The effects on the actin cytoskeleton after treatment with cytochalasins are known since long. Cytochalasin B has been shown to induce disappearance of actin filaments (*196*) and cell ruffling (*197*). Later, both cytochalasin B and D were shown to slow down actin polymerization (*198-199*). The importance of actin polymerization in fluid-phase endocytosis has been demonstrated and cytochalasin D inhibited the uptake of the fluid-phase marker Lucifer yellow in yeast cells (*200*). Amiloride and its analogues inhibit the Na^+/H^+-exchanger and causes a pH decrease close to the plasma membrane leading to inhibition of the signaling needed for vesicle initiation (*201*). In this work, the more potent analogue of amiloride, EIPA (5-(*N*-ethyl-*N*-isopropyl)-amiloride), was employed.

Clathrin-mediated endocytosis

Clathrin mediated endocytosis employ vesicles that are ~ 100 nm in diameter (*202-204*) for cargo transport. This pathway is specific and the molecule to be transported binds to its receptor which initiates the formation of "coated pits" in the plasma membrane. The coating consists of the protein clathrin and adaptor proteins which assemble after ligand binding and give rise to membrane curvature. This curvature is directed inwards and increases until that part of the membrane buds off as a coated vesicle (*205*). This pathway is important for the cellular uptake of LDL (low-density lipoprotein) and transferrin (*206-208*) from the blood stream. Labeled LDL has been shown to bind to patches in the cell membrane, identified as coated pits, and is thereafter internalized by a coated vesicle (*209*). The major protein of these coated vesicles was identified by Pearse (*210*) and given the name "Clathrin". Chlorpromazine has been shown to inhibit clathrin-mediated uptake (*203*) and causes re-localization of clathrin from the cell surface, thereby inhibiting endocytosis (*211*).

Caveolin-mediated endocytosis

With diameters of 50-100 nm (*212-214*), the vesicles resulting from the initiation of this endocytotic pathway are similar in size to clathrin-coated vesicles but there are many important differences. The definition of caveolae (vesicle of this pathway) is somewhat complicated. A review by Anderson (*214*) describes several ways of identifying a caveolae. It is not always the mere presence of caveolin, a protein found in many caveolae (*215*), that will guide the identification of these vesicles but the special membrane composition that result in low buoyant density compared to other membranous compartments in the cell (*216*). Caveolae are resistant to solubilization by Triton X-100 (*217*). This endocytotic pathway is specific and responsible for the cellular uptake of the vitamin folate (*218-224*) and several membrane receptors, transporters and signal transducers have been shown to be enriched in caveolae (reviewed by Anderson 1998 (*214*)). The high cholesterol content of caveolae is utilized when inhibiting their formation. Substances that sequester the steroid can hinder the formation of "lipid rafts", patches in the plasma membrane serving as vesicle-forming platforms (*223*). Macrolide antibiotics, such as nystatin, partitions into the plasma membrane (*225*) and interact with cholesterol (*226*) resulting in lipid raft disruption (*215, 223*) and impairment of endocytotic transport (*227*). Other cholesterol binding agents such as methyl-ß-cyclodextrin are often employed for inhibition. This substance has been reported not to exclusively impair caveolae-mediated endocytosis (*228*) and for this reason, only nystatin was used in the present study.

9.2 Intracellular fate of internalized vesicles, presentation of results from the literature

The route of uptake might explain eventual differences in subcellular distribution. In NIH3T3 cells, Khalil et al. (*229*) observed that cargo transported with macropinocytosis avoided lysosomal degradation in contrast to cargo transported with clathrin-coated vesicles. Also in A431 cells, macropinocytosed material was not directed to lysosomes (*193*) but was found later in the cytosol (*230*). In macrophages, macropinocytotic vesicles were shown to fuse with lysosomes (*231*). In HeLa cells, on the contrary, caveolin dependent endocytosis has been reported to protect against lysosomal fusion (*189*). Thus, the engulfed material reaches different post-endocytotic destinations depending on the internalization mechanism and cell type.

9.3 Tolerability of HeLa cells against inhibitors

Prior to uptake measurements, the tolerability of the cells against different inhibitors was elucidated. HeLa cells were incubated either with 25-100 µM EIPA or 10-50 µM chlorpromazine for 2.5 h and investigated under the phase contrast microscope. The uptake assay relies on the attachment of the cells to the culture flask surface throughout incubation. Detachment after treatment with substances is therefore unacceptable. The detachment of cells has been reported for both EIPA (*232*) and chlorpromazine (*233*). In the present work, chlorpromazine concentrations of 30 µM and higher were not tolerated and significant amounts of cells were detached. However, a concentration of 25 µM was accepted. For EIPA, concentrations of 100 µM and 75 µM did not give rise to detachment. Cells that were incubated with HRP together with chlorpromazine, nystatin and EIPA displayed markedly increased uptake of the enzyme (results not shown) and large amounts of cells were found detached which indicates that the cells were affected negatively. After cytochalasin D treatment, some cells had a rounded appearance, probably because of a change in cytoskeleton arrangement. However, attachment was sustained. No obvious change in cell morphology was seen after nystatin treatment.

9.4 Result of fluid-phase endocytosis inhibition on whole cell associated platinum

To test whether the platinum complexes enter the cell via one of the main endocytotic routes, (macropinocytosis, clathrin-dependent endocytosis and caveolin-dependent endocytosis) the cells were pre-incubated with inhibitors for these pathways followed by incubation with the complexes together with the inhibitors to sustain inhibition throughout the assay. HRP was used as a control for fluid-phase inhibition.

Whole cell associated platinum was unaffected by endocytosis inhibition (fig. 9.1). However, the uptake of HRP was inhibited up to 50 % by inhibitors of clathrin-dependent endocytosis (chlorpromazine) and macropinocytosis (EIPA, cytochalasin D). Results from previous works (*187*) showed that the cell accumulation of the complex mDAH4FPtDMSO was decreased with ~ 50 % by inhibitors of macropinocytosis. The only difference between mDAH4FPtDMSO and mDAH4FPtCl is the leaving group (DMSO in the former and Cl^- in the latter). The overall charge of mDAH4FPtDMSO is +4 and +2 for mDAH4FPtCl. It is possible that the higher

charge of mDAH4FPtDMSO is not accepted to the same extent by the outer cell membrane.

To make sure that the inhibition of HRP uptake by chlorpromazine is not a method artifact, HRP activity was measured after incubation of the enzyme with 0-100 µM chlorpromazine. No effect on HRP activity could be seen (data not shown). HRP has been found in coated pits of different cell-types (*234-236*). Rothberg et al. (*215*) did not find any co-localization between antibodies directed against caveolin and HRP which supports the failure of nystatin to inhibit HRP uptake in the present study. Thus, a caveolae specific control is needed.

It cannot be ruled out that the complexes enter through pathways other than macropinocytosis and clathrin- and caveolin-dependent endocytosis. There are endocytotically derived vesicles not belonging to any of the mentioned endocytosis pathways (*237*). These vesicles have been shown to contain the protein flottillin-1 and have been seen in HeLa cells, amongst others (*238-239*).

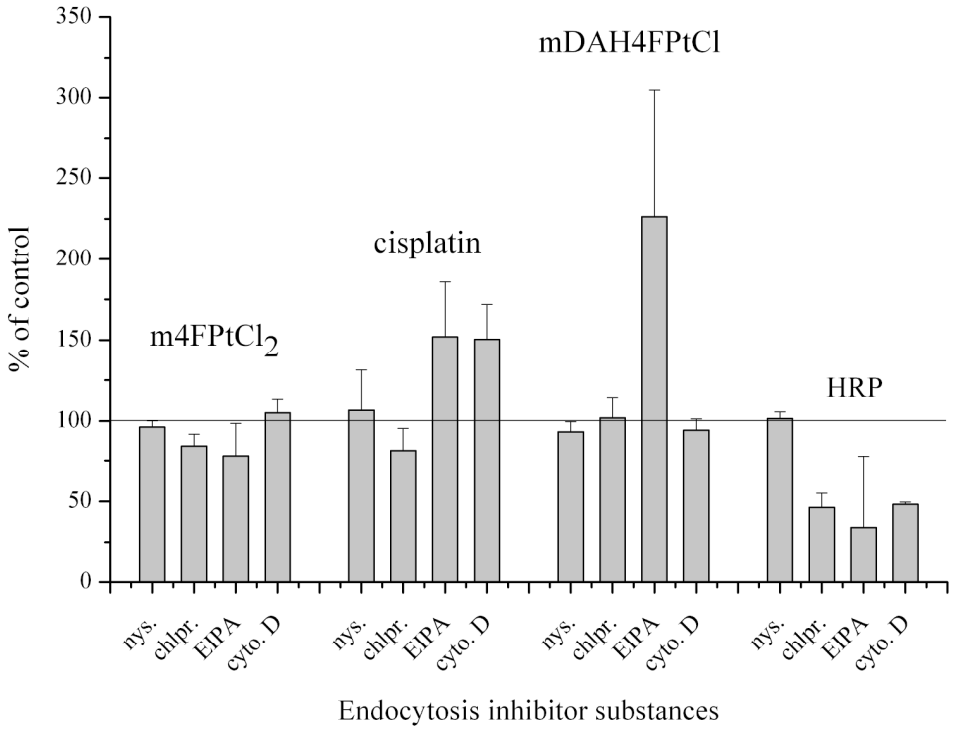

Figure 9.1. Effect of endocytosis inhibitors on HeLa cell platinum and HRP accumulation. Control cells were treated only with solvent (= DMF, 0.1 % (v/v) max). A value of 100 % of control (y-axis) = no effect of inhibitor treatment on platinum/HRP accumulation. Values are expressed as mean ± SD (if $n > 3$, otherwise range) of at least three independent experiments ($n = 2$ for cyto. D). The inhibitors did not cause significant ($p > 0.05$) changes in uptake of the platinum compounds (student's t-test, two-tailed with a significance level of 0.05, unpaired with unequal variance, it is not known if the values are normally distributed). For HRP, only EIPA displayed high SD and the values did not differ significantly ($p > 0.05$) from either 100 % or 50 % of inhibition. nys. (= nystatin, inhibits caveolin-dependent endocytosis), chlpr. (= chlorpromazine, inhibits clathrin-dependent endocytosis), EIPA (= 5-(*N*-ethyl-*N*-isopropyl)-amiloride, inhibits macropinocytosis) and cyto. D (= cytochalasin D, inhibits macropinocytosis).

10 Concentration-dependent whole cell platinum accumulation

The concentration-dependent uptake of cisplatin, $m4FPtCl_2$, $dl4FPtCl_2$ and mDAH4FPtCl was investigated in HeLa cells. The incubation time was 2 h and the concentrations ranged from 10-60 µM for all complexes except for $dl4FPtCl_2$ for which the concentrations ranged between 0.5 and 10 µM. The solubility of $dl4FPtCl_2$ (section 4.1) limits the use of higher concentrations. The uptake profiles were linear for cisplatin and mDAH4FPtCl but non-linear for $m4FPtCl_2$ and $dl4FPtCl_2$ (fig. 10.1).

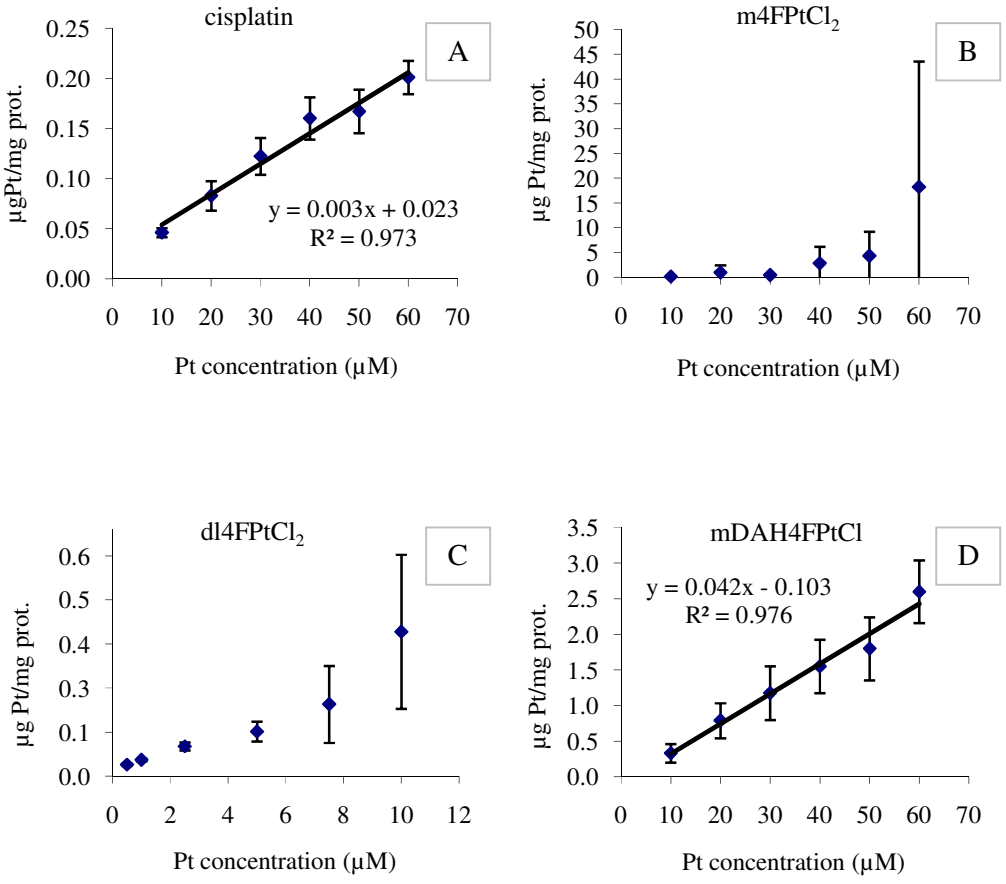

Figure 10.1. Time-dependent uptake profiles of four platinum compounds in HeLa cells. Cisplatin (A) and mDAH4FPtCl (D) exhibit linear concentration dependent uptake but the uptake profiles for $m4FPtCl_2$ (B) and $dl4FPtCl_2$ (C) are not linear. Concentrations range between 10-60 µM with an incubation time of 2 h. For $dl4FPtCl_2$ (C), the concentrations ranged between 0.5-10 µM because of solubility limitations. Values are expressed as mean ± SD from at least three independent experiments for all complexes except for cisplatin where values are expressed as mean ± range. Pt = platinum, prot. = protein.

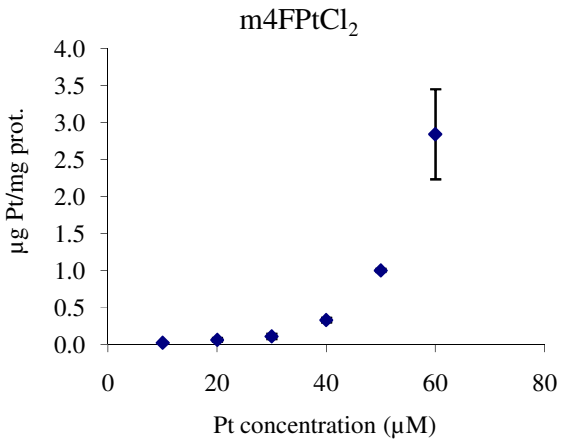

Figure 10.2. Concentration-dependent uptake of $m4FPtCl_2$ in MCF-7 cells. The relationship between concentration and uptake is exponential (R^2 = 0.989). Incubation time was 2 h. Values are expressed as mean ± SD from at least three independent experiments. Pt = platinum, prot. = protein.

A linear concentration-dependent whole cell accumulation has been reported for cisplatin in several cell lines (*62, 65, 240-242*). It is postulated that the non-linear uptake profiles of $m4FPtCl_2$ and $dl4FPtCl_2$ is a result from interactions with membrane lipids. The reason for the high deviations observed for $m4FPtCl_2$ (10.1B) and $dl4FPtCl_2$ (10.1C) is not known. The concentration dependent whole cell uptake profile of $m4FPtCl_2$ in MCF-7 cells (fig. 10.2) follows an exponential trend. A concentration dependent uptake of $m4FPtCl_2$ has been investigated in previous works, using MCF-7 cells (*106*). The uptake was linear up to 10 µM, which was also the highest concentration tested (*106*). When comparing the results from the concentration dependent uptake experiment and the whole cell associated platinum amounts from the subcellular distribution experiments (fig. 6.4), no statistical differences ($p > 0.05$, inter-experimentally) could be seen for any of the complexes except for cisplatin (two tailed student's t-test with 0.05 significance level assuming unequal variance, it is not known if the values are normally distributed). This discrepancy could not be explained.

10.1 On correlating whole cell platinum accumulation with $LogP_{o/w}$

The $LogP_{o/w}$ values of the tested platinum complexes did not differ significantly ($p > 0.05$) when culture medium was employed as aqueous phase (fig. 4.1). This is not in agreement with the cellular accumulation profiles seen for those compounds in the present work (fig. 6.4) as well as in the work of Kapp (*85*). In the present work, a significant ($p = 0.0073$) difference between the whole cell uptake of $m4FPtCl_2$ and

mDAH4FPtCl was seen (fig. 6.4). The difference between whole cell accumulation of $m4FPtCl_2$ and $dl4FPtCl_2$ was not significant in the present work (fig. 6.4) but a significant difference is expected if the initial concentrations of $m4FPtCl_2$ (now 15 µM) and $dl4FPtCl_2$ (now 10 µM) are the same. However, a difference in whole cell accumulated platinum for $m4FPtCl_2$ and $dl4FPtCl_2$ in MCF-7 cells has been reported in previous works (*85*). The difference is more prominent for cell associated platinum over time (*85*). After 2 h of incubation with 5 µM of platinum complex, the accumulation of $dl4FPtCl_2$ was at least one third higher than that of $m4FPtCl_2$ (*85*). In the present study, the substance-containing biphasic (organic and aqueous phase) system was vigorously stirred for 30 s prior to incubation at RT for 2 h but it is not sure that substance equilibrium was achieved before concentration measurements were conducted.

Differences in whole cell associated platinum between the complexes vary with concentration and time. The correlation of $LogP_{o/w}$ values with whole cell platinum accumulation might be better correlated using a model taking both concentration and time into account. This requires that the complexes do not induce changes in the membrane bilayer. Binding to membrane proteins might confound the results. The dry weight of purified HeLa cell plasma membranes is to 55 % made up of protein (*132*). Substances aiming to enter the cells are therefore not encountering a naked lipid bilayer but a lipid/protein mix.

The difference between uptakes for $m4FPtCl_2$ and $dl4FPtCl_2$ might be explained by different alignments in the lipid bilayer. Zou et al. (*243*) found that a higher rate of accumulation of 1,2-cyclohexanediamine platinum(II) complexes in red blood cells was seen for the R,R isomer than for the S,S and R,S isomers. As the differences in accumulation rate between the isomers could not be explained by different binding to sulfhydryl groups in the plasma membrane and/or the ability of the complexes to induce differences in plasma membrane permeability, the authors conclude that the plasma membrane itself is a barrier which favors molecules with a certain conformation (*243*). Bilayer selection might contribute to the lack of correlation of $LogP_{o/w}$ values with whole cell platinum association for the complexes tested in the present work.

11 Transmission electron microscopy of fractions from the subcellular fractionation

Electron microscopy (EM) can be used to visualize structures in the nm scale including cellular components such as organelles. The mitochondrial protein MTCO2, used as marker for the inner mitochondrial membrane, is present in fraction 3 and 4 (fig. 5.3). However, it is not known whether this marker represents an inner membrane that belongs to an intact or broken mitochondrial vesicle in those fractions. EM was employed in the present work to confirm or reject the assumption that the mitochondrial vesicles are broken in the subcellular fractions. Moreover, it was desired to obtain a visual profile of the fractions with respect to other cellular structures and to compare this with the western blot data.

11.1 Choosing pictures

Suitable areas on the holey carbon-coated copper grid (on which the sample is fixed) were chosen for analysis whereas regions with thick layers of sample and aggregated material were avoided. The enlarged pictures, resulting from samples imaged over the holes in the holey carbon film grids (fig. 11.3-11.8), cannot be used alone to profile the fraction because they are a selection of different structures that were found in the fractions. Still, care was taken to prevent selection bias due to the selection and presentation of one type of structures only. Within the framework of this thesis, only a qualitative analysis was preformed. A quantitative analysis requires the recording of more images which was not feasible because of the time consumption and laboriousness of the cryo-EM method.

11.2 Sample preparation and visualization

Two widely used EM methods were employed, negative staining (NS) and cryo-electron microscopy (cryo-EM). The NS analysis was done to confirm that cellular structures are present before continuing to cryo-EM. A negative stain, such as uranyl acetate, brings out shapes and cavities of the material. Uranyl acetate stains nucleic acids, proteins and ribosomes (*244*). Membranous structures are indirectly stained through stain collected around them (*244*). The samples in the present work were stained according to the negative staining carbon film method (*245-246*) without prior fixation. The analysis was done in a transmission electron microscope.

Collapsed structures arise primarily through dehydration at drying on the EM-grid after staining (fig. 11.3-11.5). Thus, cryo-EM was employed to obtain pictures of better preserved structures under conditions present in the sample suspension. The samples are shock-frozen, a process called as cryofixation, to avoid the formation of ice-crystals (*247*). The hydration of the organelles and other cellular structures is not compromised (*248*) and they maintain the shape they had in the suspension before analysis (*249*). In this solid state, they tolerate the vacuum in the electron microscope (*250*) and will not collapse due to dehydration. To maintain vitrification in the electron microscope throughout the analysis, the sample holder is cooled with liquid nitrogen. This technique also allows for the retention of diffusible macromolecules that might get lost during chemical fixation and staining and is therefore considered to be the most gentle method of sample preparation (*127*).

Cryo-EM analyses of unstained biological samples suffer low contrasts because of low signal-to-noise ratios. These samples only tolerate low electron doses and possess weak electron scattering properties. For example, the structure in figure 11.4B has been subjected to 37 e/nm^2 (electrons per square nanometer), whereas the structure shown in figure 11.7B was subjected to 749 e/nm^2. Structures with quite distinct morphology can be compared and recognized as different. Structures similar in size and morphology cannot be distinguished from each other e.g. both peroxisomes and lysosomes appear as spheres with a homogenous matrix[5]. However, the multi-vesicular appearance of some lysosomes might be recognized and distinguished from other structures in the sample.

11.3 Bubbles inside bubbles or bubbles on top of bubbles?

The samples in the present study were not subjected to slicing. A vesicle that seems to contain other vesicles in a micrograph might in fact be material clustered in the visual plane and not a true multi-vesicular structure. Also, multi-lamellar vesicles can arise during the fractionation procedure because of the tendency of biological membranes to vesiculate. An electron micrograph from a sectioned sample containing “true” multi-lamellar structures such as late endosomes is shown in figure 11.1. Multi-lamellar

[5] The term “matrix” is here referring to the compartment enclosed by the limiting membrane.

structures from an artificial membrane system, visualized with cryo-electron tomography, are shown in figure 11.2.

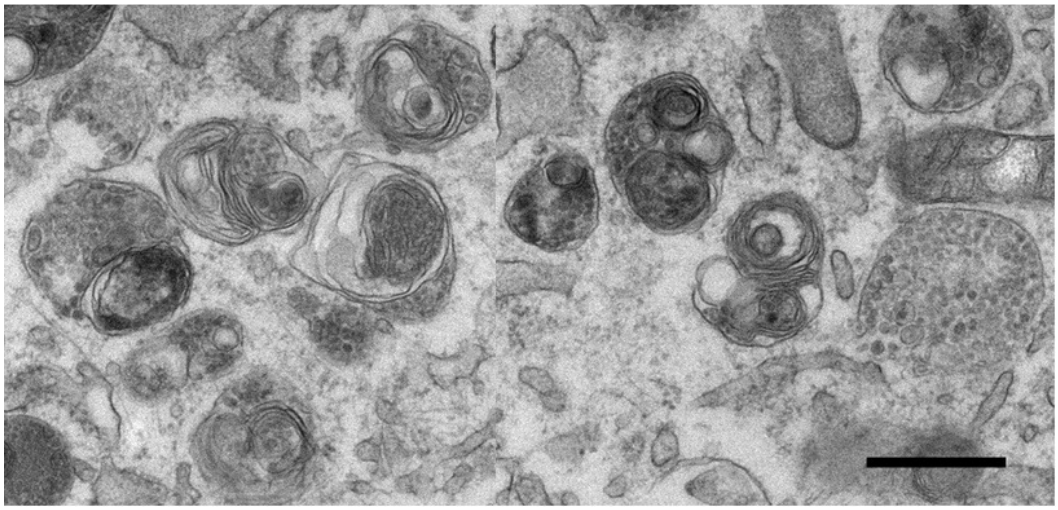

Figure 11.1. Transmission electron microscopy image showing multi-lamellar late endosomes and lysosomes from a stained and sectioned sample. Scale bar = 500 nm. Reproduced and modified with kind permission from Dr. Ian Prior, Biomedical Electron Microscopy Unit, University of Liverpool, picture obtained from: http://pcwww.liv.ac.uk/~emunit/images/endolyso.jpg.

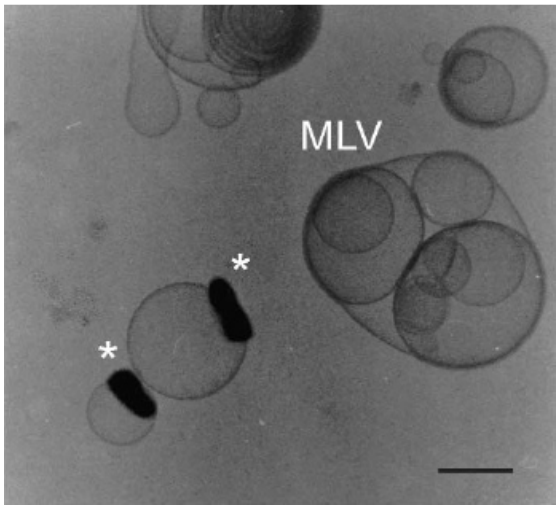

Figure 11.2. Cryo-EM micrograph of multi-lamellar liposomes (labeled as MLV in the picture) consisting of equimolar amounts of dioleyl-phosphatidylserine and dioleyl-phosphatidylcholine. Scale bar = 100 nm. Reprinted by permission from Macmillan Publishers Ltd: [Nature Medicine]((*251*) copyright (2002)).

11.4 Comparing circles with spheres

For the inexperienced eye, the availability of comparative pictures is crucial. In the literature, there are several studies available that are analyzing vitrified samples. However, picture motives constitute sectioned samples (*252-254*) or 3D analyses of tilted samples (*255-257*). Therefore, the interpretations of the pictures obtained in the present work had to be made with the aid of pictures showing samples that were prepared differentially and also analyzed employing other EM methods such as cryo-electron tomography. Many pictures in the literature are showing thin-sectioned cells where the organelles are viewed in their spatial context. In the present study, the negative staining and cryofixation procedures were performed with cellular fractions that underwent physical insults during the whole fractionation procedure as a consequence of, for example, cell homogenization and several subsequent washing steps. Slicing (sectioning of) the material will reveal the interiors of organelles and double-membrane structures might be more easily recognized than if the sample is squeezed onto the grid. Structures easily seen with one method may be looked for in vain when pictures are interpreted that were obtained using another method. Studies presenting micrographs from other cell lines were also consulted for the interpretation of the micrographs obtained in the present work.

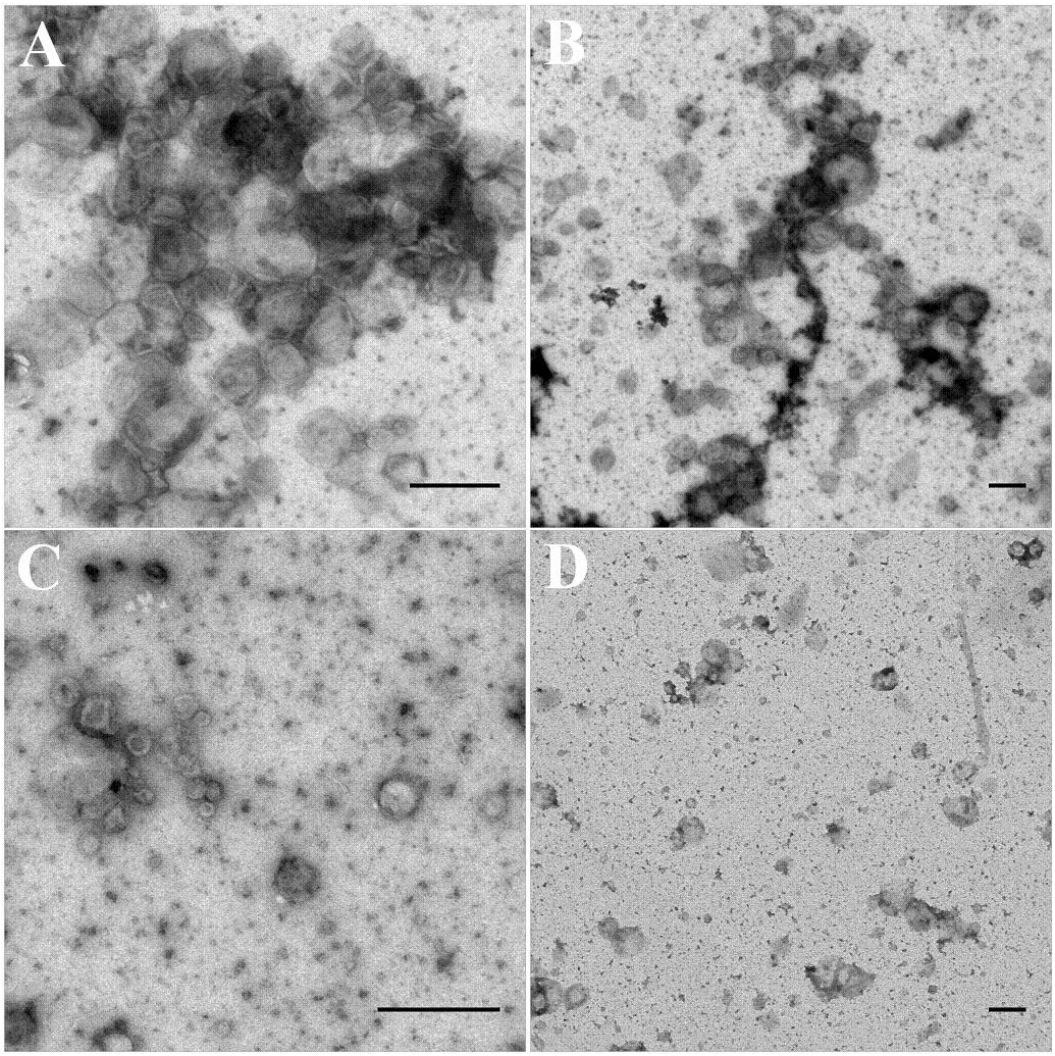

Figure 11.3. Micrographs from transmission electron microscopy of fraction 2 stained with uranyl acetate. The black speckled areas (prominent in B) are a consequence of precipitation of uranyl acetate with phosphate (*258*) present in the suspension buffer (PBS). A and B: Collapsed, relatively small, vesicles with clearly visible membrane folds. C: Membrane vesicles, many of them collapsed. Some weakly visible tubule-like structures can be seen to the right. D: Picture with less magnification, revealing some weak gray areas, maybe precipitation artifacts. Obvious cellular structures are absent. Scale bar = 500 nm.

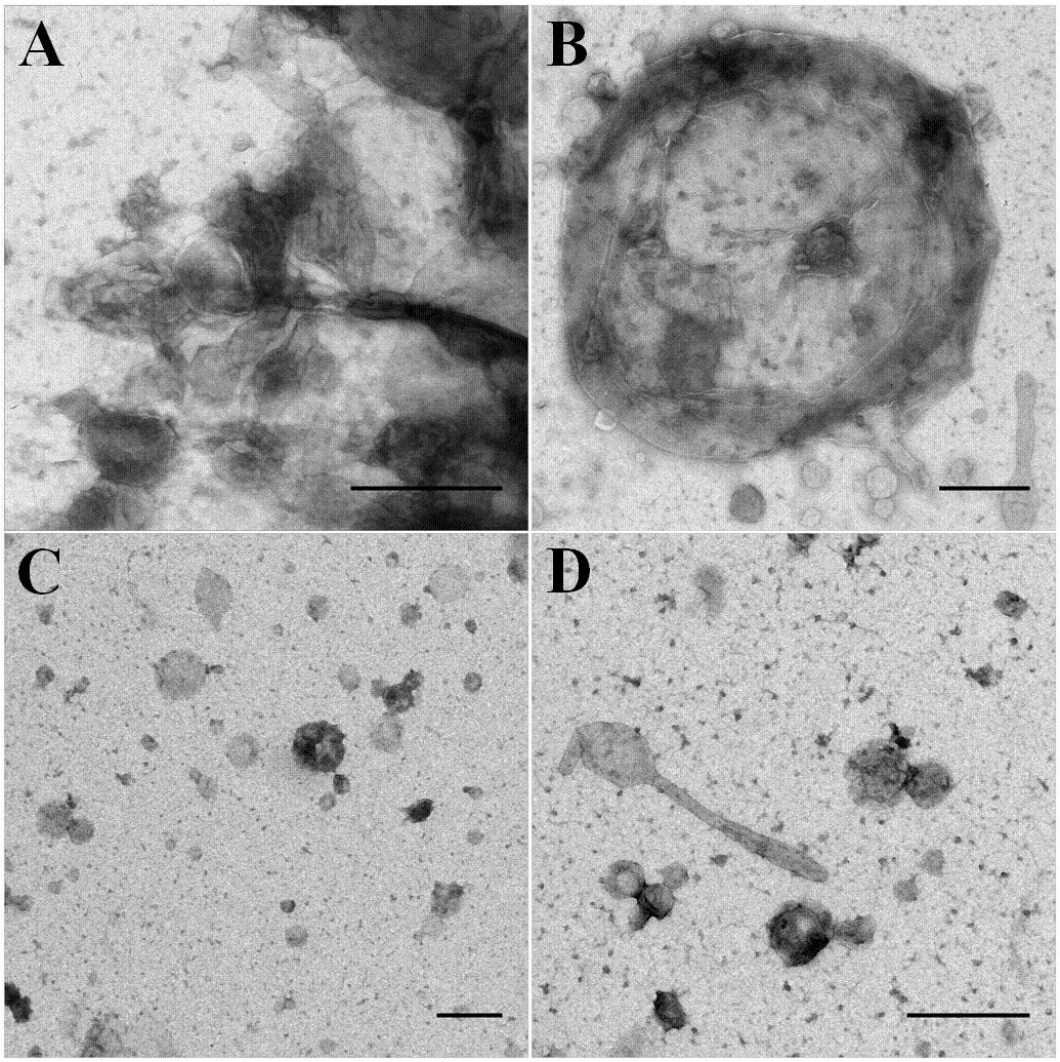

Figure 11.4. Micrographs from transmission electron microscopy of fraction 3 stained with uranyl acetate. A: Collapsed membrane structures. B: Collapsed vesicle in the lysosomal, peroxisomal, and mitochondrial size. C: Precipitation artifacts and possibly protein aggregates. D: Tubular structure extending out from a vesicle. Some small vesicles are also seen. Scale bar = 500 nm.

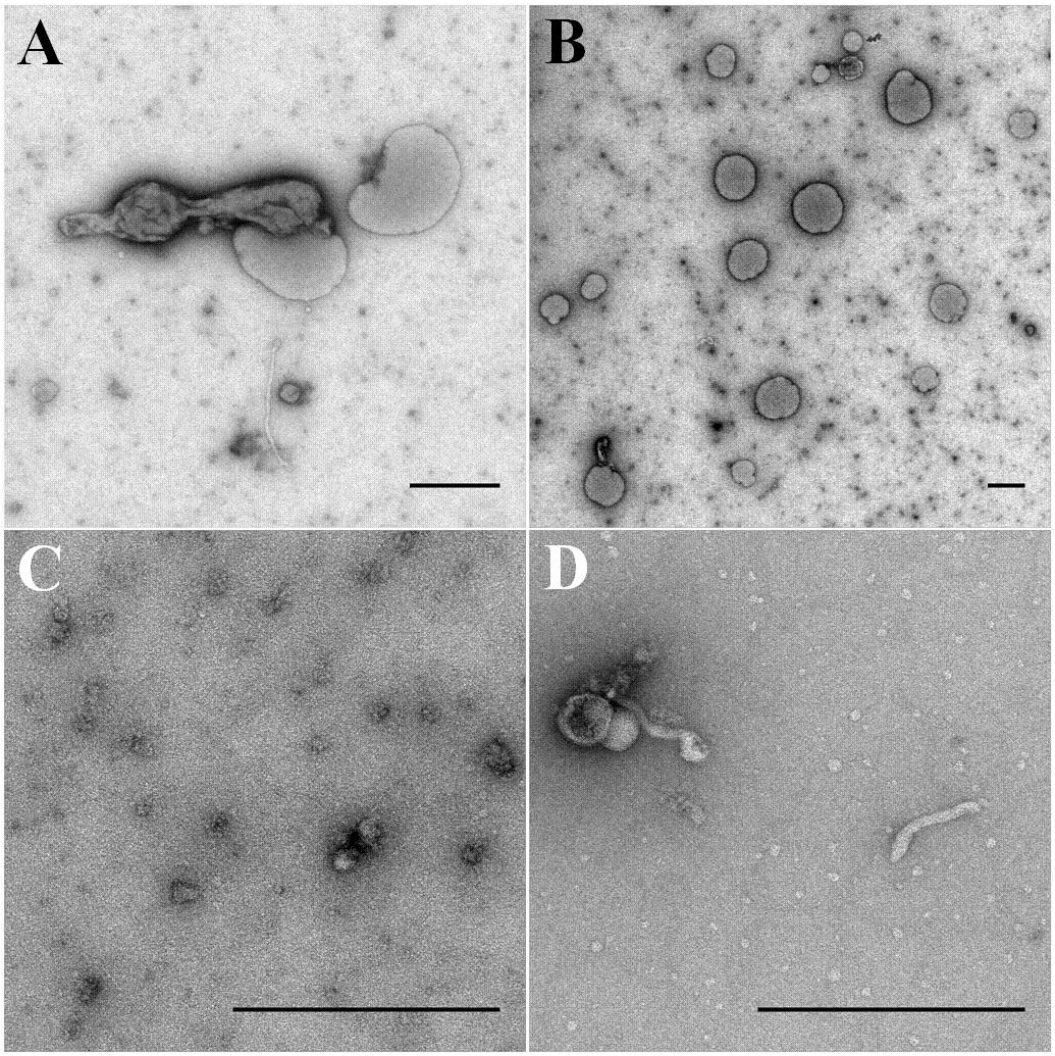

Figure 11.5. Micrographs from transmission electron microscopy of fraction 4 stained with uranyl acetate. A: Collapsed vesicle. B: Micrograph with lower magnification from one part of the grid containing many vesicle-like structures. Here, they do not appear collapsed but also not voluminous. C: Protein aggregates and/or small vesicles. D: Small vesicles (upper left corner) and tubule-like structures. Scale bar = 500 nm.

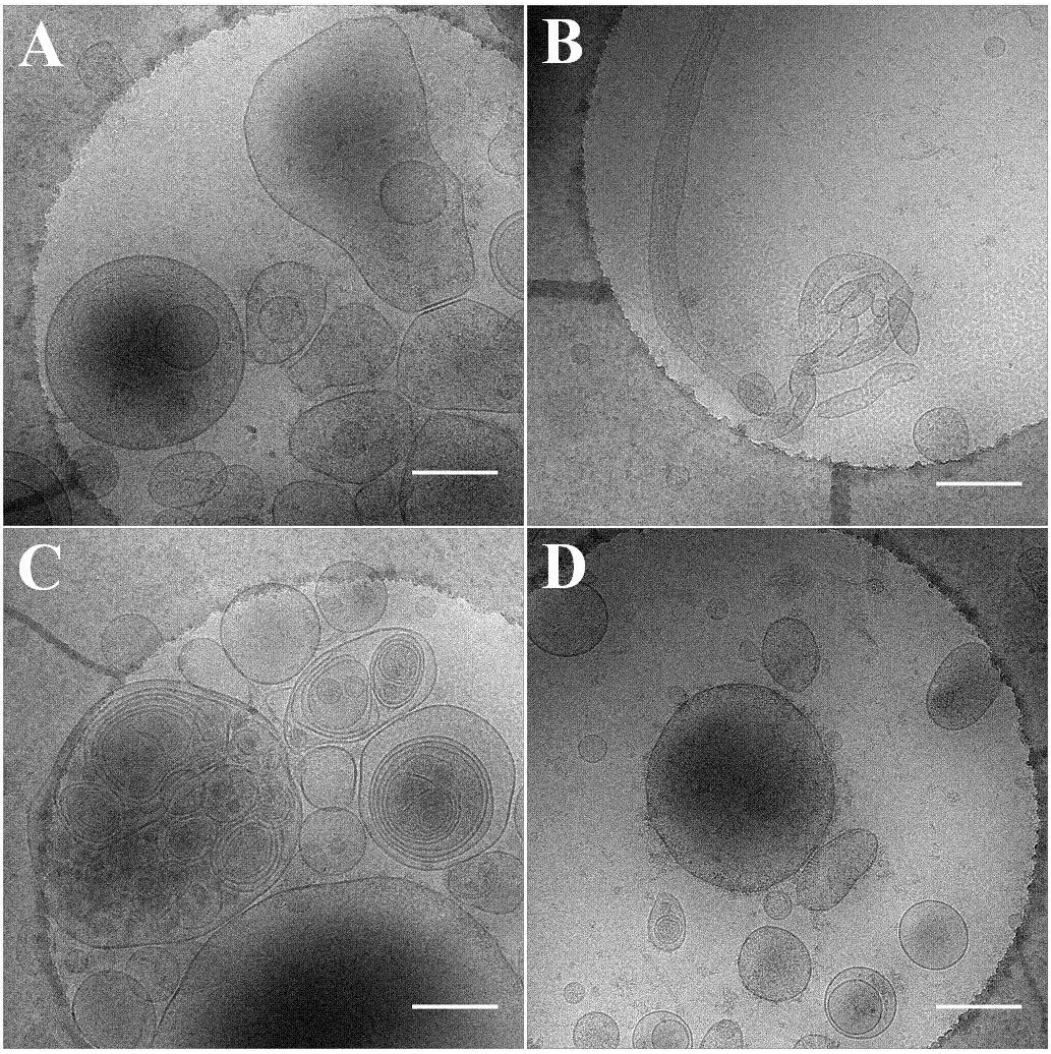

Figure 11.6. Micrographs from cryo-EM of fraction 2. A: Smaller vesicles with diameters around 200-500 nm. One vesicle is having electron dense homogenous content and might be a lysosome and/or a peroxisome. The vesicular structures are difficult to identify as they can originate from any membranous structures present in this fraction. B: Long, tubular-like structures. Maybe originating from Golgi but can also be plasma membrane fragments, as they might form stripes during the fractionation procedure. Plasma membrane derived stripes are broader than microtubule (*259*). C: In the lower part of the picture, a presumed peroxisome and/or lysosome is present. The smaller multi-vesicular membrane structures about 500 nm in diameter might be preparation artifacts. The larger multi vesicular body, 750 nm in diameter, is believed not to be an artifact because of the relatively dense packing of vesicles inside. D: The denser vesicle might be of peroxisomal and/or lysosomal origin. The origin of the smaller vesicles is unknown. Scale bar = 250 nm.

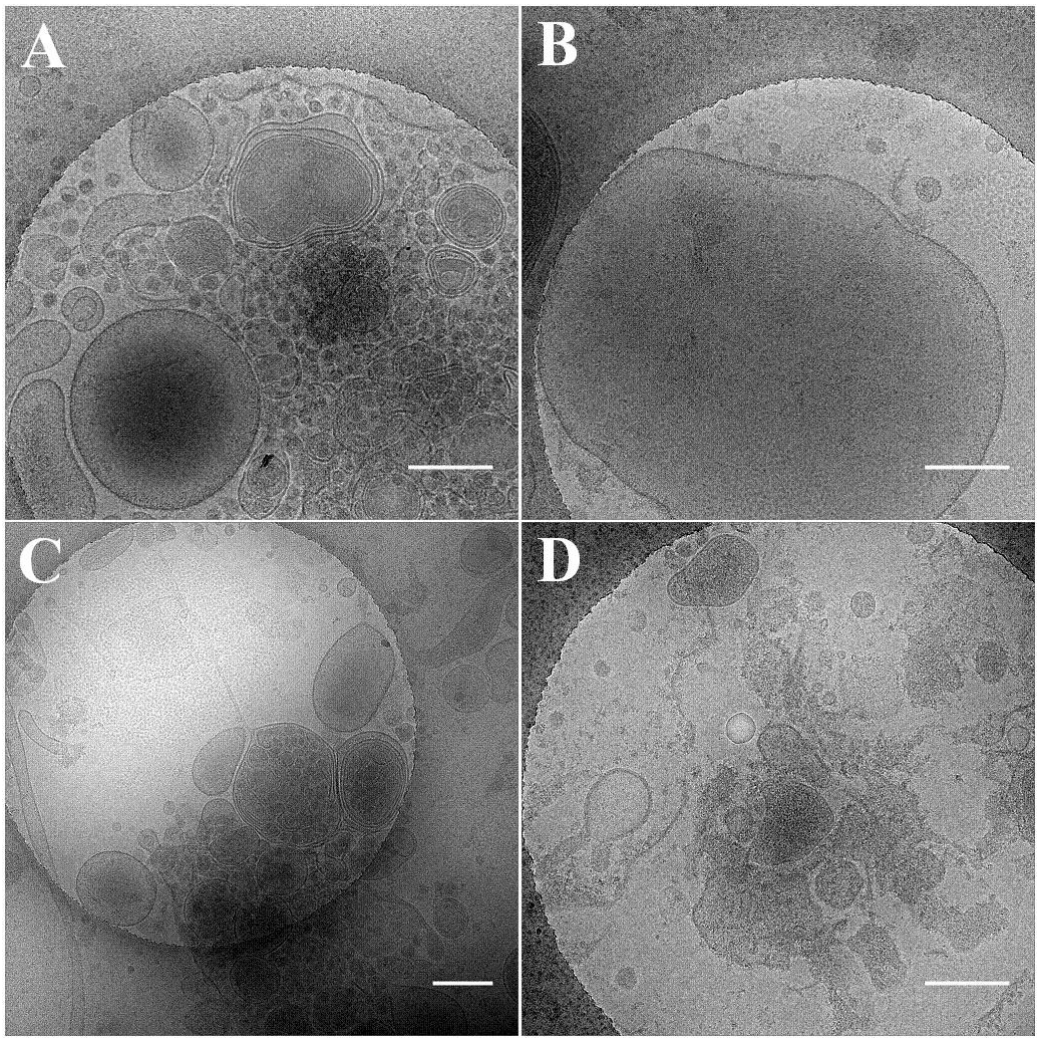

Figure 11.7. Micrographs from cryo-EM of fraction 3. A: Suspected peroxisome and/or lysosome is present (left, electron-dense matrix) together with many membranous, very heterogeneous structures that are believed to be the spilled content of a broken multi-vesicular body. The small dots (~ 50 nm) cannot be ribosomes (~ 30 nm). Some smaller multi-vesicular structures with denser content are present. B: Vesicle, roughly 1 µM in diameter with relatively weakly absorbing matrix. C: A tubule-like structure is seen on the left that is too broad to be microtubule (*259*). The multi-vesicular structures with relatively heterogeneous content are probably not artifacts. Two smaller oval vesicles with homogenous content can be seen. On looking closely, they display a one sided very weakly visible coating. Whether this is an artifact from the carbon film, ice formation or an actual coat remains uncertain. D: Broken structures giving a granular impression. Scale bar = 250 nm.

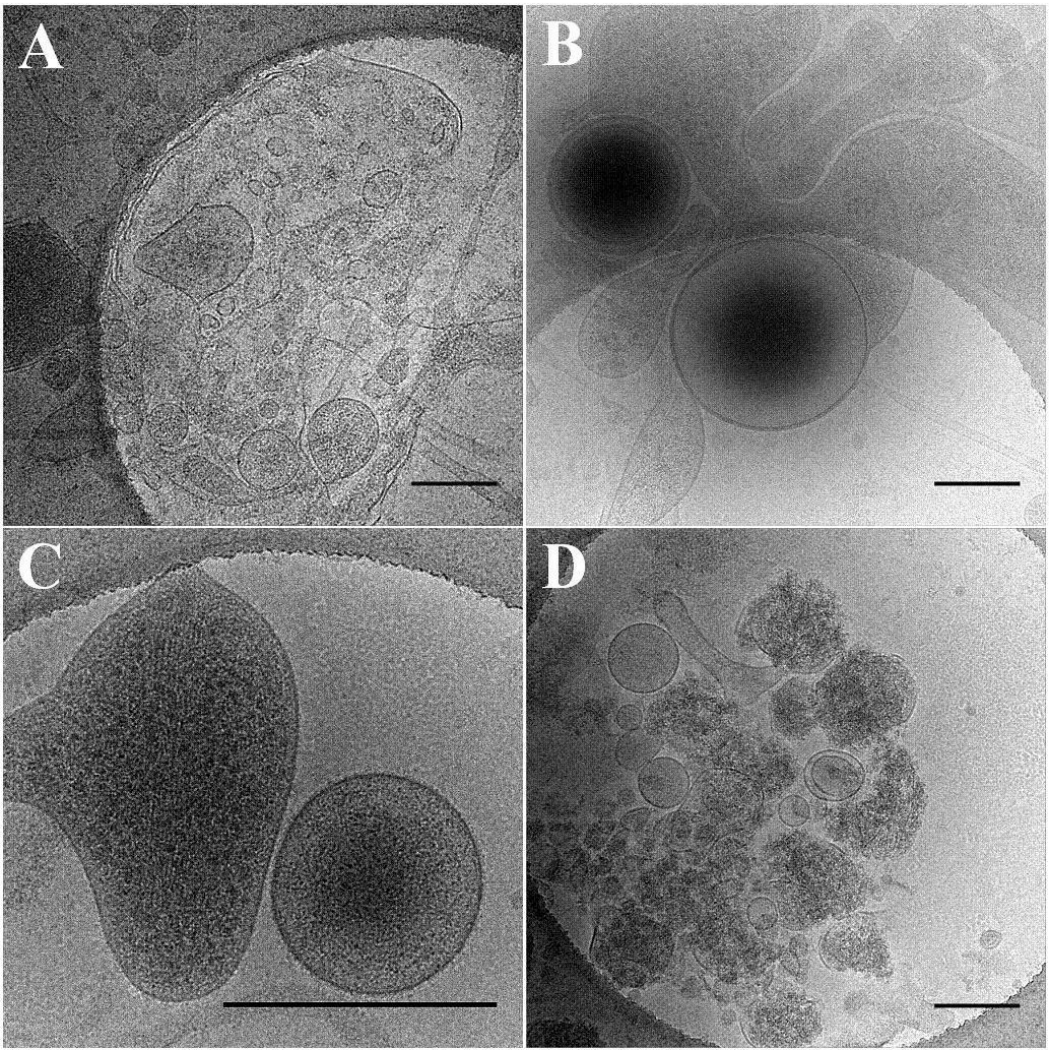

Figure 11.8. Micrographs from cryo-EM of fraction 4. A: This structure is postulated to be organelle leftovers. B: Two vesicles with diameters of ~ 500 and ~ 200 nm. Both have electron dense content and are believed to be either lysosomes and/or peroxisomes. C: Two clearly distinct structures. An oval structure is seen to the left. A closer look reveals an ordered matrix which is structured in a way that is not seen in structures present in the other fractions. This structure is believed to be a mitochondrial vesicle. The round structure to the right resembles either a peroxisome and/or primary lysosome because of its relatively dense and homogenous matrix. D: Small vesicles and granular protein aggregates, probably from lysed organelles. Scale bar = 250 nm.

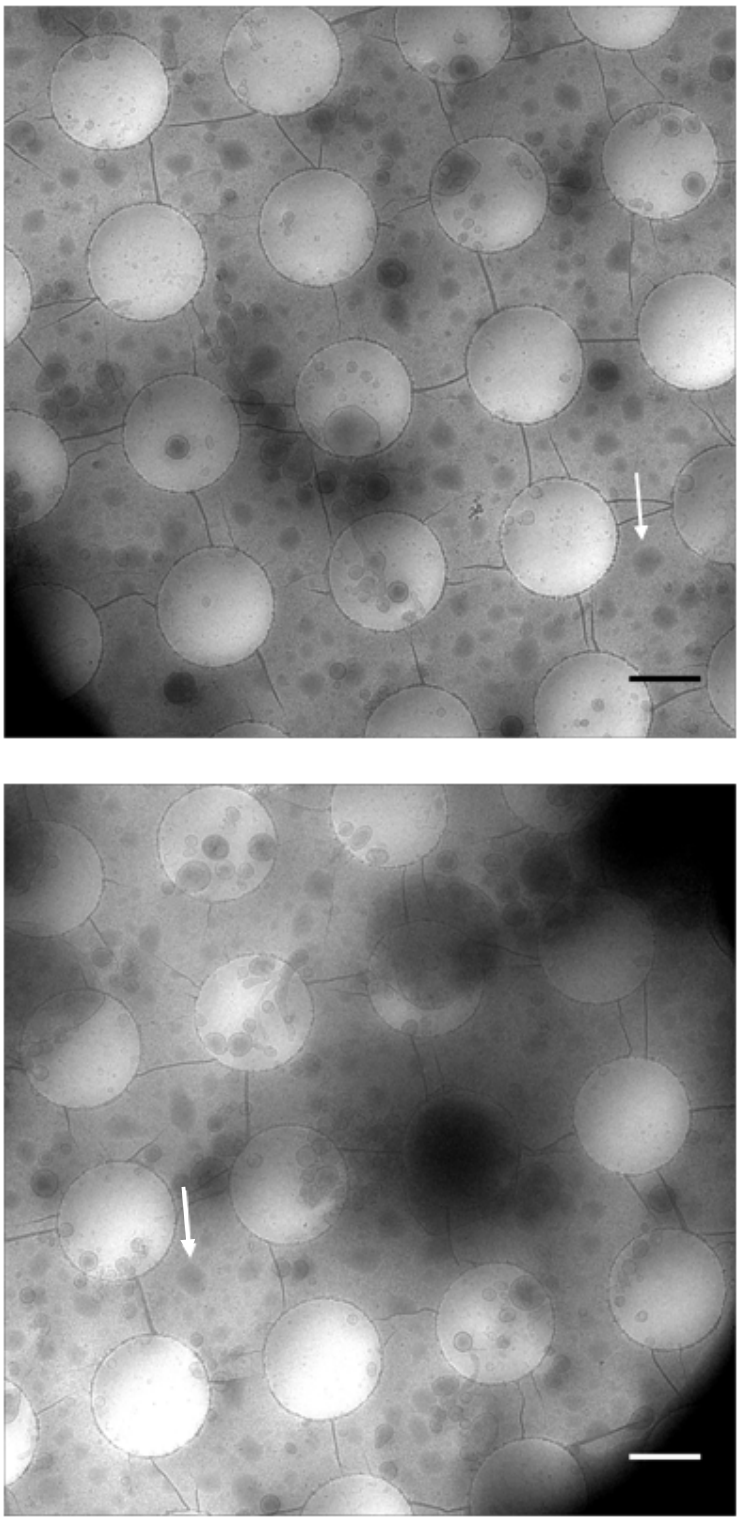

Figure 11.9. Cryo-EM overview micrographs of fraction 2. The light-gray spots with diffuse contour (indicated by arrows) might represent areas of thick ice (*260*). Scale bar = 1 µm.

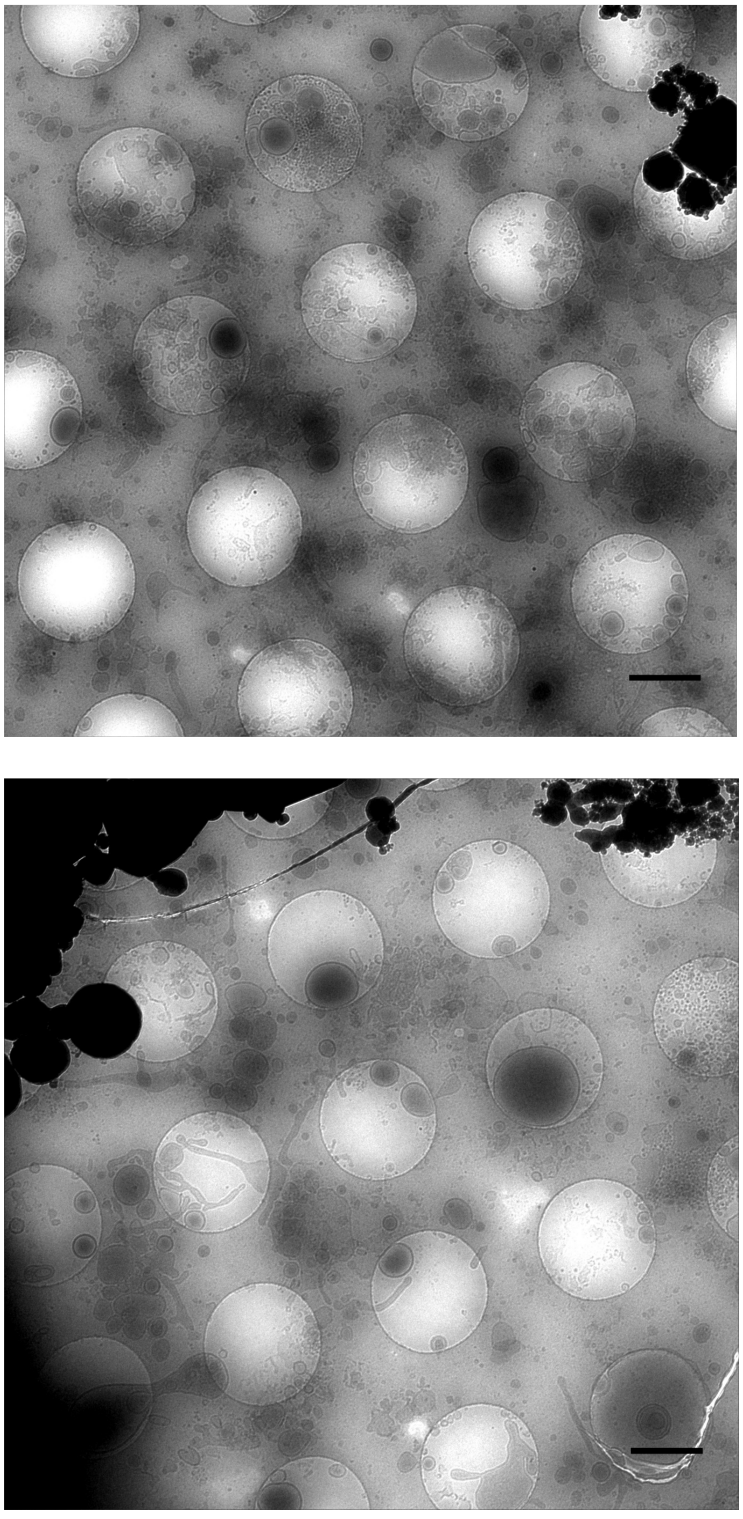

Figure 11.10. Cryo-EM overview micrographs of fraction 3. The dense black areas in the (upper) corners are large ice contaminants (*260*) through which the electron beam cannot pass. Scale bar = 1 µm.

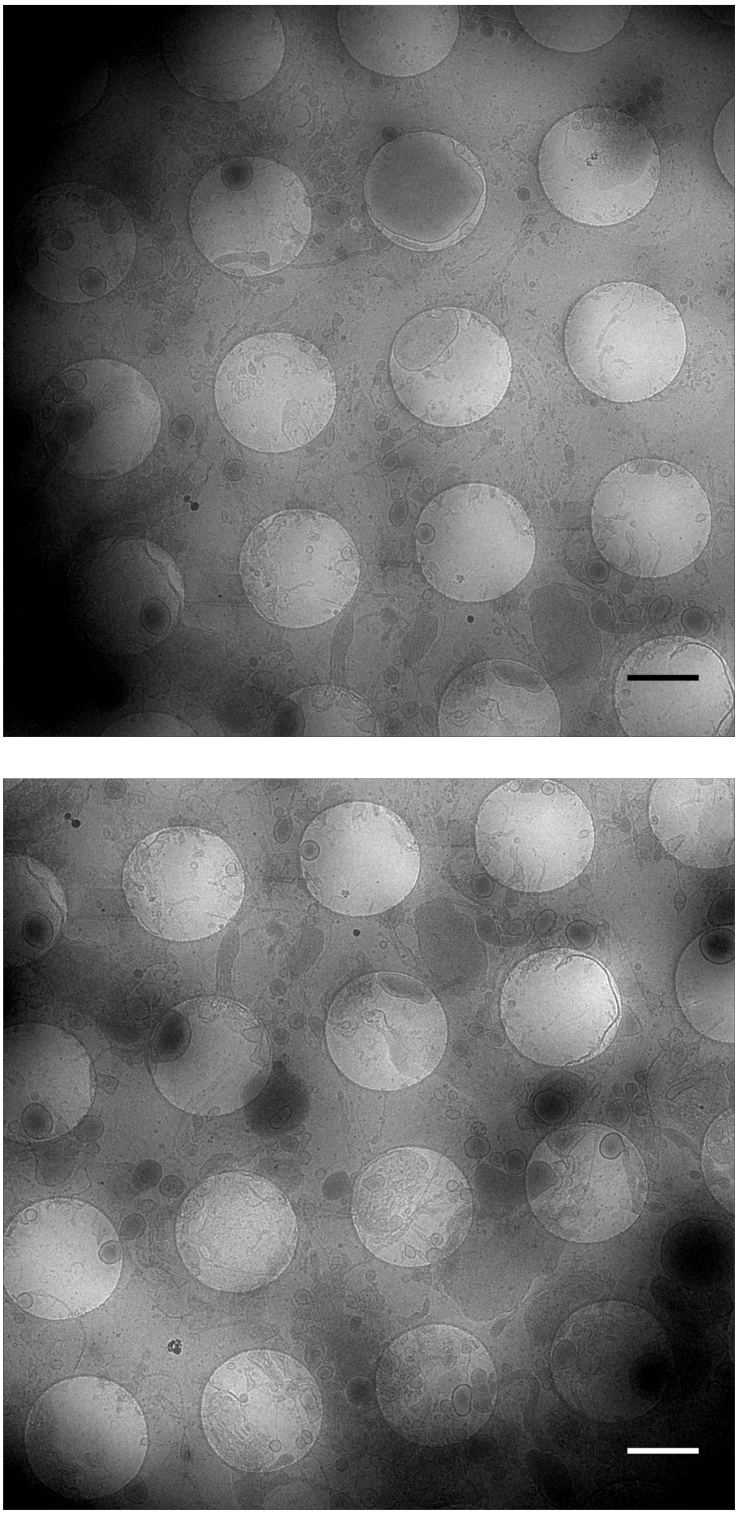

Figure 11.11. Cryo-EM overview micrographs of fraction 4. Scale bar = 1 µm.

11.5 Information from the literature used for organelle identification

The following sections present features that were used in the attempts of organelle identification in the electron microscopy micrographs obtained in the present work.

Mitochondria

The "classical" picture of a bean-shaped structure with clearly visible inner membrane invaginations were recognized in electron micrographs from sectioned cells (*253, 261-263*) but when interpreting plunged non-sectioned material, this picture has to be abandoned. Mitochondria in many mammalian cells (*264-265*), including HeLa cells (*265-267*), have been shown to form a network. In human fibroblasts, for example, the mitochondria form a filamentous network and one of those filaments can be as long as 40 µM (*264*). In electron micrographs from sectioned HeLa cells, the mitochondria display diameters of approximately 0.3-0.5 µM (*261*).

The mitochondrial networks are disrupted upon homogenization and appear as vesicles with different shapes depending on the structure of the branched tubular-like filamentous network. Prominent features of mitochondria are the double membrane and the inner membrane folds, the "cristae" (*253*). A negatively stained mitochondrial suspension obtained from different sources, such as Neurospora crassa and rat heart, has been studied with electron microscopy by Stockenius (*268*) and the partly intact mitochondria, display worm-like 30 nm broad inner membrane folds surrounded by a coat of small spherical particles, 8.5 nm in diameter, on their contour with a narrow stalk of 4-5 nm between (*268*). The appearance of the particles in the micrographs was dependent on the fixing and the staining procedure and could not be seen if the mitochondrial suspension was subjected to OsO_4 at 0 °C, $KMnO_4$ or prolonged storage of the suspension in diluted sucrose prior to dehydration and staining (*268*). Cristae from algae have been successfully visualized using cryo-EM tomography and they appear as small tubular-like structures, about 50 nm broad, coated with small protein complexes, appearing as small dots in the micrograph (see fig. 11.12) (*255*). Tilt-methods give a clearer picture about the structure than do fixed-angle methods. To conclude, typical mitochondrial features are difficult to recognize in electron micrographs with the kind of material and technique used in the present work but the presence of structures from the inner membrane folds can differentiate them from

other organelles such as peroxisomes, which are round and display a homogenous matrix.

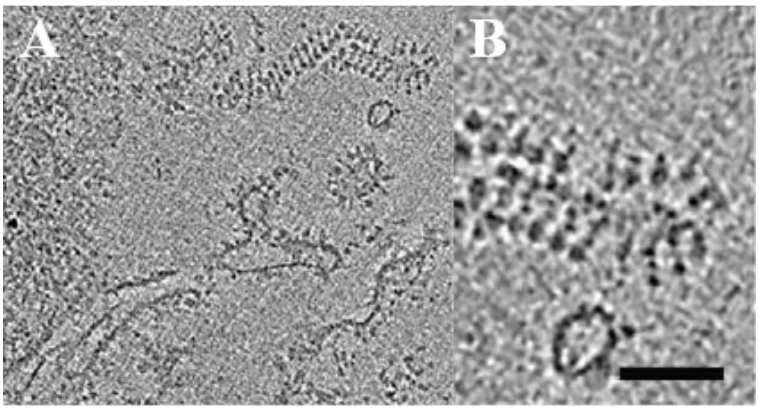

Figure 11.12. Cryo-electron tomography micrograph of cristae. B: Closer look at the tubular cristae found in the upper right corner of A. Scale bar = 50 nm. Reprinted and modified with kind permission from Egbert J. Boekema and FEBS Letters (*255*) (copyright (2010)).

Peroxisomes

Peroxisomes are spherical organelles with diameters between 0.2-1 μM (*127*). Without specific staining such as using the 3,3'-diamino-benzidine method (*269*), peroxisomes are difficult to separate from primary lysosomes because they both are spherical organelles similar in size with one limiting membrane and a homogenous matrix (*253*). Peroxisomes are sensitive to osmotic insults and may give rise to peroxisome ghosts (vesicles of peroxisomal membrane) during the purification procedure. Also, conventional purification schedules tend to promote leakage of matrix material and the organelle will give a less dense impression. This has been reported for a peroxisomal fraction purified from rat liver (*136*).

Lysosomes

There is a continuous formation and fusion of vesicles in the cell that together form larger- and multi-lamellar structures. They differ in size and morphology depending on their cargo and origin (*270*). A classical way of identifying lysosomes is the presence of hydrolytic enzymes such as acid phosphatase (*253, 271*). Unless specifically stained, it is difficult to distinguish primary lysosomes from peroxisomes. Multi-vesicular bodies will be recognized as vesicles populated by smaller vesicles and structures with multiple membrane structures. They do differ in size and can be both smaller and larger than primary lysosomes and contain many or few vesicles

(*253*). Autophagic vacuoles are vesicles containing other cell components in different stages of breakdown (*253*). Some endosomes and multi-vesicular bodies possess a coat of proteins (*272*). These vesicles are called as "receptosomes" and the proteins might be the rests from clathrin vesicle coating (*270*). Pre-lysosomal structures, such as clathrin coated vesicles, are difficult to identify with one-projection images (*273*). Caveolae might be identified as small vesicles with an irregular surface (*274*) and they can fuse with each other and form non-spherical membrane structures (*274*). These vesicles have a spiral (worm-like) coated membrane structure (*214*) which makes their surface irregular in comparison to simple membrane vesicles.

Plasma membrane

Membrane fractions prepared from several types of cells have been reported to consist of membrane strips and vesicles ranging between 100 nm and 3 µm in size (*275-279*). Shearing forces from cell homogenization and following re-suspensions of the sample prevent the plasma membranes to appear as large sheets and they will form vesicles with varying electron density (*280*). During vesicle formation, surrounding structures may be trapped in some of the vesicles.

Golgi apparatus

Intact or partly intact Golgi apparatus from rat liver in non-sectioned samples stained with phosphotungstic acid appeared as a tubular network (*252*). When disrupted, e.g. during cell homogenization (*281*), the Golgi apparatus consisted of small vesicles, varying in size with diameters between 100 nm to 300 nm, and 50 nm broad and 300 nm to 600 nm long tubule (*281*). The Golgi structures appeared smooth and lacked granularity (*281*).

Endoplasmic reticulum (ER)

In electron micrographs of sectioned cells, the RER (rough endoplasmic reticulum) and SER (smooth endoplasmic reticulum) can be identified through their spatial arrangement in the cell together with the presence or absence of ribosomes. The preparation of subcellular fractions requires subjection of the biological material to relatively harsh conditions such as cell homogenization and frequent re-suspensions. The spatial organization of ER relative to other organelles is disrupted and their morphology altered. In several preparations, mainly from investigations in rat liver,

ER membranes were found in the shape of vesicles (*282-284*). Vesicles originating from the RER are 100-250 nm in diameter and have ribosomes attached to the surface (*285-286*) whereas the vesicle population from the SER exhibit somewhat higher size heterogeneity and lacks surface particles (*283*).

In the present work, the LMF was subjected to buffers containing EDTA (see section 15.8). The release of small and/or large ribosomal subunits from microsomal membranes is promoted by magnesium chelating agents, such as EDTA (*287-288*). However, rat and guinea pig liver fractions treated with EDTA have been reported to retain some ribosomes (*289-290*). The extent of release is dependent on the amount of EDTA per weight tissue cells. In the present study, this ratio is not known.

Ribosomes

In cryo-EM micrographs, 80S ribosomes give a round and compact but granular impression and are about 30 nm in diameter (*291*).

Cytoskeletal components

Microtubule are 30 nm broad and longer than 1 µM (*259*). Actin filaments appear as very thin threads that are shorter in length than microtubule (*259*). The lengths of tubule and filaments seen in the micrographs most probably resemble shorter structures after fractionation than if viewed inside of intact cells.

11.6 Interpretation of micrographs

11.6.1 Fraction 2, general impression

Mostly membranous, round vesicular structures are present. This fraction gives a relative homogenous impression with a few structures having a denser matrix than the major part of the vesicle population. These structures are believed to be either peroxisomes and/or primary lysosomes. Some structures are too large (> 1-2 µM) to be visualized in the images of one grid hole and are only seen in the overviews (fig. 11.9). They might be multi-vesicular structures and/or large plasma membrane sheets. Tubular structures were present but few in numbers. No obvious mitochondrial structures were recognized and also no ribosomes.

11.6.2 Fraction 3, general impression

This fraction gives a heterogeneous impression, as opposed to fraction 2. A higher number of irregularly shaped membrane structures can be found in this fraction relative to round vesicles. Some material seems to be aggregated and several clusters are seen in the overview pictures (fig. 11.10) together with broken organelles and/or organelle remnants. Tubular structures are seen also in this fraction and clusters of very small and round structures, about 50 nm in diameter can be seen. They are too large to be identified as ribosomes. As stated above, no obvious mitochondrial or ribosomal structures were recognized. This fraction contains multi-vesicular structures and also vesicles with a homogenous dense matrix that are believed to be either peroxisomes and/or primary lysosomes.

11.6.3 Fraction 4, general impression

This fraction gives a damaged and heterogeneous impression (fig. 11.11) and multi-vesicular bodies were not seen. Many thin, string-like structures were present which are thought to be stripes of membranes from damaged organelles. Some of them might be microtubule. Actin filaments are too thin to be seen in the overviews. Some round vesicles with dense homogenous matrix were present which might be peroxisomes and/or lysosomes.

11.7 Cryo-electron microscopy of subcellular fractions, conclusion

The results of this method support the suspicion that the presence of mitochondrial marker (fig. 5.3) in western blot analysis of fraction 3 is a consequence of mitochondrial disruption during the fractionation procedure. One vesicle that is assumed to be of mitochondrial origin was seen in fraction 4 (fig. 11.8C) but not in fraction 3. Fraction 4 was devoid of typical lysosomal and endosomal structures such as multi-vesicular bodies, seen in fractions 2 and 3 (fig. 11.6C and 11.7A and C).

12 Resistant cells

If cytotoxic substances are added to culture cells, they have to adapt to survive. The nature of the induced changes depends on the substance, cell type and dosage scheme (*292*). The higher the toxic challenge, the greater the changes the cells need to adopt to survive in their new environment. The cells that survive and grow in the presence of the toxic substance have developed resistance. The grade of resistance, RF (resistant factor), is calculated as: IC_{50} (solvent treated cells)/IC_{50} (resistant cells).

12.1 Establishing resistance

Resistant cell lines can be established in several ways. Some protocols are selecting resistant clones in a cell culture after single or a few multiple step substance additions (*293-294*). However, survival after few doses indicates inherent resistance, a consequence of genetic diversity in a cell culture population (*295*). Acquirement of resistance needs continuous- or pulse-wise subjection of the cells to the toxic substance, often over longer time periods such as several months. Mese et al. and Shen et al. (*294, 296*) used a mutagen together with cisplatin to speed up the selection process. In the present work, substances were added weekly at the time of cell passage. If few cells were left attached (< 20 % cell coverage of flask surface), the culture was left to recover before further stressing the cells. Figure 12.1 shows results from tests with MCF-7 cells treated with substances for about 16 months (recovery phases included). The reactive nature of platinum complexes enable several targets in the cell and force the cells to respond by changing several mechanisms at once which might explain the long adjustment times.

12.2 Usefulness of resistant cell lines

Resistant cell cultures can be used to investigate cross resistance, i.e. if the mechanism developed against the toxicity of one substance also protects against the toxicity of another substance. The mechanism of action of the toxic substance will direct the adaption process of the cells i.e. a complex that cannot bind to DNA will not induce changes in the cell DNA repair machinery during resistance development. Cross resistance is often seen between platinum complexes (*25, 65, 241, 297-299*), e.g. between cisplatin and carboplatin in several cell lines with acquired resistance (*294, 300-301*). This is an indication that those complexes share at least some mechanisms of action. Resistance against cisplatin does not always and exclusively lead to cross

resistance to other platinum complexes (*298*) but can lead to cross resistance to platinum lacking substances, such as doxorubicin (*242, 296, 302*). For cisplatin and other platinum complexes, resistance is often accompanied by a reduction in cell uptake (*25, 62, 65, 240-242, 294, 297-299, 303-304*). If the uptake of another complex is reduced in cisplatin resistant cells, they probably have one or several uptake- and/or efflux mechanisms in common.

12.3 How do the cells acquire resistance to platinum substances?

The literature describing resistance development of platinum complexes, particularly cisplatin, is mainly mentioning the change in DNA repair mechanisms (*65, 298, 304-305*) and increased glutathione (*56, 242, 301*) and metallothionein concentrations (*242*) as mechanisms of adaption. Reduced uptake (see references above) and/or increased efflux (*62*) resulting in a net reduction of cellular accumulation of complexes have also been reported in cells with acquired resistance. Many other changes have been described for cell lines resistant to cisplatin such as impaired pinocytosis (*306*) and altered mitochondrial morphology (*307*). During resistance development, cells might answer to the insult by changing their growth rate. Decreased (*292, 300*), increased (*242, 300, 302*) and unchanged (*65, 241, 294, 297, 299-300, 304*) growth rates have been reported for several cancer cell lines with acquired tolerance to various platinum complexes. In the present work, the MCF-7 cell cultures treated with platinum complexes displayed reduced growth rates. This reduction seemed most prominent in the cisplatin and dl4FPtCl_2 resistant cultures and was previously reported for cisplatin resistant MCF-7 cells (*308*).

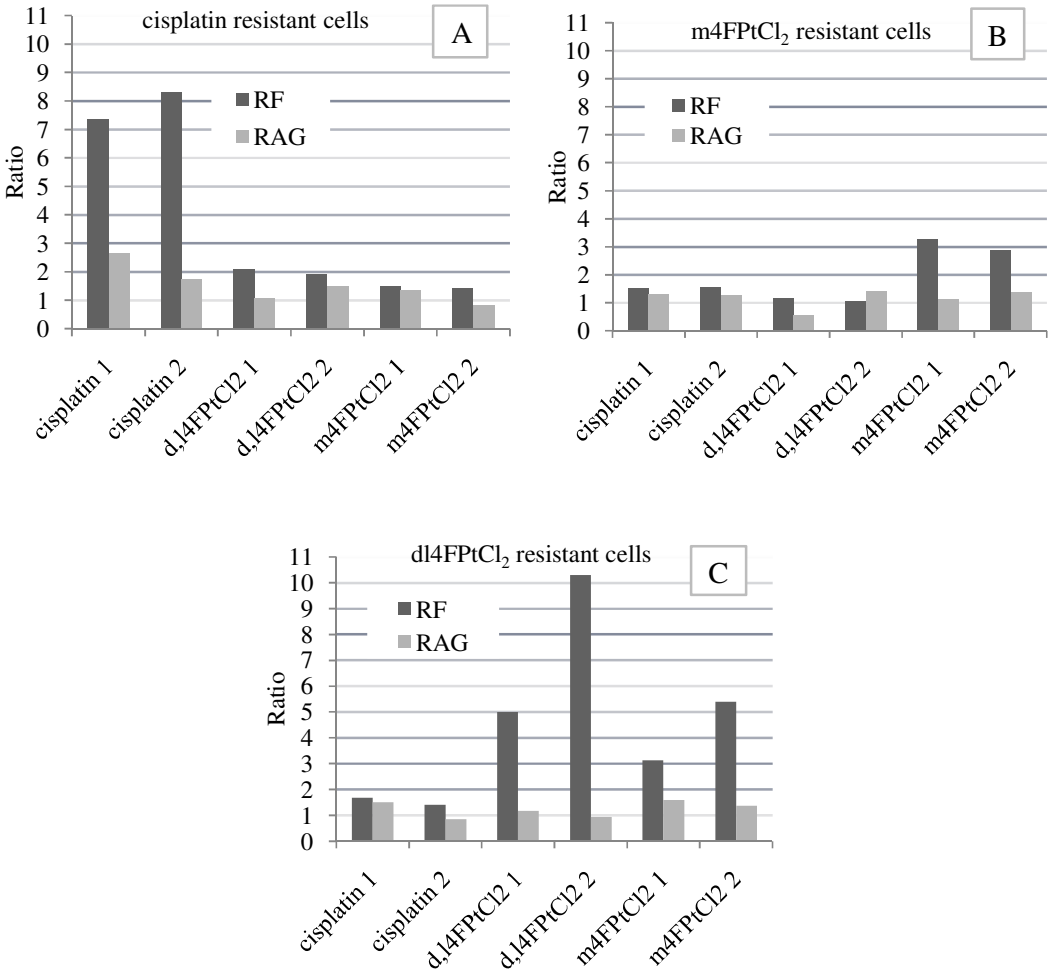

Figure 12.1. Resistance factor and relative accumulation grade of cisplatin, m4FPtCl$_2$ and dl4FPtCl$_2$ in MCF-7 cells with acquired resistance. Cells resistant to cisplatin (A), m4FPtCl$_2$ (B) and dl4FPtCl$_2$ (C) were incubated with all complexes except mDAH4FPtCl to measure the resistance factor (RF) and relative accumulation grade (RAG). Resistance factor is defined as the IC$_{50}$ of the complex in resistant cells divided by the IC$_{50}$ in the control cells. Accumulation grade is the concentration of platinum in the cell volume (calculated using protein amounts) divided by the initial medium concentration (*90*). The RAG is the AG in sensitive cells divided by the AG in resistant cells. The number after the name of the complex in the y-axis is the experiment number. For the whole cell uptake measurements, the substances were incubated for 2 h at concentrations of 30, 15 and 5 µM for cisplatin, m4FPtCl$_2$ and dl4FPtCl$_2$ respectively. For the concentration dependent cytotoxicity measurement, concentrations of 0.1, 0.5, 1, 5, 10, 25 and 50 µM were used for all complexes and the incubation time was 96 h.

12.4 MCF-7 cells with acquired resistance, investigations of cross-resistance and whole cell associated platinum

In the present work, MCF-7 cells were cultured in the presence of cisplatin, m4FPtCl$_2$ or dl4FPtCl$_2$ to acquire resistance. The resistant cell lines were used to investigate cross-resistance of the complexes and the effect of resistance on whole cell associated platinum.

12.4.1 Cross-resistance

In the present study, only very low mutual cross resistance was observed between the diastereomers (m4FPtCl$_2$ and dl4FPtCl$_2$) and cisplatin (fig. 12.1). The resistance factor of m4FPtCl$_2$ was similar in m4FPtCl$_2$-resistant and dl4FPtCl$_2$-resistant cells (fig. 12.1B and 12.1C). However, no resistance towards dl4FPtCl$_2$ was seen in m4FPtCl$_2$-resistant cells. These results suggest that the mechanisms of resistance to dl4FPtCl$_2$ are protecting the cells towards cytotoxicity of m4FPtCl$_2$. The initial rate of resistance development, see fig. 12.2, suggests that the mechanisms required for resistance towards m4FPtCl$_2$ might be more easily adopted by the cells than the mechanisms required for resistance towards dl4FPtCl$_2$. The RF values were low for the cells that had grown in the presence of m4FPtCl$_2$ (fig. 12.1B). This was not expected since at the time of resistance development, they could withstand relatively high concentrations in the cell culture medium (> 30 µM). The culture was growing a few weeks in substance-free culture medium before the cells were ready to be seeded for cytotoxicity and uptake tests. Widely speculating, the cells might during this time have adapted to the new conditions by starting to phase out the mechanisms responsible for resistance. The resistant cell cultures growing with different platinum complexes were individually treated and should not be directly compared.

12.4.2 Whole cell associated platinum

The uptake of cisplatin in the cisplatin resistant cells was only slightly lowered (fig. 12.1A). In the literature, many examples can be found where concentration- and/or time-dependent cellular cisplatin accumulation has been investigated (see section 12.2). The uptake of m4FPtCl$_2$ and dl4FPtCl$_2$ was not affected except for the humbly decreased uptake for m4FPtCl$_2$ in cells resistant to dl4FPtCl$_2$ (fig. 12.1C). However, more investigations are needed. Single-point measurements at low concentrations

and/or short incubation times might not show significant accumulation differences between resistant and sensitive cells, even if mechanisms such as increase in exodus and/or decrease in uptake are active.

12.4.3 Results from uptake measurements of cisplatin in cell lines with acquired cisplatin resistance, presentation of results from the literature

Andrews et al. (*62*) investigated concentration dependent cisplatin uptake in a 3.3-fold cisplatin resistant human ovarian carcinoma cell line (2008). They found half as much cisplatin after 1 h in the tolerant cells as in the sensitive cells when the initial medium concentration of cisplatin was 30 µM. When the concentration was kept constant at 10 µM and the incubation time varied, the same result could be seen after 2 h of incubation. Ma et al. (*65*) conducted concentration-dependent uptake using a human ovarian adenocarcinoma cell line (IGROV-1) with 8.4-fold cisplatin resistance. After 2 h of incubation with 33.3 µM cisplatin, the sensitive cells had accumulated 2.5 times more cisplatin than their resistant counterparts. In a 9-fold cisplatin resistant rat hepatoma cell line (H4-II-E), Kishimoto et al. (*240*) found 2.5 times more cisplatin in sensitive cells than resistant cells after 2 h of incubation with 33 µM cisplatin. Mese et al. (*294*) could first see differences in cisplatin accumulation between a 3.1- fold resistant and sensitive human epidermoid carcinoma cell line (A431) after 3 h in a time dependent test with 67 µM cisplatin. For a 3.25-fold resistant human colon carcinoma cell line (LoVo), the time dependent accumulation of cisplatin differed from the accumulation in the sensitive line after between three and four hours of incubation time with an initial cisplatin concentration of 40 µM (*303*). For a 6-fold cisplatin resistant human osteosarcoma cell line (U2-OS), treated 1 h with 33 µM cisplatin, the accumulation in resistant cells was half the amount in cisplatin sensitive cells (*304*).

12.5 Resistance development time course

The time it takes for the cells to develop resistance to the complexes tested in the present work differ. The addition of substances was ceased at the same time for all complexes and the concentrations in the culture medium at the last substance addition were 8 µM, 30 µM and 30 µM for cisplatin, m4FPtCl$_2$ and dl4FPtCl$_2$ respectively. Initially during resistance development, the cells reacted strongly to small increases in the dl4FPtCl$_2$ concentration (fig. 12.2) which is similar to the behavior of the cells

incubated with cisplatin. After reaching a concentration of about 5 µM, the cells were less susceptible to increases in dl4FPtCl$_2$ concentration. Because of solubility limitations, it is difficult to know the "true" concentration of dl4FPtCl$_2$. According to solubility measurements (see section 4.1) this substance precipitates at concentrations > 10 µM and at those concentrations, the cells grow in the presence of crystals, as seen under the phase contrast microscope. The solubility limitation of dl4FPtCl$_2$ might explain the sudden tolerance of the cells to the increase in concentration around passage number 90 (fig. 12.2A).

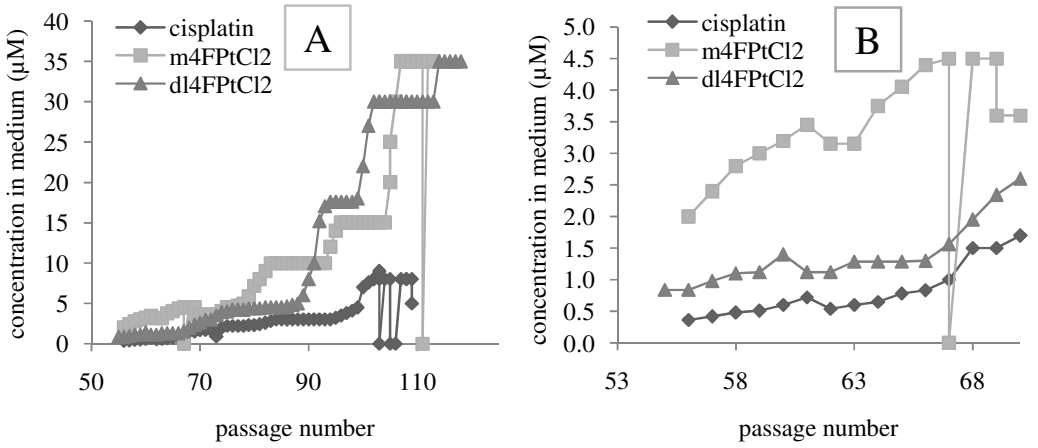

Figure 12.2. Documentation during resistance development. A: Concentration in the culture medium of cisplatin, m4FPtCl$_2$, and dl4FPtCl$_2$ (expressed in µM) plotted against the cell passage number. B: Enlarged view of A showing the concentrations in the culture medium of cisplatin, m4FPtCl$_2$ and dl4FPtCl$_2$ during the first 16 passages. The amount of cells that was transferred to new bottles at the time of passage was not documented.

13 Cellular fractionation and other techniques for investigating subcellular distribution of platinum complexes

There are several methods that can be used to investigate the subcellular distribution of platinum complexes. Visual techniques, such as those employing fluorescence, allow the viewing of labeled platinum complexes in living cells. Electron microscopy and synchrotron radiation-induced X-ray emission cannot be used for visualization in living material. However, an advantage of these techniques is that the platinum atom is the species being visualized (direct method) and not a fluorescent tag (indirect method). All visual methods analyze material with a preserved spatial organization of the organelles and artifacts arising during sample handling are absent. For methods using live imaging fluorescence microscopy, the integrity of the organelles is preserved because of the sustained natural environment and absence of mechanical and osmotic insult. The complexes can be studied using relatively low concentrations and after incubation times ranging from a few minutes to several hours. After short incubation times, the intracellular path of the complexes can be followed by live viewing. But labels are often large and it is questionable if a labeled complex will display the same subcellular distribution as the unlabeled platinum complex concerning the difference in size and possibly lipophilicity. In the following section, several investigations of fluorescently labeled platinum complexes are presented and the time dependent subcellular distribution from some investigations is summarized in flow charts (charts 13.1, 13.2 and 13.3) and some of the tested structures are shown in figure 13.1 and 13.2.

13.1 Techniques using fluorescence microscopy for subcellular localization of platinum complexes, presentation of studies from the literature

Jansen and Kalayda et al. (*95-96, 309*) investigated amongst other cytotoxicity, DNA binding, cellular accumulation and subcellular distribution of dinuclear *N,N*'-bis(aminoalkyl)-1,4-diaminoanthraquinone-platinum complexes in A2780 human ovarian carcinoma cells with (A2780cisR, RF = 6) and without (A2780) acquired cisplatin resistance. Subcellular distribution was also tested in U2-OS human osteosarcoma cells with (RF = 2.5) and without acquired cisplatin resistance. The complexes and the anthraquinones possessed varying aminoalkyl lengths. The results of subcellular distribution of one of the platinum complexes (PAQ2, fig 13.1) and the

respective label (AQ2, fig. 13.1) are presented here and summarized in chart 13.1. No difference in subcellular distribution was seen between the compounds in their respective groups (*95, 309*) (complexes and labels). The authors found that the platinum linked anthraquinones did accumulate less efficiently than their unlinked counterparts (chart 13.1) (*309*). As the fluorescent platinum complexes display cross-resistance with cisplatin, the authors conclude that some or all mechanisms of action are common. Jansen et al. (*309*) report that after 2 h of incubation in A2780 cells, AQ2 and PAQ2 were found in cytoplasm surrounding nucleus, confirmed not to be Golgi membranes (chart 13.1). After 24 h PAQ2, but not AQ2, was found in acidic vesicles in A2780 cells (*309*). In A2780cisR cells, the distribution was not different than in A2780 cells for AQ2 but PAQ2, on the other hand, was seen in acidic vesicles already after 20 min and did not spread to other compartments (*95*). No accumulation in nucleus could be seen for PAQ2 and this was confirmed to be due to fluorescence quenching by the DNA because DNA binding in A2780 cells was confirmed to be even greater for PAQ2 than for cisplatin (*309*). The lysosomal sequestration seen in A2780cisR cells for PAQ2 was not seen in cisplatin resistant U2-OS cells and the overall subcellular distribution was similar in sensitive U2-OS cells. AQ2 was seen first to co-localize with Golgi marker and later in the acidic compartments but PAQ2 was still accumulated in the Golgi complex (*96*). The authors concluded that accumulation in lysosomal vesicles is a part of the resistance mechanism towards cisplatin as the resistance factor for PAQ2 was low in the cisplatin resistant U2-OS cells as compared to A2780cisR cells (*96*). They also showed that a change in lysosomal pH was seen in the resistant ovarian carcinoma cell line and not in the resistant osteosarcoma cell line and reached to the conclusion that changes in lysosomal processing is likely to play a role in the resistance mechanism.

Alderden et al. (*98*) investigated cytotoxicity and subcellular distribution of a mononuclear anthraquinone linked platinum complex (Pt-1C3), structurally similar to the complexes described by Jansen and Kalayda et al. (*95-96, 309*) (fig. 13.2), in a human colon adenocarcinoma cell line, DLD-1. No difference in subcellular distribution between the fluorescent platinum complex and the anthraquinone ligand was seen. After 4-5 h of incubation, both compounds were seen in structures accumulating LysoTracker Green (lysosomal marker). No accumulation in nucleus was apparent and it was confirmed that the fluorescence was not quenched by DNA

interaction. The cytotoxicity of the platinum complex was not significantly different from the cytotoxicity of the ligand (*98*).

Molenaar et al. (*100*) used fluorescence-labeled and hapten-labeled ethylenediamine platinum complexes (CFDA-Pt and DNP-Pt respectively) (fig. 13.2) for their investigations of subcellular distribution in U2-OS human osteosarcoma cells. They found that CFDA-boc (fluorescent control) and CFDA-Pt entered the cells rapidly and after 1-2 h, the platinum complex and the control were seen localized to the nuclei (chart 13.2A). After 6-8 h, the fluorescence of the platinum complex co-localized with a Golgi marker and was still accumulated in Golgi after 24 h of incubation whereas the fluorescence in nucleus had disappeared. At this point, the fluorescence from the control compound was diminished and was until this point not yet seen to localize to Golgi. DNP-Pt was distributed in a similar fashion as CFDA-Pt and differently as compared to DNP-boc. Thus, the authors concluded that the subcellular distribution is determined by the platinum moiety. DNP-Pt was reported to bind to guanosine in the same manner as cisplatin in an experiment with free guanosine dinucleotides. The same results were obtained for these compounds in cisplatin-sensitive U2-OS as in U2-OS cells with acquired resistance to cisplatin (RF = 6 (*304*)) and their IC_{50} values in both cell lines exceed 50 (*97*).

Safaei et al. (*310*) investigated the subcellular distribution of a fluorescein-labeled ethylenediammine dichloroplatinum(II) complex (F-DDP) and the label (CHMA-F) (fig. 13.2) in cisplatin-sensitive (2008) and cisplatin-resistant (2008/C13*5.25) 2008 human ovarian carcinoma cells. F-DDP displayed cross-resistance with cisplatin with RF values of 5.3 and 5.7 for cisplatin and F-DDP respectively. After one hour, only 26 % of the amount of F-DDP accumulated in 2008 cells compared to 2008/C13*5.25 cells. The subcellular distribution of F-DDP differed between the cell lines (chart 13.2 B). After 1 h of incubation, F-DDP was reported to localize to several compartments in 2008 cells such as nuclei and cytoplasmic vesicles. Diffuse staining in areas between cell nuclei, plasma membrane and the cytoplasmic vesicles was also seen. The distribution in 2008/C13*5.25 cells was quite different with accumulation only at the cell periphery. No distribution in nuclei was seen and only very weak cytoplasmic staining. Differences in the subcellular distribution between CHMA-F and F-DDP were also seen in 2008/C13*5.25 cells. The authors reported that F-DDP also localized to mitochondria (*310*). Safaei et al. (*310*) investigated more closely the cell

entry of F-DDP. Culture medium solution containing the complex was applied to 2008 cells and then immediately washed away. F-DDP was first spotted at the cell surface but after few minutes localized to cytoplasmic organelles and after 10-30 min the fluorescence reached the nuclei. After 1 h of incubation, the platinum complex was present in the nucleus and vesicular structures near the nucleus whereas CHMA-F co-localized with a marker for filamentous actin. Also, some vesicles labeled with a trans-Golgi marker golgin97 (secretory pathway) and vesicles labeled with a lysosomal marker (LysoTracker Red) contained F-DDP. F-DDP was also seen in vesicles containing the copper efflux transport protein ATP7A and the multidrug resistant protein MDR2, as determined by co-localization of F-DDP with antibodies against these proteins (*310*). Wortmannin treatment resulted in a ~ 30 % increase in total cell accumulated F-DDP and a change in localization of the complex to vesicles, that under normal circumstances did not exhibit accumulation. Also total cell accumulation of cisplatin was induced by this agent (*310*). No co-localization of F-DDP with early endosomal markers was seen after 1 h of incubation.

Liang et al. (*99*) studied, amongst other, accumulation and intracellular distribution of Alexa Fluor 546 labeled cisplatin (Alexa Fluor 546-cisplatin) in KB epidermoid carcinoma cell lines that are sensitive (KB-3-1) and resistant (KB-CP.5) to cisplatin. The KB-CP.5 cells were obtained through a single step selection after incubation with 0.5 µM cisplatin. Co-localization of Alexa Fluor 546-cisplatin and the Golgi label NBD-C6-Ceramide was seen during the first 30 min of incubation (chart 13.3). Between 30 min and 1 h, the platinum complex also gathered in nuclei. After 2 h, fluorescence was seen in both Golgi and cell nuclei. For the KB-CP.5 cells, most Alexa Fluor 546-cisplatin was seen in Golgi after 1 h of incubation and very weak fluorescence was seen in nuclei. The complex was reported to localize to nuclei first after 2 h with fluorescence also seen in Golgi. Also, the fluorescence was less evenly distributed and localized to spots compared to the pattern seen in the sensitive cell line. In both cell lines, Alexa Fluor 546-cisplatin also escaped to non-Golgi vesicles after accumulation in Golgi but the signals were overall weaker in the resistant cell line. Uptake of Alexa Fluor 546 alone was fast and fluorescence was seen throughout the cell already after 5 minutes of incubation.

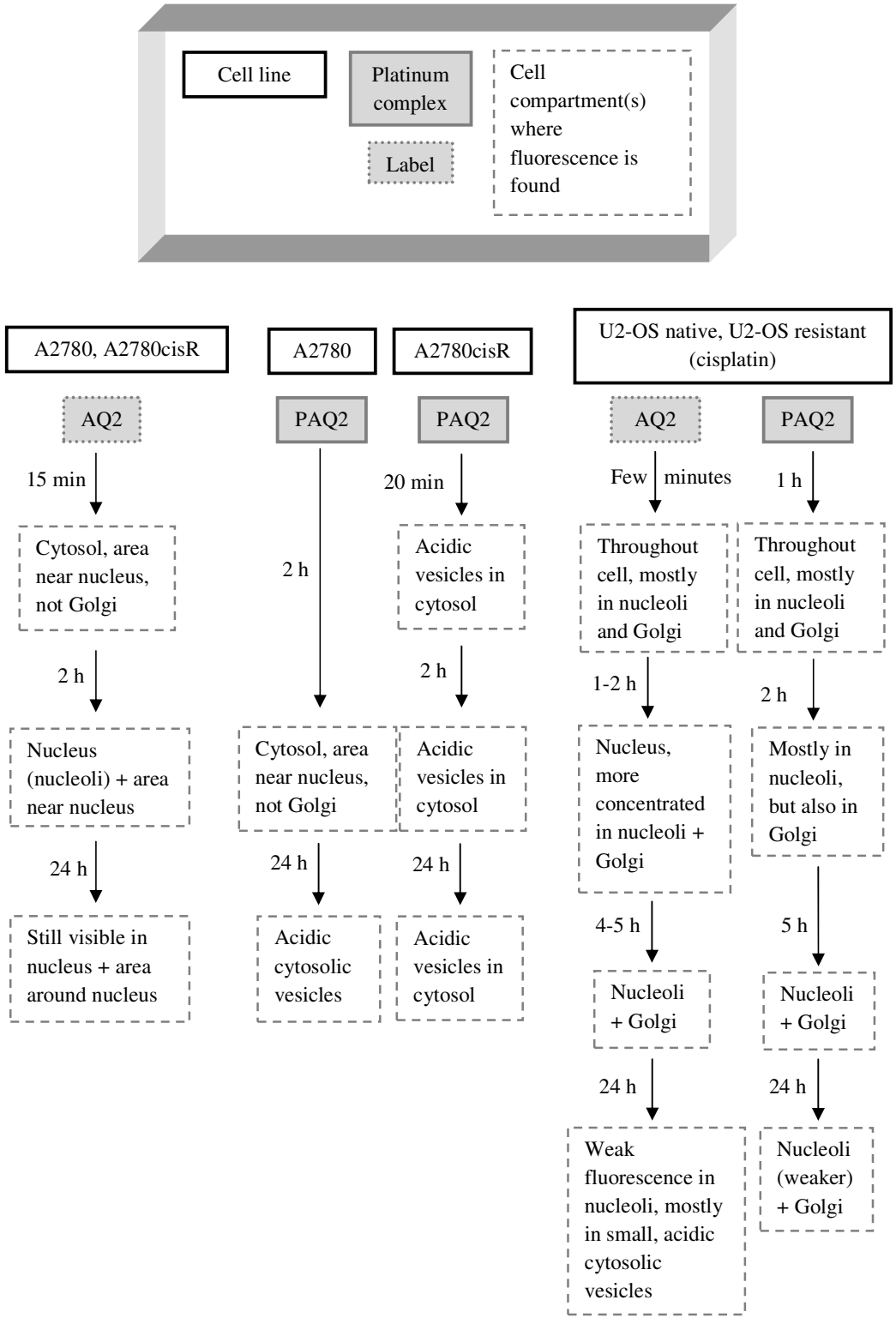

Chart 13.1. Flow chart summarize of results obtained by Jansen and Kalayda et al. (*95-96, 309*)**.**
For chemical structures, see fig. 31.1.

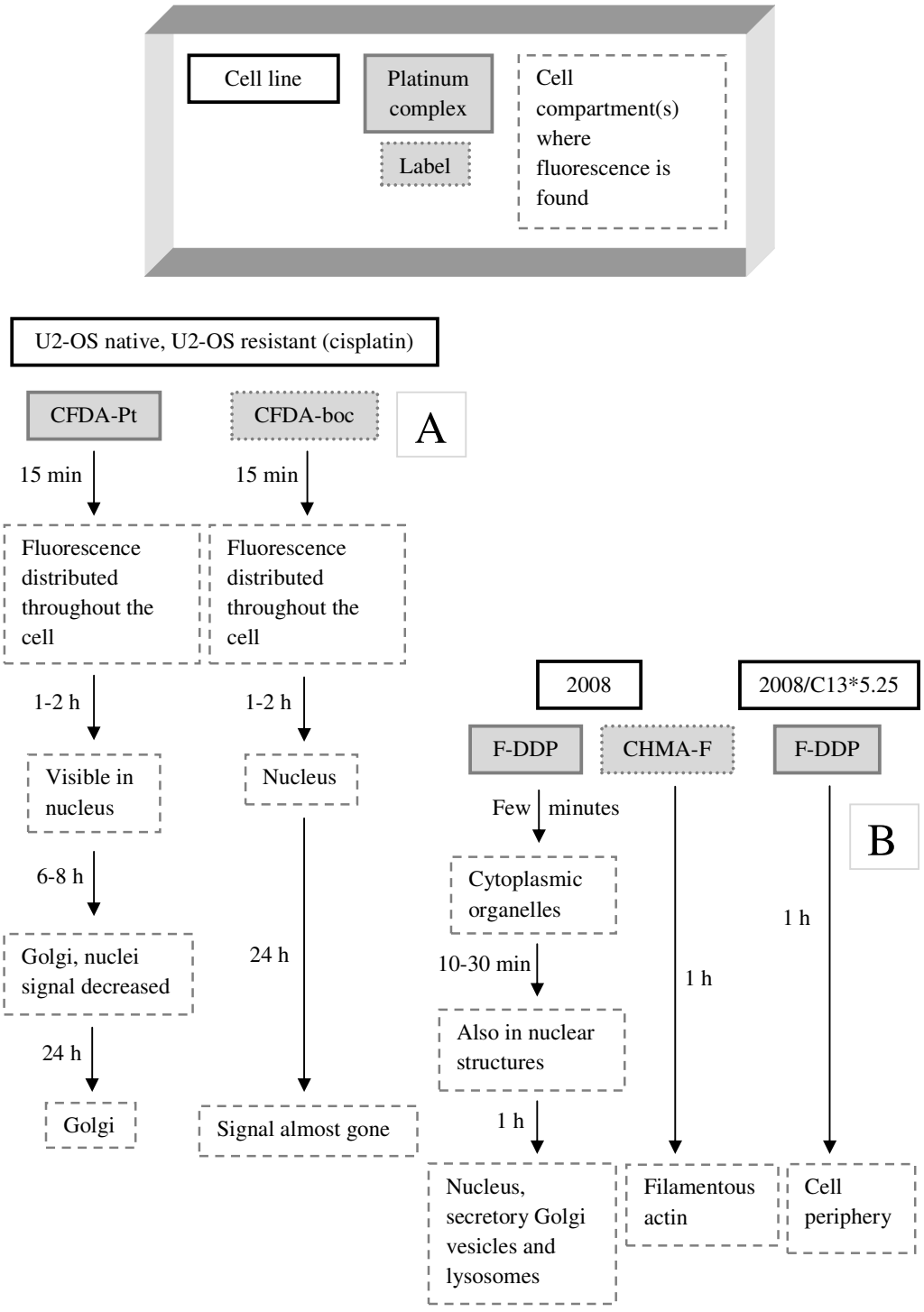

Chart 13.2. Flow chart summarize of results obtained by A: Molenaar et al. (*100*) **and B: Safaei et al.** (*310*)**.** For chemical structures, see fig. 13.2.

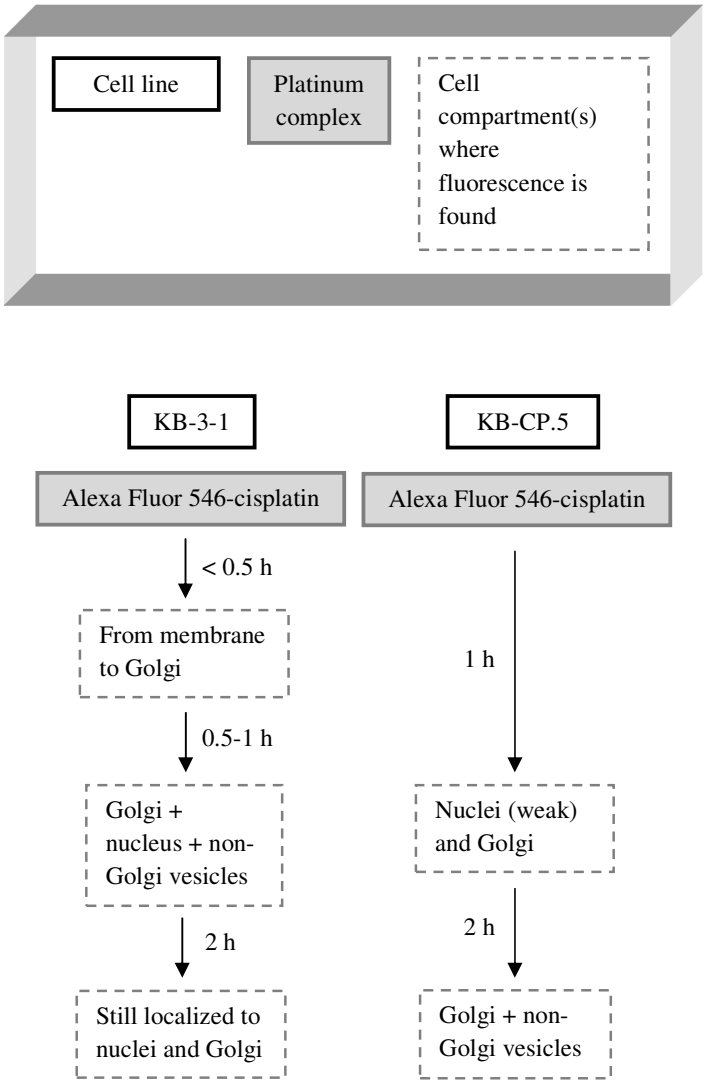

Chart 13.3. Flow chart summarize of results obtained by Liang et al. (*99*)**.** The structure of Alexa Fluor 546-cisplatin is not available.

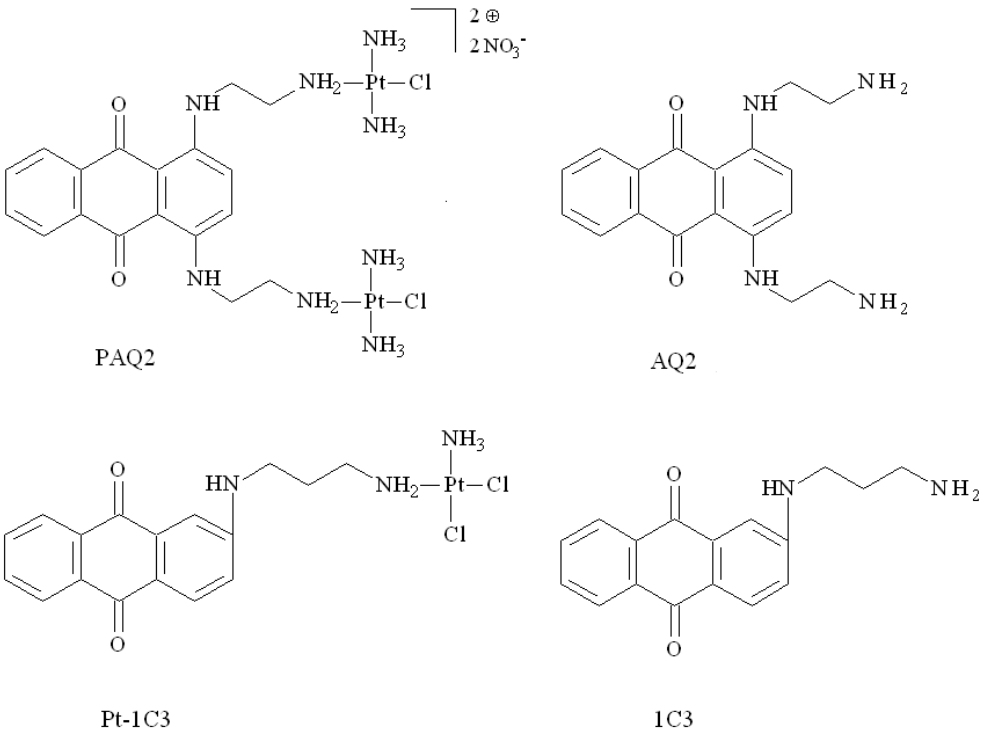

Figure 13.1. Structures of labels and complexes used in the literature *(95-96, 98, 309)*.

13.2 Direct visual techniques for investigation of subcellular localization of platinum complexes, presentation of studies from the literature

Beretta et al. (*92*) used electron microscopy to follow the subcellular path of cisplatin in cells of the human ovarian carcinoma cell line A2780/BBR3464 with resistance to the trinuclear platinum complex BBR3463 and slight cross resistance to cisplatin. Deposits of cisplatin could be seen at the plasma membrane and the nuclear envelope after 5 and 15 min respectively after incubation of the cells with 100 µM. Inside of the nucleus, several platinum deposits could be seen in nucleoli after 30 min of incubation. Presence in organelles apart from those mentioned above was not reported.

Hall et al. (*94*) used synchrotron radiation-induced X-ray emission to investigate the subcellular distribution of cisplatin in A2780 human ovarian cancer cells after 24 h of incubation with 20 µM. Platinum was reported to be situated in the nucleus.

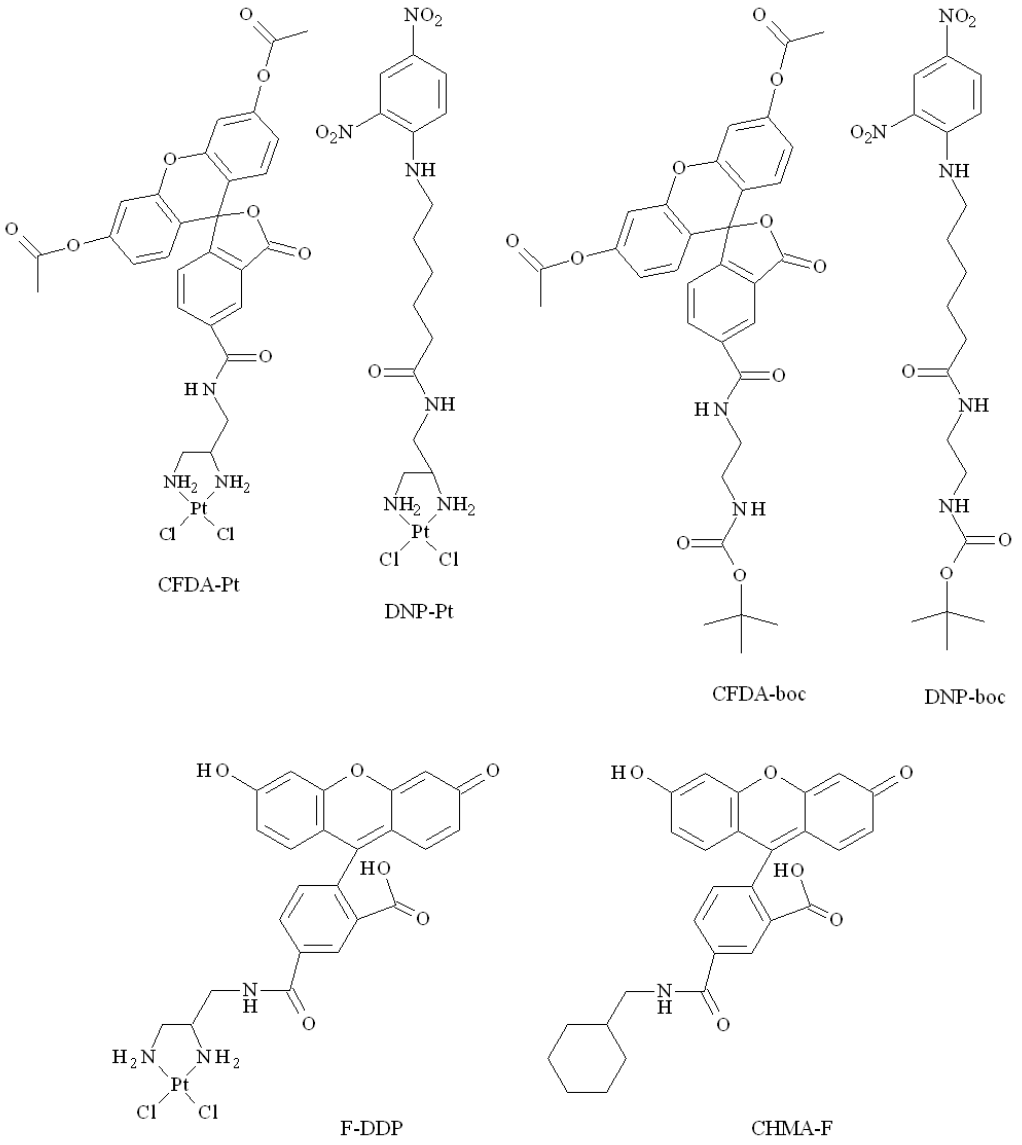

Figure 13.2. Structures of labels and complexes used in the literature (*100, 310*)**.**

Using particle induced X-ray emission, Moretto et al. (*311*) found a homogenous subcellular distribution of cisplatin in cells of the ovarian carcinoma cell line IGROV1-p.

As early as 1978, Khan et al. (*93*) investigated the intracellular distribution of cisplatin in HeLa cells using scanning transmission electron microscopy (STEM) after incubation of cells with 200 µM cisplatin during 4 h. Electron dense areas were reported in nuclear compartments such as nucleoli and the inner nuclear membrane.

Using electron probe microanalysis, the authors confirmed the electron dense areas to be platinum. Little platinum was found in the cytoplasm (*93*).

13.3 Discussion, indirect and direct methods

The methods of determining subcellular platinum distributions presented in section 13.1 and 13.2 are using cisplatin (direct method) or fluorescently labeled platinum complexes with either cisplatin or a complex similar to cisplatin as platinum moiety (indirect method). Therefore, the determination of subcellular localization of this complex will be discussed.

The complex Pt-1C3, investigated by Alderden et al. (*98*), was reported not to localize to nuclei. For the labeled complexes CFDA-Pt (*100*), DNP-Pt (*100*) and Alexa Fluor 546-cisplatin (*99*), binding to cellular DNA was not investigated but it was mentioned that the complexes are able to bind to N7 (see fig. 1.4) in guanine bases. F-DDP was reported to be localized to nuclei after 1 h (*310*) but that was the last time point included and DNA binding was not investigated. Molenaar et al. (*100*) could not find any co-localization of their fluorescently labeled platinum complex (CFDA-Pt) with markers for mitochondria. Some of the direct methods (section 13.2) do not report cisplatin accumulation to mitochondria.

While the direct methods mainly detected platinum in the nuclei, the indirect methods also pointed out cytoplasmic organelles such as the Golgi apparatus and lysosomes as important contributors to the distribution of the complexes inside the cells. The use of different cell lines, sample preparation and detection methods, loading- and incubation times make direct comparisons difficult. Some loss of diffusible material occurs during sample preparation prior to electron microscopy investigations whereas this is not the case for live imaging techniques. A subcellular fractionation method might be a good complement to the indirect visual methods and more questions can be answered concerning the representativeness of the labeled complexes for the corresponding unlabelled platinum complexes regarding subcellular distribution. A combination of both visual and fractionation methods might therefore give a better view of the intracellular distribution pattern of platinum complexes than the methods alone.

The method presented in the present work is different from the visual techniques in many aspects. Some of its advantages and disadvantages are summarized below (section 13.4). The results presented here show that platinum from cisplatin, $m4FPtCl_2$, $dl4FPtCl_2$ and mDAH4FPtCl is found in both the cell nuclei fraction, the three fractions originating from density centrifugation of LMF and the plasma membrane fraction (fig. 6.1-6.3) after an incubation time of 2 h with the complexes.

13.4 Advantages, disadvantages and considerations of the subcellular fractionation method used in the present study

- There is no need for a fluorescent tag because it is the platinum atom in the complexes that is the subject for detection.
- The material from all cells in a culture flask is analyzed and it is the distribution in the majority of the cells that is represented.
- There is an overlap of organelle markers between the fractions (fig. 5.1 and 5.3) and it is therefore difficult to assign the presence of platinum in one fraction to a certain population of organelles.
- The presence of organelle markers does not necessarily guarantee the presence of intact organelles.
- The number and length of possible incubation times of cells with substances are limited by:
    - the need to purify the material directly after incubation.
    - the toxicity, or lack thereof, of the tested complexes.
- Since the purification time is longer than the incubation time, there is a risk that the quantities of substance in the collected fractions are underestimated because of diffusion.
- The protocol might need changes if a different cell line is to be used.
- The path of the complexes inside of the cells over time cannot be followed i.e. short incubation of the cells with complex followed by wash and analysis at subsequent time points is not feasible which is partly due to the required purification time. Instead, the complexes are present in the culture medium until the cells are collected.
- All cellular compartments are not represented, e.g. cytosol.

14 Conclusion

The aim of the present work was to develop methods for the investigation of subcellular distribution of the platinum complexes cisplatin (fig. 1.1), m4FPtCl_2, dl4FPtCl_2 and mDAH4FPtCl (fig. 1.7) in cancer cell monolayer cultures. This was achieved by employing subcellular fractionation to generate different fractions in which the platinum content could be determined using FAAS after incubating the cells (HeLa) with the complex of interest. In previous works, cisplatin, m4FPtCl_2, dl4FPtCl_2 and mDAH4FPtCl have been shown to display differences regarding cytotoxicity, protein- and DNA binding and total accumulation in nuclei and in whole cells (*85*). It was desired in the present work to investigate if these four complexes also display different subcellular distributions. The methods developed and used here have also been critically canvassed and compared with other methods that aim to map the subcellular distribution of platinum complexes.

Differences between the complexes in their relative subcellular distribution were small (fig. 6.1-6.3). This might partly be explained by organelle overlap between the fractions, as seen in western blot analysis (fig. 5.3). The cryo-electron microscopy analysis indicates that the mitochondria are broken since obvious mitochondrial structures were absent in fraction 3. A vesicle suspected to be of mitochondrial origin was seen in fraction 4 (fig. 11.8C). This was also concluded for some of the peroxisomes because of the low banding densities of the peroxisomal marker in the density gradient (fig. 5.3). This was believed to be the consequence of hypotonic lysis and frequent re-suspensions during sample processing and a more gentle disruption procedure than the hypotonic lysis method used in the present work might enhance the gradient separation efficiency. The non-quantifiable HRP concentrations in fraction 4 (fig. 8.1) could be explained by the lack of sufficient endocytotic structures (endosomes, lysosomes) which was supported by cryo-electron microscopy (fig. 11.8 and 11.11) and a weak LAMP1 band in this fraction relative to the other fractions in the western blot (fig. 5.3).

The subcellular distribution of HRP (fig. 8.1) in fractions 2, 3, 4 and M differed from the subcellular distribution of the platinum complexes (fig. 6.1-6.3). The differences were smaller than expected because HRP uptake is dependent on endocytosis. However, the results for HRP might have been biased by enzymatic digestion (section

5.10.1). Diffusion is thought to be a contributing factor to the whole cell accumulation of cisplatin and mDAH4FPtCl because the accumulation was not saturable up to 60 μM (fig. 10.1) and not mediated by one of three common endocytosis pathways (see below). For $m4FPtCl_2$ and $dl4FPtCl_2$, the relation between whole cell associated platinum and concentration seemed to follow a non-linear fashion (fig 10.1 and 10.2). The accumulation of $m4FPtCl_2$ was shown also not to be inhibited by inhibitors of three endocytotic pathways (see below). The highest percent of platinum was found in the cell nuclei (~ 10-25 %, depending on complex) (fig. 6.2) fraction for all complexes but this fraction is also the fraction richest in material and the selectivity was not different compared to the other fractions (fig. 6.1).

The contribution of three different fluid-phase endocytosis pathways to the whole cell accumulation of cisplatin, $m4FPtCl_2$, mDAH4FPtCl and HRP was investigated (fig. 9.1). The uptake of HRP was reduced with ~ 50 % by inhibitors for the two pathways macropinocytosis and clathrin-dependent endocytosis but not by an inhibitor for caveolae-dependent endocytosis. None of the inhibitors caused a decrease in whole cell accumulation of any of the tested platinum complexes.

To investigate if the complexes are capable of entering the mitochondria and to bind to mitochondrial DNA, mitochondrial DNA was collected after incubation of the cells with the complexes. The associated amounts of $m4FPtCl_2$ and cisplatin with collected mitochondrial and genomic DNA after 24 h of incubation (fig. 6.5) were similar. This is interesting because cisplatin is poorly accumulated in the cells compared to the other complexes (fig. 6.4). Similar DNA associated amounts of $dl4FPtCl_2$ were found despite the use of a concentration four times lower than for the other complexes.

The octanol/water distribution of the complexes was similar for all complexes except cisplatin (fig. 4.1) when culture medium was employed as aqueous phase.

To investigate if $m4FPtCl_2$ and $dl4FPtCl_2$ employ common uptake mechanisms with cisplatin and/or with each other, resistant MCF-7 cells were developed with tolerance to each of the three platinum complexes. The cross-resistance of cisplatin with $m4FPtCl_2$ and $dl4FPtCl_2$ was very low. However, cells resistant to $dl4FPtCl_2$ displayed some tolerance against $m4FPtCl_2$ which might be an indication that they share some mechanisms of action (fig. 12.1). The uptake of cisplatin was reduced by half in the resistant cells compared to control cells. For $m4FPtCl_2$ and $dl4FPtCl_2$,

uptake did not seem to play a role in the resistance mechanism. However, additional tests are needed for substantial results. The rate at which the cells adapted to m4FPtCl_2 was faster than for cisplatin for which the cells were more sensitive to small increases in concentration.

The present work lists many important aspects one needs to consider before starting up accumulation tests of platinum complexes in whole cells and subcellular fractions. It also presents the applied methods in a critical way e.g. what limitations they have in the context of platinum accumulation in cells and in subcellular fractions. If subjected to further optimization, the methods might yield stronger conclusions regarding subcellular distribution of platinum complexes.

15 Materials and methods

15.1 Cell culture and test preparations

MCF-7 and HeLa cells were passaged weekly and at least twice a week respectively. After washing with PBS, a small volume of trypsin solution was added and after visible detachment from the flask surface, the cells were suspended in Dulbecco's modified Eagle Medium (DMEM) containing 5 % foetal bovine serum (FBS). For HeLa cells, DMEM without phenol red was used. For MCF-7 cells, 1 ml of cell suspension from a 75 cm^2 culture flask with 75-80 % confluency was transferred to a new flask containing 10 ml fresh culture medium (FBS supplemented DMEM). For HeLa cells, 0.5 ml of suspension was transferred. Prior to seeding out for a test in culture plates, the cell suspension was counted using an Ussing chamber.

15.2 Whole cell uptake

The uptake tests were performed when the cells had reached a confluency of 70-80 %, usually after 5 days. To prevent the cells from growing into multiple layers, the plates were shaken mildly once daily the first four days of incubation (37 °C, 5 % CO_2) and only wells containing mono-layers were used. For uptake measurements with cells growing in 175 cm^2-flasks, 1 ml of a HeLa cell suspension (in a total of 26 ml cell culture medium) from a 75-80 % confluent cell culture was sufficient to reach the same flask surface coverage after four days of incubation. When HeLa cells were seeded out to 6-well microtiter plates, 2 ml of cell suspension with 2 x 10^5 cells/ml were transferred to each well and the cells incubated for five days prior to substance addition. For MCF-7 cells, 2 ml of a suspension with 5 x 10^5 cells/ml were transferred to each well.

15.3 Platinum quantification using FAAS

Prior to all sample measurements, a standard curve was measured from freshly prepared standard solutions with the concentrations 0/10/25/50/100/200/300 and 400 µg/L platinum using a platinum standard (platinum standard = hexachloroplatinic acid in hydrochloric acid). If Triton X-100 was used for sample stabilization (generally for whole cell lysates) the calibration solutions contained the same concentration of this agent. Hydrochloric acid was added to the calibration solutions to the final concentration of 3 % (25 µl of 18 % HCl in a total of 150 µl). All solutions were

measured using the settings presented in table 15.1. All samples were sonicated prior to analysis (see section 15.4). All solutions were measured twice and if the relative standard deviation exceeded 5 % (95.4 % significance level), the solutions were prepared new and/or measured again with thorough mixing prior to each measurement. The auto sampler tubing was flushed in cycles of 5 after every measurement. One extra step of cleaning was performed after completion of the standard curve.

Background correction	Field-mode	Field-strength (T)	Wavelength of analysis (nm)	Lamp current (mA)	Width of slit (nm)	Volume injected (µl)
Zeeman	2	0.9	265.9	6.0	0.2	20

Table 15.1. Fixed parameters used during the platinum quantification with FAAS. T= tesla, A= ampere.

15.4 Sonication of cells and subcellular fractions

Prior to measurements of whole cells, whole cell homogenates and cell fractions where a fine suspension and disruption of organelles was needed, the samples were sonicated (sonotrode) 6 times with the maximal power switch positioned at MS72/D and sound duration of 35 cycles (repeats).

15.5 Protein determination

The ready-to-use Bradford reagent solution used for protein quantification was prepared by diluting the concentrated solution 1:5 with bi-distilled water. An aliquot of the lysate was diluted with bi-distilled water and 20 µl (three wells per sample) of the diluted lysate were transferred to 200 µl of Bradford reagent in microtiter plates. After mixing using a multichannel micropipette, the plate was left to equilibrate for 20 min followed by absorption measurement at 590 and 450 nm respectively. If detergent (Triton X-100) was present in the samples, the same amount of detergent was added to the calibration solutions. The ratio of absorption at 590 nm to 450 nm (A_{590}/A_{450}) was plotted against the protein concentration. The standard curve contained solutions of 0.0, 0.025, 0.05, 0.075, 0.1, 0.125, 0.15, and 0.175 mg/ml HSA from which 20 µl was added to the Bradford reagent. When only sparse amounts of sample were available, 10 µl of sample suspension and 100 µl of Bradford reagent were used instead.

15.6 Chemosensitivity test, crystal violet assay

The cells were washed in PBS, suspended (described in section 15.1) and seeded into 96-well microtiter plates with 100 µl/well of a suspension containing 7500 MCF-7 cells/ml or 2500 HeLa cells/ml. The cells were left in the incubation chamber (37 °C, 5 % CO_2) for 72 h prior to the addition of test substances. The substances were diluted in cell culture medium from stock solutions and 100µl/well were added for final concentrations of 0.1-50 µM (one row per concentration, maximal solvent concentration = 0.1 % (v/v)). After 96 h of incubation, the culture medium was sucked off and the cells fixed with 100 µl of 1 % glutardialdehyde in PBS. After removal of the fixing solution, 180 µl of PBS was added and the plates stored at 4 °C until analysis. To stain remaining biomass, the PBS was removed and 100 µl/well of crystal violet solution was added and left for 30 min at room temperature. By leaving the plates in a water bath for 15 min, the excess of stain was removed. After removal of water, 180 µl/well of 70 % ethanol was added and the plates were shaken mildly for 3-4 h. Absorbance was measured at 590 nm.

15.7 Incubation of cells with substances for uptake studies

After the cells had reached a confluence of 70-80 %, the old culture medium was removed and new FBS-lacking culture medium, containing the test substances, was added. Stock solutions with appropriate concentrations were used to avoid solvent (DMF) concentration exceeding 0.1 % (v/v). Volumes of culture medium were 25 ml for 175 cm^2 culture flasks and 2 ml for wells of the 6-well plates.

15.8 Subcellular fractionation

After incubation with test substance, the cells were suspended as described in section 15.1. The cell suspension was centrifuged at 339 g at 4 °C for 3 min, washed twice in PBS and finally collected at 693 g for 3 min at 4 °C for a more firmly packed pellet. The supernatant was sucked off, leaving as little buffer as possible without disturbing the pellet. Each pellet from one 175 cm^2 culture flask was re-suspended in 3 ml of ice-cold RSB using a micropipette and left to swell for 10 min on ice. For each substance, two flasks (175 cm^2) were used and the suspensions (3 ml each) were carefully combined (by pouring) in a Dounce glass homogenizer (15 ml capacity). The swollen cells were mechanically lysed with 20 strokes (pestle B). Before the addition of 2 ml ice-cold sucrose stabilization solution and 100 µl of protease inhibitor cocktail (not in

the MOM experiment (section 5.10)), a small aliquot of lysate was collected and immediately stored at -20 °C.

Nuclei and undisrupted cells were removed at 1300 g for 5 min at 4 °C. The supernatant was collected and re-spun. The resulting supernatant (PNF) was distributed in 1.5 ml micro tubes. Care was taken not to collect the layer close to the small nuclei pellet which consisted of non-pelleted nuclei. The PNF was controlled for nuclei contamination under the phase contrast microscope. The supernatant was spun at 15000 g for 10 min at 4 °C and the resulting supernatant collected (fraction M). The resulting pellets (LMF) were washed once in isotonic sucrose and re-spun. After discarding the supernatant, the pellets were re-suspended in 1 ml of iodixanol solution A and 5 µl of protease inhibitor cocktail was added (not in the MOM experiment (section 5.10)) followed by storage on ice. The gradient medium solutions were prepared by diluting the 50 % iodixanol solution with iodixanol solution A for concentrations of 5, 10, 17, 20, 25 and 30 % iodixanol. The solutions were controlled refractometrically and deviations higher than ± 0.0005 from the values in the manufacturer's description (Axis shield) were corrected by the addition of iodixanol solution A or 50 % iodixanol solution.

For the preparation of density gradients, 1 ml of 30 % iodixanol was added to centrifugation tubes (14 x 89 mm) using a micropipette and 1.5 ml of the gradient solutions were added carefully using a 1 ml syringe and a 20 G x 2 3/4 needle. The gradients were prepared on ice and all the solutions were pre-cooled. One centrifugation tube containing fraction M was used to calibrate one density gradient by the addition of isotonic sucrose. The density gradients and their respective fraction M were centrifuged at 28400 rpm (= 100000 g_{av} = 138868 g_{max}) for 1.5 h at 4 °C in a SW41T_i rotor. The cell material gathered at the density layer interfaces was collected using the same type of syringe and needle that was used for preparation of the density gradients. Each collected fraction (approximately 300-320 µl) was diluted with 100 µl of PBS and distributed in two centrifugation tubes (7 x 20 mm). The diluted fractions were spun at 55000 rpm (= 13200 g_{max} = 117000 g_{av} = 102000 g_{min}) for 20 min at 4 °C in a TLA100 rotor. The pellets were re-suspended in ice-cold PBS and solutions originating from the same fraction were combined in one tube. After centrifugation (same time and speed), the resulting pellets were re-suspended in 150 µl of ice cold PBS. For the pellets resulting from fraction M, the supernatant was poured off and the

pellet was re-suspended in 500 µl of ice cold PBS and 250 µl transferred to two centrifuge tubes and collected and washed as described for the material from the density gradient. The resulting pellet was re-suspended in 250 µl of ice cold PBS. All the collected samples were stored at -20 °C until analysis.

15.9 Western blot

15.9.1 SDS-PAGE

For each gel (15 pockets), 6 µl of gel sample buffer was added to 20 µl of sample suspension and the mixture heated to 95 °C for 5 min except for those samples being blotted with anti-Na^+/K^+-ATPase which were instead subjected to 60 °C for 5 min. For samples being blotted with anti-Giantin, RIPA buffer was added prior to heating. If nothing else stated, 4.8 µg of protein was loaded on the gel for all samples except for the lysate that was added in five times that amount. The gels were run at 30 mA/gel and 180 V. All gels, except for gels being blotted with anti-Giantin, contained 12 % acrylamide. Because of the large size of Giantin, gels containing 8 % acrylamide were used instead. A size marker containing proteins in the size range of 10-250 kD was applied onto each gel.

15.9.2 Western Blot transfer, antibody incubation and development

The protein transfer was done over night to nitrocellulose membranes with 0.45 µm pore size in transfer buffer containing 10 % ethanol. Transfer buffer for membranes being blotted with anti-Giantin contained 20 % ethanol and 0.1 % (w/v) SDS. As transfer control, Ponceau reagent was added to the membranes after one wash in distilled water. For removal of dye, the membranes were washed three times with PBS. After the addition of 10 % (w/v) fat-free milk (dry powder dissolved in PBS), the membranes were blocked for one hour under mild shaking. For membranes being blotted with anti-Giantin and anti-PMP70, 5 % fat-free milk diluted in TBST buffer was used.

After blocking, only membranes being blocked with 10 % milk were washed three times with PBS prior to the addition of first antibody (primary antibody solutions: anti-Giantin (dilution 1/5000) in TBST buffer containing 5 % fat-free milk, anti-Na^+/K^+-ATPase (dilution 1/5000) in PBS, anti-PMP70 (dilution 1/1000) in TBST buffer containing 5 % fat-free milk, anti-LAMP1 (dilution 1/400) in PBS, anti-

Calnexin (dilution 1/2000) in PBS, anti-MTCO2 (dilution 1/1000) in PBS. Sodium azide was added to all antibody solutions to a final concentration of 0.02 % (w/v)). After incubation at room temperature during mild shaking, the solutions were poured off and excess of antibody was removed by washing the membranes three times with PBS. Membranes incubated with anti-Giantin or anti-PMP70 were washed three times with TBST buffer.

After the washing step, secondary antibodies (anti-rabbit or anti-mouse) were added in a concentration of 1/10000 in PBS containing 5 % fat-free milk. Membranes incubated with anti-Giantin or anti-PMP70 were subjected to secondary antibodies diluted in TBST buffer containing 5 % fat-free milk. All membranes were left for one hour at room temperature and mild shaking. After incubation with secondary antibody, the membranes were washed with distilled water. Each membrane was then exposed to 1 ml of ECL (enhanced chemoluminescence) liquid and the emitted light immediately caught on an X-ray film and developed, mostly after an exposure time of 2 min.

15.10 Purification of cell nuclei

The cells were collected as described in section 15.1 and the freshly prepared cell pellets (corresponding to cells from one 175 cm^2 culture flask) were suspended in 1 ml of RSB and incubated on ice for 10 min. The swollen cells were collected at 600 g for 5 min at 4 °C and re-suspended in 1 ml of ice-cold nuclei lysis buffer and vortexed for 10 s. After the addition of 100 µl citric acid solution, the suspension was vortexed for 10 s. The released nuclei were collected at 600 g for 5 min at 4 °C and the resulting pellet suspended in 500 µl of isotonic sucrose. A small volume was taken out and carefully diluted with a methylene blue solution in PBS and checked for complete cell lysis under the phase contrast microscope. The suspension was under layered with 0.5 ml of 0.88 M sucrose (prepared in bi-distilled water) using a micropipette and the two layers centrifuged at 5000 g for 10 min at 4 °C. Without disrupting the pellet, the uppermost layer together with as much as possible from the denser fraction was carefully removed with a micropipette. After suspending the pellet in 1 ml of PBS, the nuclei were collected at 1000 g for 5 min at 4 °C and stored at -20 °C until analysis.

15.11 Preparation of a HeLa cell membrane fraction (ghosts)

All centrifugation steps were performed in a centrifuge cooled to 4 ºC and all solutions and suspensions were kept on ice. Purification of ghosts from cells that had been

incubated with one substance was made using at least four 175 cm^2 culture flasks with a cell confluence of 60-70 %. Multi-layers and high cell confluency (~ 80 %) lower the yields and the ghosts that were seen after cell lysis were smaller. Consequently, flasks containing multi-layers or a high confluence were not used.

After suspending the cells (as described in section 15.1), they were collected at 339 g at 4 °C for 3 min and washed twice with EBSS (Earle's balanced salt solution) and subsequently collected at 693 g. The supernatant was sucked off and every pellet re-suspended in 10 mM Tris-HCl (pH 8) in a volume corresponding to 20 times the pellet volume. After 10 min of incubation on ice, the cells were lysed using 3-5 slow strokes with pestle B in a Dounce glass homogenizer with 15 ml capacity. After 90 % lysis (or maximum 5 strokes), as seen under the phase contrast microscope, 10 % of the lysate volume of nuclei stabilization buffer was added and an aliquot of the lysate was saved and immediately stored at -20 °C until analysis (if not the same day).

Nuclei and undisrupted cells were collected at 998 g for 2 min and the supernatants collected. The absence of nuclei was controlled under the phase contrast microscope. The longer the delay of the addition of nuclei stabilization buffer, the more difficult it is to pellet the nuclei at the conditions applied in the present work. Membrane ghosts can be recovered from the nuclei pellet and sometimes this was performed successfully but most of the times the ghost fraction was heavily contaminated by nuclei. If recovery was desired, nuclei pellets from four culture flasks were re-suspended in approximately 8 ml of RSB and distributed in two centrifuge tubes. The nuclei were pelleted at 1000 g for 1 min and the supernatant collected. The membrane ghosts were collected at 3056 g for 3 min and the supernatants discarded followed by careful re-suspension of the pellets in approximately 10 ml of RSB/pellet. This step was repeated five times. At this point, the supernatant was left with little contaminating material, as seen under the phase contrast microscope. Further washing steps were assumed to disrupt the ghosts because of the mechanical insult and did not seem to lead to obvious changes in purity when the suspension was investigated under the phase contrast microscope. The final membrane pellet was kept at -20 °C after re-suspension in a small amount of RSB.

15.12 Preparation of mitochondrial and genomic DNA from HeLa cells

The washed cell pellets (section 15.1) were suspended in mtDNA homogenization buffer and after 10 min of incubation on ice (3 ml of buffer to a pellet from one 175 cm^2 flask), lysed with 15 strokes (pestle B) in a Dounce glass homogenizer with 15 ml capacity. After stabilization by the addition of mtDNA sucrose stabilization buffer in a volume corresponding to one third of the lysate volume, the nuclei and undisrupted cells were collected at 1300 g for 5 min at 4 °C. Most of the supernatant was collected and care was taken not to collect the non-pelleted nuclei that were often seen in the two ml closest to the pellet.

The supernatant was re-spun and the remaining solution free of nuclei (as seen under the phase contrast microscope) was distributed in micro tubes with 2 ml capacity. The LMF was collected at 15000 g for 15 min at 4 °C in an Eppendorf centrifuge with a fixed-angle rotor. The supernatants were discarded and each pellet washed three times with 1 ml of mtDNA isotonic sucrose buffer. The resulting pellets were re-suspended in a total of 1 ml of STE/$CaCl_2$ buffer and 20 % (w/v) SDS was added dropwise until the supernatant cleared (approximately 50 µl) followed by addition of proteinase K solution to a total enzyme concentration of 100 µg/ml. The mitochondrial lysate was incubated for one hour at 37 °C and 300 rpm in an Eppendorf thermo mixer. After protein digestion, 1 ml of Tris-equilibrated phenol was added and the fluids mixed gently by inversion. The layers were centrifuged at 20000 g for 30 min at room temperature. The aqueous phase was washed several times with a mixture of phenol/chloroform/isoamyl alcohol (relative volumes = 25:24:1) until the white layer of proteins was absent at the layer interface (usually after three to four washes). After two washes with chloroform, the aqueous phase was washed twice with diethyl ether.

The micro tubes were left open at room temperature for evaporation of the diethyl ether residues. After the addition of 100 µl of 1 M sodium acetate and careful mixing, 700 µl of absolute ethanol was added and the tube turned carefully until the solvents were completely mixed. The DNA was left to precipitate over night at -20 °C. The precipitate was collected at 15000 g for 30 min at 4 °C. After careful removal of the solvent, the DNA left on the walls of the tube was collected by an additional spin for 15 min at the same speed. If the solvent residues could not be removed without disturbing the pellet, the tubes were warmed to 70 °C at 300 rpm in an Eppendorf

thermo mixer but care was taken not to evaporate all fluid. If the pellet is left to dry, the DNA is more difficult to dissolve and the complete loss of solvent can lead to DNA breakage.

The pellet was dissolved in 500 µl of STE buffer and if this was not readily accomplished, the micro tubes were left at 50 °C at 300 rpm for at least 1 h. For the digestion of RNA, RNase A and RNase T_1 was added to final concentrations of 100 µg/ml and 700 units respectively and left at 37 °C and 300 rpm for 1 h. After a second deproteinization, the DNA was precipitated as described above. The DNA pellet was washed once with ice cold ethanol. The ethanol was removed by gentle heating of the tube but the pellet was not left completely dry. The residues were dissolved in 100 µl of bi-distilled water prior to analysis.

15.13 DNA Restriction analysis

Agarose (0.8 % (w/v)) was dissolved in TAE buffer by heating in a microwave oven and Safe Red® was added (final dilution 1: 20000) after cooling and just before gelation. For a total volume of 40 µl, 1 µl of restriction enzyme, 1 µl of 10 % BSA and 4 µl of restriction buffer (New England Biolabs Inc., USA) were added to sample and water. The solutions were mixed carefully with a micropipette. After one hour at 37 °C and 300 rpm in an Eppendorf thermo mixer, 8 µl of DNA loading buffer were added and after careful mixing with a micropipette, 30 µl were loaded on the gel. The gel was run at 150 mA and 200 V and the bands visualized in and captured with a gel documentation camera.

15.14 Endocytosis inhibitor assay

Cells were pre-incubated for 0.5 h with the following inhibitors (final concentrations in brackets) in culture medium lacking FBS: EIPA (70 µM), cytochalasin D (10 µM), chlorpromazine (20 µM) and nystatin (30 µM). To the control cells and to the cells incubated with inhibitor substances that were dissolved in water, solvent (DMF) was added. After pre-incubation, platinum complexes (60 µM cisplatin, 15 µM m4FPtCl_2, 15 µM mDAH4FPtCl) or HRP (0.1 mg/ml) were added together with the inhibitor substances and the cells were further incubated for 2 h. After incubation, the cells were collected, washed and collected as described (see 15.1). The cells incubated with enzyme were shock-frozen in liquid nitrogen and stored at -20 °C together with the other samples prior to analysis.

15.15 Assay of HRP activity

All the samples were sonicated (see section 15.4) and 30 µl transferred to one well in a 96-well microtiter plate. After addition of 270 µl HRP assay buffer and thorough mixing using a micropipette, the cyclic absorption measurements (60 repeats) at 460 nm were immediately started. The cycle number was plotted against the absorption and the small time delays between measurements were ignored (one well at the time is measured and one cycle corresponds to the time it takes for the reader to measure all included wells). Not more than 12 wells were measured at one time. Only the linear part of the curve was used for the calculation of the slope, which in turn was used as a measure of activity.

15.16 Na^+/K^+-ATPase assay

Prior to incubation, 25 µl of sample (purified HeLa cell membrane ghosts or cell lysate) was mixed with 125 µl enzyme release buffer, vortexed, and incubated at room temperature for 10 min. After addition of 350 µl of incubation buffer containing or lacking ouabain, the solutions were left for 30 min in a water bath, warmed to 37 °C. To stop the enzymatic reaction, 500 µl of ice-cold solution 2 was added and the samples left on ice for 10 min followed by the addition of 750 µl of solution 3 and incubation for 10 min at 37 °C.

The standard solutions (50 µl) were transferred directly to the 96-well plate in replicates of three. After addition of 100 µl of solution 2 and incubation on ice, 150 µl of solution 3 was added and the plate incubated at 37 ºC in an incubation chamber. The sample solutions were transferred to the plate in volumes of 300 µl/well (in replicates of four). Bubbles were carefully removed using an injection needle. The absorbance was measured at 710 nm or 590 nm and the amount of released PO_4^{3-} in every fraction calculated from the standard curve.

For absorbance at 710 nm, the calibration curve was not linear beyond 45 µM PO_4^{3-}. When absorbance was measured at 590 nm, the linearity was extended to higher concentrations because of the decline in sensitivity. For every sample, three solutions were prepared. One solution was incubated with a final concentration of 1 mM of the inhibitor ouabain, one without the inhibitor and one lacking sample solution at the time of incubation (control). Sample solution was added to the control after addition of

solution 2. The control solution compensates for the already in the sample existing phosphate and for non-specific release during the assay.

For preparation of standards solutions, K_2HPO_4 was dissolved in bi-distilled water for concentrations in the range of 0-300 µM in the solution that was added to the wells. It was noticed that the samples needed some time after addition of solution 3 and the following incubation to stabilize in colour. After that, the solutions were stable for at least one hour. It is important that the standard solutions are treated with solution 2 and 3 in close time proximity to the samples. The measured release of PO_4^{3-} was expressed as µmol PO_4^{3-}/mg protein.

15.17 Resistant cells

Substances were added to cell culture medium (supplemented with 5 % FBS) at every (weekly) passage with initial concentrations of 0.35 µM for cisplatin and 2 µM for $m4FPtCl_2$ and $dl4FPtCl_2$ respectively. A control culture without substances was kept parallel and all cultures were growing with culture medium containing the same amount of solvent (DMF) with concentrations never exceeding 0.1 % (v/v). The cells reacted by growing slower and the substances had different impacts on growth. As a consequence, different amounts of cell suspension had to be transferred to new flasks from the cultures treated with different platinum complexes to synchronize passage intervals.

Before seeding out cells for whole cell uptake and chemosensitivity assays, the cells were passaged at least once with culture medium lacking both solvent and platinum complexes. The results shown in the present work were obtained with cells surviving approximately 52 passages in substance-containing cell culture medium.

15.18 Transmission electron microscopy

15.18.1 Negative staining

Approximately 2 to 5 µl of sample suspension containing about 100 ng/µl protein were placed on a carbon-coated glow-discharged 400 mesh copper grid (QuantifoilTM, Jena, Germany) and stained with 2 % aqueous uranyl acetate (EMS, Hatfield, PA 19440). Excess of liquid was blotted off using filter paper and the grid was left to dry at room temperature. The sample was examined using a Philips CM100

(FEI, Hillsboro; OR, USA) transmission electron microscope (TEM) and imaged using a Fastscan CCD camera (TVIPS, Gauting, Germany).

15.18.2 Cryofixation

After suspending the final pellets from the subcellular fractionation (fig. 5.1) in a total of 150 µl sterile-filtered PBS, they were further diluted with sterile-filtered PBS prior to analysis. The protein amount was not quantified prior to analysis but fractions 2 and 4 were diluted by 1/2 and fraction 3 by 1/10 to obtain similar amounts of material in the fractions and to avoid thick samples that might resist vitrification. A small volume (3.5 µl) of the sample suspension was applied on a freshly glow discharged 400 mesh carbon coated holey grid (QuantifoilTM, Jena, Germany) at 4 °C and blotted for 10 s before plunge frozen into liquid ethane cooled by liquid nitrogen using a semi-automated Vitrobot^{TM} plunge-freezer (FEI). After vitrification, the grid was placed in a cryo storage box and kept in liquid nitrogen until analysis. The sample was then placed in a Gatan (Pleasanton, CA, USA) cryo holder and analyzed using a 120 kV Tecnai Spirit (FEI) cryo electron microscope, equipped with a 2k Eagle CCD (FEI).

16 Buffers and reagents

The salts and reagents were always dissolved in bi-distilled water, if nothing else stated.

20 % SDS: 2 g SDS in 10 ml bi-distilled water. If precipitated, the tube was hold under warm water until a clear solution was obtained.

50 % Iodixanol solution (12 ml): 2 ml of iodixanol solution B is mixed with 10 ml of OptiPrep™.

Bradford reagent (5 x): 250 ml Serva Blue G, 250 ml 96 % ethanol, 500 ml bi-distilled water and 500 ml 85 % H_3PO_4

Citric acid solution (11 % (w/v)): 1.1 g citric acid, 11 mM $MgCl_2 \cdot 6H_2O$ in 10 ml bi-distilled water

Crystal violet solution (0.02 % (w/v)): 100 mg of crystal violet is dissolved in 500 ml distilled water.

DNA loading buffer (6 x): 30 % glycerol, 0.1 % bromophenol blue

EBSS (Earle's Balanced Salt Solution): 34.5 mM NaCl, 1.26 mM KCl, 0.83 mM $MgSO_4$ x $7H_2O$, 1.17 mM KH_2PO_4, 2.71 mM $NaHCO_3$, 5.55 mM D-Glucose

ECL liquid: 1 ml of ECL solution A is mixed with 0.1 ml of ECL solution B and 0.3 µl of 35 % H_2O_2. The solution is prepared just before usage.

ECL solution A: 50 mg luminol in 20 ml 0.1 M Tris-HCl (pH 8.6), stored at 4 °C

ECL solution B: 22 mg *trans*-4-hydroxycinnamic acid is dissolved in 20 ml DMSO and stored at room temperature in the dark.

Enzyme release buffer (pH 7.0): 0.06 % (w/v) sodium deoxycholate, 25 mM imidazole

Gel sample buffer (4 x): 200 mM Tris-HCl (pH 6.8), 1.43 M β-mercaptoethanol 40 % (v/v) glycerin, 4 % (w/v) SDS and 0.3 mM bromophenol blue.

Glutardialdehyde (fixative) solution (1 % (v/v)): 2 ml of a 25 % glutardialdehyde solution is diluted with PBS to a total volume of 50 ml.

HRP assay buffer (6 ml): 300 µl 1 M KH_2PO_4 (pH 4), 50 µl 1 % (w/v) *o*-dianisidine, 60 µl 0.3 % (v/v) H_2O_2, 67 µl 10 % (v/v) Triton X-100.

Incubation buffer (pH 7.2): 143 mM NaCl, 28.6 mM KCl, 71.43 mM Tris-HCl, 4.29 mM $MgCl_2$, 4.3 mM ATP. Prior to incubation together with the samples, the incubation buffer was mixed with ATP for a total concentration of 4.3 mM. This solution was used to obtain solutions with 1.43 mM ouabain.)

Iodixanol solution A: 10 mM HEPES (pH 7.4), 1 mM EDTA disodium salt, 250 mM sucrose

Iodixanol solution B: 60 mM HEPES (pH 7.4), 6 mM EDTA disodium salt, 250 mM sucrose

Isotonic sucrose: 10 mM Tris-HCl (pH 7.4), 2.5 mM $MgCl_2$, 250 mM sucrose

Methylene blue solution: A spattle tip of methylene blue is solved in PBS and sonicated before use to dissolve eventual crystals.

mtDNA homogenization buffer: 10 mM Tris-HCl (pH 7.4), 1 mM EDTA, 2.5 mM $CaCl_2$

mtDNA isotonic sucrose buffer: 10 mM Tris-HCl (pH 7.4), 250 mM Sucrose, 20 mM EDTA

mtDNA sucrose stabilization buffer: mtDNA homogenization buffer in 1 M sucrose

Nuclei lysis buffer: 10 mM Tris-HCl (pH 7.4), 3 mM $MgCl_2$, 10 mM NaCl, 0.5 % (v/v) Triton X-100

Nuclei stabilization buffer: 10 mM Tris-HCl (pH 7.4), 30 mM $MgCl_2$, 100 mM NaCl

PBS: 8 g NaCl, 0.2 g KCl, 0.2 g KH_2PO_4 and 1.4 g $Na_2HPO_4 \cdot 2H_2O$ in a total of 1 l water

Ponceau reagent (100 x): 2 g Ponceau S, 30 g trichloroacetic acid, 30 g 5-sulfosalicylic acid dihydrate, milli-Q water is added to a total volume of 100 ml.

Preparation of stacking- and separating gels: The volumes of solutions required for gels of concentrations 8 and 12.5 % are listed in table 16.1. After mixing, the solutions were poured into sealed casting forms. Sufficient space was left for the stacking gel in

the forms. A layer of isopropanol was added carefully and the gels were left to polymerize. Before the addition of the stacking gel solution, the alcohol was carefully poured off and the remains sucked off with a paper towel. The stacking solution was added right after the mixing of the ingredients and the gel left to polymerize after insertion of the comb.

Separating gel
4 gels with 15 pockets respectively

Final concentration	Rotiphorese	Tris-HCl (pH 8.8)	20 % SDS	Water (Milli-Q)	Temed	APS
%	ml	ml	µl	ml	µl	µl
8	12	8.4	225	24	225	22.5
12.5	18.75	8.4	225	17.25	225	22.5

Stacking gel
4 gels with 15 pockets respectively

Final concentration	Rotiphorese	Tris-HCl (pH 8.8)	20 % SDS	Water (Milli-Q)	Temed	APS
%	ml	ml	µl	ml	µl	µl
5	2.5	1.875	75	10.5	75	15

Table 16.1. Volumes of solutions required for preparation of SDS-PAGE gels.

Proteinase K solution: 1 mg/ml proteinase K in bi-distilled water, stored at -20 °C

RIPA Buffer (5 x): 750 mM sodium chloride, 5 % (v/v) Triton X-100, 2.5 % (w/v) sodium deoxycholate, 0.5 % (w/v) sodium dodecyl sulphate and 250 mM Tris-HCl (pH 8)

RNase A solution: 10 mg/ml RNase A in 0.15 M NaCl, stored at -20 °C

RSB: 10 mM Tris-HCl (pH 7.4), 3 mM $MgCl_2$, 10 mM NaCl

SDS-PAGE run buffer: 25 mM Tris base, 250 mM glycine, 0.1 % (w/v) SDS

Solution 1 (1 ml): 100 mg ammonium molybdate in 1 ml bi-distilled water

Solution 2 (20 ml): 600 mg of ascorbic acid is dissolved in 1 ml of bi-distilled water and 10 ml of 1 M hydrochloric acid is added and the solution left on ice for at least ten minutes. After addition of solution 1 (1 ml), a shift from colourless to bright yellow should be seen. If the solution turns blue-green, it has to be discarded. Thereafter, 3 ml of 20 % (w/v) SDS is added and the solution kept on ice throughout the assay.

Solution 3 (30 ml): 1050 mg bismuth citrate is dissolved in 10 ml of 1 M hydrochloric acid and subsequently 1050 mg sodium citrate is added. It is important that the first salt is fully dissolved before the addition of the second salt.

STE buffer: 50 mM Tris-HCl (pH 7.4), 100 mM NaCl

STE/$CaCl_2$ buffer: 50 mM Tris-HCl (pH 7.4), 100 mM NaCl, 2.5 mM $CaCl_2$

Sucrose stabilization solution: 1 M sucrose

TAE buffer: 40 mM Tris base, 40 mM acetic acid, 1 mM EDTA

TBST-buffer: 50 mM Tris-HCl, 150 mM NaCl, 0.05 % (v/v) Tween 20 in milli-Q water

Transfer buffer: 25 mM Tris base, 10 % (v/v) 96 % ethanol, 192 mM glycine

Trypsin solution (0.17 % (w/v)): 500 mg trypsin and 200 mg EDTA disodium salt were dissolved in 300 ml PBS solution and sterile filtered through a 0.22 µm pore-size filter.

17 Instrumentation and materials

17.1 Instrumentation

Adjustable multichannel pipettes

8 and 12 channel Eppendorf Research, 30-300 µl (Eppendorf AG, Germany)

Transferpette-12, 20-200 µl (Brand GmbH, Germany)

Adjustable single channel pipettes

Eppendorf Research, 0.5-10 µl, 10-100 µl, 20-200 µl, 100-1000 µl (Eppendorf AG, Germany)

Transferpette 2-20 µl (Brand GmbH, Germany)

Analytical scale

BP 211D (Sartorius AG, Germany)

BP 210D (Sartorius AG, Germany)

Atomic absorption spectrometer

ZEEnit 600 (Analytik Jena, Germany)

Autoclave

Systec 2540 EL (Systec GmbH, Germany)

Balance

MP-300 electronic balance (Chyo, Japan)

L2200 P (Sartorius AG, Germany)

Benchtop centrifuges

5417R (Eppendorf AG, Germany)

Megafuge 1.0 R (Heraeus, USA)

Benchtop ultracentrifuge

Optima^{TM} TL (Beckman, USA)

Bio waste flask 4 l polypropylene (Integra Biosciences GmbH, Germany)

Dry block heater

UBD (Grant, UK)

Electrophoresis cells

For SDS-PAGE: Mini-protean tetra system (Biorad, USA)

For transfer: Transblot-cell (Biorad, USA)

Electrophoresis power supply

EPS 301 (Amersham Biosciences, Switzerland)

Agarose gel horizontal electrophoresis system (In-house production at ZMBH,

Heidelberg University)

Gel imaging system

AlphaImager 2200 (Biozym, Germany)

Hemocytometer

Neubauer improved (Marienfeld, Germany)

Incubation chamber

HERAcell 240 (Thermo Scientific, Germany)

Microplate readers

FLASHScan S12 (Analytik Jena, Germany)

Viktor^2 1420 Multilabel counter (Perkin Elmer, Finland)

pH meter

761 Calimatic (Knick, Germany)

Portamess 911 (Knick, Germany)

Phase contrast microscope

Axiovert 25 (Carl Zeiss, Germany)

Axiovert 40 CFl (Carl Zeiss, Germany) equipped with a digital color camera Imaging source CC6 (Inteq, Germany)

Power supply

2000/200 (Biorad, USA)

EPS 301 (Amersham, USA)

Safety cabinet

Hera Safe Heraeus (Thermo Scientific, Germany)

Scanner

Perfection 3200 Photo (Epson, Germany)

Serological pipette controller Pipetboy acu with 8-channel suction mouthpiece

(Integra Biosciences, Germany)

Shaking tables

CAT ST5 (Neolab, Germany)

Gerhardt LS10 (Gerhardt, Germany)

Sonotrode

Generator Sonopuls GM 70 (Bandelin, Germany)

Tip SH 70 G (Bandelin, Germany)

Spectrophotometer

Nanodrop1000 (Thermo Scientific/PeqLab, Germany) for UV-Vis

Thermomixer

Eppendorf thermomixer comfort 1.5 ml (Eppendorf AG, Germany)

Ultracentrifuge

L-60 (Beckman, USA)

Ultrasound bath

Sonorex RK100 (Bandelin, Germany)

Vacuum pump

Laboport (KNF Neuberger, Germany)

Vortex mixer

Vortex Genie 2 (Scientific Industries, USA)

Reax 2000 (Heidolph, Germany)

VF2 (Janke & Kunkel, Germany)

Water bath

Köttermann (Köttermann, Germany)

X-Ray film processor

Cawomat 2000 IR (Cawo, Germany)

17.2 Cell lines

MCF-7 was a kind gift from Prof. Dr. Stefan Wölfl, University of Heidelberg.

HeLa, cervical adenocarcinoma cell line (ATCC-LGC Standards, USA)

17.3 Chemicals and Reagents

If nothing else is written, all chemicals (analytical grade or higher) were purchased from Sigma-Aldrich (Fluka included), USA.

1 kB DNA ladder (Invitrogen, USA)

2-Mercaptoethanol

3-Methylbutanol

5-(N-Ethyl-N-isopropyl) amiloride

Acetic acid (Roth, Germany)

Agarose (Invitrogen, USA)

Albumin from human serum

Amiloride hydrochloride hydrate

Ammonium molybdate tetrahydrate

Antibodies

Primary antibodies were purchased from Abcam, United Kingdom

Anti-aktin (Chemicon International, USA)

Anti-mouse (Promega, USA)

Anti-rabbit (Promega, USA)

APS (Roth, Germany)

Argon (Air Liquide, Germany)

ATP

Bismuth (III) citrate

BSA (New England Biolabs Inc., USA)

Bromophenol blue (Serva, Germany)

Coomassie Brilliant Blue R (Serva, Germany)

Chloroform

Chlorpromazine hydrochloride

Citric acid

Crystal violet (Roth, Germany)

Cytochalasin D from *Zygosporium mansonii*

D-(+)-Glucose anhydrous

Developer and fixing fluid (Unimatic, Calbe Fotochemie GmbH, Germany)

DMEM, with and without phenol red (PAA Laboratories GmbH, Austria)

DMSO (Roth, Germany)

EDTA disodium salt dihydrate (Acros Organics, USA)

Ethanol 96 % (Merck, Germany)

FBS (Biochrom AG, Germany)

Glutardialdehyde (Merck, Germany)

Glycerol (Roth, Germany)

Glycine (Roth, Germany)

HEPES

H-Gly-Phe-βNA (Bachem, Germany) (GPN)

H-Met-OMe x HCl (Bachem, Germany) (MOM)

Hydrochloric acid (Fischer scientific, Germany)

Hydrogen peroxide

Imidazole

Isopropanol (Brenntag AG, Germany)

Iodixanol density gradient medium OptiPrep™ (Axis-shield, Norway)

L (+)-Ascorbic acid (Merck, Germany)

Luminol

Magnesium chloride hexahydrate

Magnesium sulphate heptahydrate (Acros Organics, USA)

Methanol (Brenntag AG, Germany)

Methylene blue (Merck, Germany)

Nitric acid

N, N-Dimethylformamide

Non-fat dry milk, frema Reform (Granovita, Germany)

Nystatin

o-dianisidine

Octanol (Merck, Germany)

Ouabain

Percoll®

Peroxidase, from horseradish

Ponceau S (Roth, Germany)

Potassium chloride (Merck, Germany)

Potassium phosphate dibasic anhydrous

Potassium phosphate monobasic

Protease inhibitor cocktail

Proteinase from *Tritirachium album*

Proteinase K from baker's yeast (*S. cervisiae*)

Platinum-standard solution

Pyruvic acid sodium salt (Carl Roth, Germany)

Restriction enzymes

Hind III, *Bam* HI (New England Biolabs Inc., USA)

Ribonuclease A from bovine pancreas

Ribonuclease T_1 from *Aspergillus oryzae*, ammonium sulphate suspension

Rotiphorese® GEL 30, 30 % Acrylamide, 0.8 % Bisacrylamide (Carl Roth, Germany)

SafeRed Nucleic acid stain (Intron Biotechnology Inc., Korea)

Size Marker for Slab Gels (Biorad, USA)

Sodium acide

Sodium chloride

Sodium citrate tribasic dehydrate

Sodium deoxycholate (Acros Organics, USA)

Sodium dodecyl sulphate (Merck, Germany)

Sodium hydrogen carbonate (Alfa Aesar, USA)

Sodium phosphate dibasic dehydrate

Sucrose

Sulfosalicylic acid dihydrate

Temed (Pharmacia, Sweden)

trans-4-Hydroxycinnamic acid

Trichloroacetic acid (Merck, Germany)

Tris-equilibrated phenol solution

Triton™ X-100

Trizma® hydrochloride

Trypsin from porcine pancreas

Tween® 20

17.4 Consumables

Cell culture flasks

- 25 cm^2, 175 cm^2 (Sarstedt AG, Germany)
- 75 cm^2 (TPP, CH)

Centrifuge tubes

- 15 ml, 50 ml (Sarstedt AG, Germany)
- 7 x 20 mm, 14 x 89 mm (Beckman Coulter, Germany)

Filter paper

- Whatman 3MM (Whatman International Ltd., Great Britain)

Gloves

- Latex gloves (VWR International GmbH, Germany)
- Kolibri latex gloves (Igefa, Germany)
- Rotiprotect nitril (Roth, Germany)

Hypodermic needle

- Sterican® (B. Braun, Germany)

Kimtech cleaning wipes (Kimberly-Clark, GB)

Microtiter plates 96-well (Nunc, DK)

Nitrocellulose membrane

- Porablot NCP, 0.45 µM pore-size (Macherey-Nagel, Germany)

Parafilm (Pechiney Plastic Packaging, USA)

Pasteur pipettes (Carl Roth, Germany)

Pipette tips

10 µl (Eppendorf AG, Germany)

200 µl, 250 µl, 1000 µl (Sarstedt AG, Germany)

Micro tubes 1.5 ml, 2 ml (Sarstedt AG, Germany)

Sample vials for FAAS

0.5 ml and 1.5 ml, polystyrene (Analytik Jena, Germany)

Serological pipettes sterile

2 ml, 5 ml, 10 ml, 25 ml (Sarstedt AG, Germany)

Sterile filter

500 ml Steritop 0.22 µM (Millipore, Germany)

Millipore Express™ plus 0.22 µM (Millipore, Germany)

Syringe filters Rotalibo 0.22 µM (Carl Roth, Germany)

Syringes 1 ml, 5 ml 10 ml and 50 ml (B.Braun, Germany)

Tissue culture plates 6-well (Sarstedt INC, USA)

X-Ray film (Konica Minolta/Hartenstein, Germany)

17.5 Software

Acrobat reader (Adobe systems, USA)

Epson perfection 3200 (Epson, Germany)

ImageJ (National Institutes of Health (*312*), USA, http://rsb.info.nih.gov/ij/)

IQ Easy Measure (Inteq, Germany)

Microsoft Office (Microsoft, USA)

Nanodrop1000 software (Thermo Scientific/PeqLab, Germany)

Origin (OriginLab Corporation, USA)

Paint (Microsoft, USA)

Wallac 1420 workstation (Perkin Elmer, Finland)

WinAAS® (Analytik Jena, Germany)

Winflash (Analytik Jena, Germany)

18 Zusammenfassung

Platinkomplexe haben eine wichtige Position in der heutigen Krebstherapie. Hoden- und Ovarialkrebs können damit erfolgreich behandelt werden. Cisplatin ist der erste therapeutisch verwendete Platinkomplex. Seit dem Entdecken seiner biologischen Wirkung in den sechziger Jahren, ist ein erhebliches Forschungsfeld im Gang gesetzt werden im welchen ein Vielzahl von chemischen Modifizierungen von Cisplatin untersucht worden sind. Das Ziel ist einen neuen Komplex mit erhöhter Zytotoxizität und weniger Nebenwirkungen zu finden. Um ihre Zytotoxizität zu bewerten, werden neue Platinkomplexe häufig in Zellkulturen von Krebszellen getestet. Weitere Methoden um der Interaktion zwischen biologisches Material und Platinkomplexe zu charakterisieren, sind Untersuchungen wie Zellaufnahme und subzelluläre Distribution wie z.B. Platinmengen assoziiert mit der Zellkern und/oder Bindung des Platins am Erbgut. Der Schwerpunkt dieser Arbeit liegt an den Untersuchungen der subzellulären Distribution von den Platinkomplexen cisplatin, m4FPtCl_2, dl4FPtCl_2 und mDAH4FPtCl (zwei Platinatome). Vorherige Arbeiten haben gezeigt dass die Komplexe Unterschiede bezüglich Zytotoxizität, Assoziation mit Zellen, Zellnuklei und Bindung an der Zellulären DNA aufweisen. Um weitere Informationen über die subzelluläre Distribution der Komplexe zu erhalten, sind in der jetzigen Arbeit verschiedene Zentrifugierungsmethoden benutzt worden um subzelluläre Fraktionen von HeLa Zellen zu erhalten in welchen Platin mittels Atomabsorptionsspektrometrie quantifiziert worden sind. Die Unterschiede in subzellulärer Distribution zwischen den Platinkomplexen nach 2 Std Inkubationszeit waren klein. Dies galt für Prozentuale- sowie auf Protein normalisierten Platinmengen. Die höchsten Platinmengen sind in die Zellnukleifraktion gefunden worden (~ 10-25 % je nach Komplex) aber die Unterschiede zwischen Fraktionen mit auf Protein normalisierte Platinmengen waren relativ klein. Es wird vermutet dass der Densitätsgradient nicht fein genug ist um niedrige Unterschiede in subzellulären Verteilung zwischen Komplexe bemerkbar zu machen. Die Lage des peroxisomalen Markerprotein im Densitätsgradient lässt die Vermutung nahe, dass die Peroxisomen beschädigt sind. Cryo-elektronmikroskopische Analyse der Fraktionen weist darauf hin dass die Mitochondrien als nicht intakt vorliegen. Eine schonende Probenaufarbeitung wurde mutmaßlich die Organellenintegrität besser erhalten und infolgedessen den Abscheidegrad des Gradients erhöhen. Der Zellaufnahmemechanismus kann die subzelluläre Distribution

beeinflussen und deswegen wurden drei Endozytosehemmer eingesetzt. Weder Hemmsubstanzen der Makropinozytose oder Hemmsubstanzen der klathrin- und kaveolinabhängige Endozytose konnte die Zellaufnahme von cisplatin, m4FPtCl_2 oder mDAH4FPtCl beeinflussen. Das Enzym Meerettichperoxidase (HRP) unterschied sich von den Platinkomplexen in seiner subzellulären Distribution und höhere Anreicherung konnte in Fraktionen, die das lysosomale Markerprotein LAMP1 enthalten, gesehen werden. Dennoch können diese Ergebnisse nur benutzt werden um einen Unterschied zwischen Protein und Komplexe festzustellen. Wegen vermuteter lysosomaler Verdauung des Enzyms sind andere Aussagen ausgeschlossen. Die Zellaufnahme von HRP konnte durch Hemmung der Makropinozytose und der klathrinabhängige Endozytose erniedrigt werden. Demzufolge kann die unterschiedliche intrazelluläre Distribution von den Platinkomplexen und das Protein zumindest Teils von unterschiedlichen Zellaufnahmemechanismen erklärt werden.

Quantifizierung des Platins in aufgereinigter mitochondrialer DNS nach Inkubation von HeLa-Zellen mit den Komplexen zeigte dass alle Komplexe mit der DNS assoziiert sind. Vorherigen Arbeiten haben markante Unterschiede in Zellakkumulierung zwischen den Komplexen in MCF-7 Zellen nach 24 Std festgestellt und cisplatin ist in Hinsicht auf die totale Platinmenge in den Zellen, am effektivsten an DNS gebunden. MCF-7 Zellen wurden entweder mit cisplatin, m4FPtCl_2 oder dl4FPtCl_2 kultiviert um Resistenz zu entwickeln. Die cisplatinresistente Zellen waren nicht resistent gegen m4FPtCl_2 oder dl4FPtCl_2. Allerdings zeigten m4FPtCl_2 gewisse Kreuzresistenz gegen dl4FPtCl_2 in Zellen mit Resistenz gegen dl4FPtCl_2. Platinmengen waren niedriger in cisplatinresistente Zellen als in Kontrollzellen nach Inkubation mit cisplatin. Dementsprechend galt nicht für m4FPtCl_2 oder dl4FPtCl_2 in deren respektive resistenten Zelllinien. Es wird vermutet dass der Aufnahmeweg für diese Komplexe nicht mit in den Resistenzmechanismus mit beteiligt ist obwohl mehrere Experimente sind nötig um dies zu befestigen.

19 Abstract

Platinum complexes are frequently employed in the therapy of several cancers such as testicular- and ovarian cancer. The first therapeutically used platinum complex, cisplatin, has been the subject of extensive research since its therapeutic potential was discovered in the Sixties. Ever since, a vast number of chemical modifications have been exploited with the aim to reduce the side effects and enhance cytotoxicity. New platinum complexes are often tested in cancer culture cells to evaluate their cytotoxic potential. To further characterize the complexes, other investigations such as whole cell uptake and subcellular distribution are often conducted e.g. amount in cell nuclei and/or binding to DNA. In the present work, emphasis has been given to the investigation of the subcellular distribution of four platinum complexes, cisplatin, m4FPtCl_2, dl4FPtCl_2 and mDAH4FPtCl (two platinum atoms). In previous works, these complexes have displayed differences regarding cytotoxicity, whole cell- and nuclei accumulation and binding to genomic DNA. To further investigate their subcellular distribution, different centrifugation methods were used in the present work to collect subcellular fractions from HeLa cells where flameless atomic absorption spectrometry was employed for the quantification of platinum. Moreover, the cross-resistance and whole cell associated platinum in MCF-7 cells with acquired resistance was investigated. The differences in subcellular distribution between the platinum complexes were small after 2 h of incubation and this was true for the recovered percentage in each fraction as well as for the protein normalized amounts. The highest platinum amount was found in the cell nuclei fraction (~ 10-25 % depending on the complex) but the differences in protein normalized amounts between the fractions were relatively small. It is suspected that the density gradient is too crude to differentiate between complexes with small differences in their subcellular distribution. The results from the western blot analysis of the subcellular fractions from the density gradient indicate that the peroxisomes might be damaged. Cryo-electron microscopy of the fractions led to the assumption that the integrity of the mitochondria is assaulted. It is believed that a gentler sample preparation method would better preserve organelle integrity and therefore increase gradient separation efficiency. Since the cell entry mechanism might affect the subcellular distribution, the role of three fluid-phase endocytosis mechanisms in whole cell accumulation of cisplatin, m4FPtCl_2 and mDAH4FPtCl were investigated. Inhibitors of

macropinocytosis and clathrin- and caveolin dependent endocytosis did not lower the cell associated platinum amounts for any of the tested complexes. The subcellular distribution of the enzyme horseradish peroxidase (HRP) was different than for the platinum complexes (uptake in nuclei and plasma membrane fractions was not investigated) and a higher accumulation in fractions containing the lysosomal marker protein LAMP1 was seen. However, the results from the subcellular fractionation can only be used to show that the distribution is different for the enzyme than for the platinum complexes because of presumed lysosomal breakdown of HRP. The uptake of HRP was lowered by inhibitors of macropinocytosis and clathrin-dependent endocytosis. Thus, different cell accumulation mechanisms of the platinum complexes and the protein HRP might partly explain differences in subcellular distribution.

Subsequent purification of the mitochondrial DNA after incubation of HeLa cells with the complexes, revealed all complexes to be associated with the DNA. If the whole cell accumulation data is considered, cisplatin is more efficiently bound to HeLa cell DNA compared to the other complexes. MCF-7 cells were cultivated in the presence of cisplatin, m4FPtCl_2 and dl4FPtCl_2 to acquire resistance. MCF-7 cells with resistance to cisplatin were not resistant to m4FPtCl_2 or dl4FPtCl_2. However, m4FPtCl_2 displayed cross resistance to dl4FPtCl_2 in cells tolerant against dl4FPtCl_2. Whole cell associated platinum was lowered for cisplatin in cisplatin resistant cells. No obvious differences in cell uptake were seen for m4FPtCl_2 and dl4FPtCl_2 in any of the tolerant cell lines. It is postulated that the uptake of these complexes is not playing an important role in the resistance mechanisms but more experiments are required to confirm this.

20 References

1. Rosenberg, B. (1965) Inhibition of cell division in Escherichia coli by electrolysis products from a platinum electrode, *Nature 205*, 698-699.
2. Rosenberg, B. (2006) Platinum complexes for the treatment of cancer: Why the search goes on, In *Cisplatin*, pp 1-27, Verlag Helvetica Chimica Acta.
3. Peyrone, M. (1844) Ueber die einwirkung des ammoniaks auf platinchlorür, *Justus Liebigs Annalen der Chemie 51*, 1-29.
4. Kauffman, G. B. (1997) Alfred Werner's research on the platinum metals, A centennial retrospect, *Platinum Metals Review 41* 34-40.
5. Rosenberg, B. (1969) Platinum compounds: A new class of potent antitumor agents, *Nature 222*, 385-386.
6. O'Dwyer, P. J., Stevenson, J. P., and Johnson, S. W. (1999) Clinical status of cisplatin, carboplatin, and other platinum-based antitumor drugs, In *Cisplatin*, pp 29-69, Verlag Helvetica Chimica Acta.
7. Einhorn, L. H., and Donohue, J. (1977) Cis-diamminedichloroplatinum, vinblastine, and bleomycin combination chemotherapy in disseminated testicular cancer, *Annals of Internal Medicine 87*, 293-298.
8. Gonzalez-Vitale, J. C., Hayes, D. M., Cvitkovic, E., and Sternberg, S. S. (1977) The renal pathology in clinical trials of cis-platinum (II) diamminedichloride, *Cancer 39*, 1362-1371.
9. Cvitkovic, E., Spaulding, J., Bethune, V., Martin, J., and Whitmore, W. F. (1977) Improvement of cis-dichlorodiammineplatinum (nsc 119875): Therapeutic index in an animal model, *Cancer 39*, 1357-1361.
10. Hayes, D. M., Cvitkovic, E., Golbey, R. B., Scheiner, E., Helson, L., and Krakoff, I. H. (1977) High dose cis-platinum diammine dichloride. Amelioration of renal toxicity by mannitol diuresis, *Cancer 39*, 1372-1381.
11. Giaccone, G. (2000) Clinical perspectives on platinum resistance, *Drugs 59*, 9-17.
12. Wheate, N. J., Walker, S., Craig, G. E., and Oun, R. (2010) The status of platinum anticancer drugs in the clinic and in clinical trials, *Dalton Transactions 39*, 8113-8127.
13. Lee, F. H., Canetta, R., Issell, B. F., and Lenaz, L. (1983) New platinum complexes in clinical trials, *Cancer Treatment Reviews 10*, 39-51.
14. Canetta, R., Bragman, K., Smaldone, L., and Rozencweig, M. (1988) Carboplatin: Current status and future prospects, *Cancer Treatment Reviews 15, Supplement B*, 17-32.
15. Lokich, J., and Anderson, N. (1998) Carboplatin versus cisplatin in solid tumors: An analysis of the literature, *Annals of Oncology 9*, 13-21.
16. Curt, G. A., Grygiel, J. J., Corden, B. J., Ozols, R. F., Weiss, R. B., Tell, D. T., Myers, C. E., and Collins, J. M. (1983) A phase I and pharmacokinetic study of diamminecyclobutanedicarboxylatoplatinum (nsc 241240), *Cancer Research 43*, 4470-4473.
17. Mangioni, C., Bolis, G., Pecorelli, S., Bragman, K., Epis, A., Favalli, G., Gambino, A., Landoni, F., Presti, M., Torri, W., Vassena, L., Zanaboni, F., and Marsoni, S. (1989) Randomized trial in advanced ovarian cancer comparing cisplatin and carboplatin, *Journal of the National Cancer Institute 81*, 1464-1471.
18. Giacchetti, S., Perpoint, B., Zidani, R., Le Bail, N., Faggiuolo, R., Focan, C., Chollet, P., Llory, J. F., Letourneau, Y., Coudert, B., Bertheaut-Cvitkovic, F.,

Larregain-Fournier, D., Le Rol, A., Walter, S., Adam, R., Misset, J. L., and Lévi, F. (2000) Phase III multicenter randomized trial of oxaliplatin added to chronomodulated fluorouracil–leucovorin as first-line treatment of metastatic colorectal cancer, *Journal of Clinical Oncology 18*, 136.

19. de Gramont, A., Figer, A., Seymour, M., Homerin, M., Hmissi, A., Cassidy, J., Boni, C., Cortes-Funes, H., Cervantes, A., Freyer, G., Papamichael, D., Le Bail, N., Louvet, C., Hendler, D., de Braud, F., Wilson, C., Morvan, F., and Bonetti, A. (2000) Leucovorin and fluorouracil with or without oxaliplatin as first-line treatment in advanced colorectal cancer, *Journal of Clinical Oncology 18*, 2938-2947.
20. André, T., Boni, C., Navarro, M., Tabernero, J., Hickish, T., Topham, C., Bonetti, A., Clingan, P., Bridgewater, J., Rivera, F., and de Gramont, A. (2009) Improved overall survival with oxaliplatin, fluorouracil, and leucovorin as adjuvant treatment in stage II or III colon cancer in the mosaic trial, *Journal of Clinical Oncology 27*, 3109-3116.
21. Chabner, B. A., and Longo, D. A., (Eds.) (2010) *Cancer chemotherapy and biotherapy: Principles and practice*, Lippincott Williams & Wilkins, Philadelphia.
22. Becouarn, Y., Ychou, M., Ducreux, M., Borel, C., Bertheault-Cvitkovic, F., Seitz, J., Nasca, S., Nguyen, T., Paillot, B., Raoul, J., Duffour, J., Fandi, A., Dupont-Andre, G., and Rougier, P. (1998) Phase II trial of oxaliplatin as first-line chemotherapy in metastatic colorectal cancer patients. Digestive group of french federation of cancer centers, *Journal of Clinical Oncology 16*, 2739-2744.
23. Levi, F., Perpoint, B., Garufi, C., Focan, C., Chollet, P., Depres-Brummer, P., Zidani, R., Brienza, S., Itzhaki, M., Iacobelli, S., Kunstlinger, F., Gastiaburu, J., and Misset, J.-L. (1993) Oxaliplatin activity against metastatic colorectal cancer. A phase II study of 5-day continuous venous infusion at circadian rhythm modulated rate, *European Journal of Cancer 29*, 1280-1284.
24. Stordal, B., Pavlakis, N., and Davey, R. (2007) Oxaliplatin for the treatment of cisplatin-resistant cancer: A systematic review, *Cancer Treatment Reviews 33*, 347-357.
25. Rixe, O., Ortuzar, W., Alvarez, M., Parker, R., Reed, E., Paull, K., and Fojo, T. (1996) Oxaliplatin, tetraplatin, cisplatin, and carboplatin: Spectrum of activity in drug-resistant cell lines and in the cell lines of the national cancer institute's anticancer drug screen panel, *Biochemical Pharmacology 52*, 1855-1865.
26. Sternberg, C. N., Petrylak, D. P., Sartor, O., Witjes, J. A., Demkow, T., Ferrero, J.-M., Eymard, J.-C., Falcon, S., Calabrò, F., James, N., Bodrogi, I., Harper, P., Wirth, M., Berry, W., Petrone, M. E., McKearn, T. J., Noursalehi, M., George, M., and Rozencweig, M. (2009) Multinational, double-blind, phase III study of prednisone and either satraplatin or placebo in patients with castrate-refractory prostate cancer progressing after prior chemotherapy: The sparc trial, *Journal of Clinical Oncology 27*, 5431-5438.
27. Reishus, J. W., and Martin, D. S. (1961) Cis-dichlorodiammineplatinum(II). Acid hydrolysis and isotopic exchange of the chloride ligands, *Journal of the American Chemical Society 83*, 2457-2462.
28. Cleare, M. J., Hydes, P. C., Malerbi, B. W., and Watkins, D. M. (1978) Anti-tumour platinum complexes : Relationships between chemical properties and activity, *Biochimie 60*, 835-850.

29. Zhang, Y., Guo, Z., and You, X.-Z. (2001) Hydrolysis theory for cisplatin and its analogues based on density functional studies, *Journal of the American Chemical Society 123*, 9378-9387.
30. Martin, R. B. (2006) Platinum complexes: Hydrolysis and binding to N(7) and N(1) of purines, In *Cisplatin*, pp 181-205, Verlag Helvetica Chimica Acta.
31. Howe-Grant, M., Wu, K. C., Bauer, W. R., and Lippard, S. J. (1976) Binding of platinum and palladium metallointercalation reagents and antitumor drugs to closed and open DNAs, *Biochemistry 15*, 4339-4346.
32. Butour, J.-L., and Macquet, J.-P. (1977) Differentiation of DNA · platinum complexes by fluorescence, *European Journal of Biochemistry 78*, 455-463.
33. Barry, M. A., Behnke, C. A., and Eastman, A. (1990) Activation of programmed cell death (apoptosis) by cisplatin, other anticancer drugs, toxins and hyperthermia, *Biochemical Pharmacology 40*, 2353-2362.
34. Ormerod, M. G., O'Neill, C. F., Robertson, D., and Harrap, K. R. (1994) Cisplatin induces apoptosis in a human ovarian carcinoma cell line without concomitant internucleosomal degradation of DNA, *Experimental Cell Research 211*, 231-237.
35. Perego, P., Righetti, S., Supino, R., Delia, D., Caserini, C., Carenini, N., Bedogné, B., Broome, E., Krajewski, S., Reed, J., and Zunino, F. (1997) Role of apoptosis and apoptosis-related proteins in the cisplatin-resistant phenotype of human tumor cell lines, *Apoptosis 2*, 540-548.
36. Zhou, S., Lin, J., Du, W., Zhang, Z., Luo, Q., Liu, B.-F., and Dai, Y. (2006) Monitoring of proteinase activation in cell apoptosis by capillary electrophoresis with bioengineered fluorescent probe, *Analytica Chimica Acta 569*, 176-181.
37. Maldonado, V., Melendez, J., Gonzalet, H., and Ortega, a. (1995) Internucleosomal DNA cleavage in HeLa cells exposed to cisplatin, *Biochemistry and Molecular Biology International 37*, 691-696.
38. Mansy, S., Chu, G. Y. H., Duncan, R. E., and Tobias, R. S. (1978) Heavy metal nucleotide interactions. 12. Competitive reactions in systems of four nucleotides with cis- or trans-diammineplatinum(II). Raman difference spectrophotometry of the relative nucleophilicity of guanosine, cytidine, adenosine, and uridine monophosphates and analogous DNA bases, *Journal of the American Chemical Society 100*, 607-616.
39. Mandic, A., Hansson, J., Linder, S., and Shoshan, M. C. (2003) Cisplatin induces endoplasmic reticulum stress and nucleus-independent apoptotic signaling, *Journal of Biological Chemistry 278*, 9100-9106.
40. Meyn, R. E., Jenkins, S. F., and Thompson, L. H. (1982) Defective removal of DNA cross-links in a repair-deficient mutant of chinese hamster cells, *Cancer Research 42*, 3106-3110.
41. Sorenson, C. M., and Eastman, A. (1988) Influence of cis-diamminedichloroplatinum(II) on DNA synthesis and cell cycle progression in excision repair proficient and deficient chinese hamster ovary cells, *Cancer Research 48*, 6703-6707.
42. Caradonna, J. P., Lippard, S. J., Gait, M. J., and Singh, M. (1982) The antitumor drug cis-dichlorodiammineplatinum forms an intrastrand d(GpG) crosslink upon reaction with [d(ApGpGpCpCpT)]2, *Journal of the American Chemical Society 104*, 5793-5795.

43. Takahara, P. M., Frederick, C. A., and Lippard, S. J. (1996) Crystal structure of the anticancer drug cisplatin bound to duplex DNA, *Journal of the American Chemical Society 118*, 12309-12321.
44. Bellon, S. F., Coleman, J. H., and Lippard, S. J. (1991) DNA unwinding produced by site-specific intrastrand crosslinks of the antitumor drug cis-diamminedichloroplatinum(II), *Biochemistry 30*, 8026-8035.
45. Rosenberg, B., Van Camp, L., Grimley, E. B., and Thomson, A. J. (1967) The inhibition of growth or cell division in Escherichia coli by different ionic species of platinum(IV) complexes, *Journal of Biological Chemistry 242*, 1347-1352.
46. Cleare, M. J., and Hoeschele, J. D. (1973) Studies on the antitumor activity of group VIII transition metal complexes. Part I. Platinum (II) complexes, *Bioinorganic Chemistry 2*, 187-210.
47. Leonard, B. J., Eccleston, E., Jones, D., Todd, P., and Walpole, A. (1971) Antileukaemic and nephrotoxic properties of platinum compounds, *Nature 234*, 43-45.
48. Fichtinger-Schepman, A. M. J., van Oosterom, A. T., Lohman, P. H. M., and Berends, F. (1987) Cis-diamminedichloroplatinum(II)-induced DNA adducts in peripheral leukocytes from seven cancer patients: Quantitative immunochemical detection of the adduct induction and removal after a single dose of cis-diamminedichloroplatinum(II), *Cancer Research 47*, 3000-3004.
49. Plooy, A. C., Van Dijk, M., and Lohman, P. H. (1984) Induction and repair of DNA-cross-links in chinese hamster ovary cells treated with various platinum coordination compounds in relation to platinum binding to DNA, cytotoxicity, mutagenicity, and antitumor activity, *Cancer Res 44*, 2043-2051.
50. Zwelling, L. A., Bradley, M. O., Sharkey, N. A., Anderson, and Kurt W. Kohn, T. (1979) Mutagenicity, cytotoxicity and DNA crosslinking in V79 chinese hamster cells treated with cis- and trans-Pt(II) diamminedichloride, *Mutation Research/Genetic Toxicology 67*, 271-280.
51. Zwelling, L. A., Anderson, T., and Kohn, K. W. (1979) DNA-protein and DNA interstrand cross-linking by cis- and trans- platinum(II) diamminedichloride in l1210 mouse leukemia cells and relation to cytotoxicity, *Cancer Research 39*, 365-369.
52. Plooy, A. C. M., Fichtinger-Schepman, A. M. J., Schutte, H. H., van Dijk, M., and Lohman, P. H. M. (1985) The quantitative detection of various Pt-DNA-adducts in chinese hamster ovary cells treated with cisplatin: Application of immunochemical techniques, *Carcinogenesis 6*, 561-566.
53. Eastman, A. (1986) Reevaluation of interaction of cis-dichloro(ethylenediamine)platinum(II) with DNA, *Biochemistry 25*, 3912-3915.
54. Boubakari, Bracht, K., Neumann, C., Grünert, R., and Bednarski, P. J. (2004) No correlation between GSH levels in human cancer cell lines and the cell growth inhibitory activities of platinum diamine complexes, *Archiv der Pharmazie 337*, 668-671.
55. Bracht, K., Boubakari, Grünert, R., and Bednarski, P. J. (2006) Correlations between the activities of 19 anti-tumor agents and the intracellular glutathione concentrations in a panel of 14 human cancer cell lines: Comparisons with the national cancer institute data, *Anti-Cancer Drugs 17*, 41-51.
56. Godwin, A. K., Meister, A., O'Dwyer, P. J., Huang, C. S., Hamilton, T. C., and Anderson, M. E. (1992) High resistance to cisplatin in human ovarian cancer

cell lines is associated with marked increase of glutathione synthesis, *Proceedings of the National Academy of Sciences 89*, 3070-3074.
57. Ishikawa, T., and Ali-Osman, F. (1993) Glutathione-associated cis-diamminedichloroplatinum(II) metabolism and ATP-dependent efflux from leukemia cells. Molecular characterization of glutathione-platinum complex and its biological significance, *Journal of Biological Chemistry 268*, 20116-20125.
58. Hishikawa, Y., Abe, S., Kinugasa, S., Yoshimura, H., Monden, N., Igarashi, M., Tachibana, M., and Nagasue, N. (1997) Overexpression of metallothionein correlates with chemoresistance to cisplatin and prognosis in esophageal cancer, *Oncology 54*, 342-347.
59. Surowiak, P., Materna, V., Maciejczyk, A., Pudełko, M., Markwitz, E., Spaczyński, M., Dietel, M., Zabel, M., and Lage, H. (2007) Nuclear metallothionein expression correlates with cisplatin resistance of ovarian cancer cells and poor clinical outcome, *Virchows Archiv 450*, 279-285.
60. Andrews, P. A., Murphy, M. P., and Howell, S. B. (1987) Metallothionein-mediated cisplatin resistance in human ovarian carcinoma cells, *Cancer Chemotherapy and Pharmacology 19*, 149-154.
61. Hall, M., Okabe, M., Shen, D.-W., Liang, X.-J., and Gottesman, M., M. (2008) The role of cellular accumulation in determining sensitivity to platinum-based chemotherapy, *Annual Review of Pharmacology and Toxicology 48*, 495-535.
62. Andrews, P. A., Velury, S., Mann, S. C., and Howell, S. B. (1988) Cis-diamminedichloroplatinum(II) accumulation in sensitive and resistant human ovarian carcinoma cells, *Cancer Research 48*, 68-73.
63. Hromas, R. A., North, J. A., and Burns, C. P. (1987) Decreased cisplatin uptake by resistant l1210 leukemia cells, *Cancer Letters 36*, 197-201.
64. Kelland, L. R., Mistry, P., Abel, G., Loh, S. Y., O'Neill, C. F., Murrer, B. A., and Harrap, K. R. (1992) Mechanism-related circumvention of acquired cis-diamminedichloroplatinum(II) resistance using two pairs of human ovarian carcinoma cell lines by ammine/amine platinum(IV) dicarboxylates, *Cancer Res 52*, 3857-3864.
65. Ma, J., Maliepaard, M., Kolker, H. J., Verweij, J., and Schellens, J. H. M. (1997) Abrogated energy-dependent uptake of cisplatin in a cisplatin-resistant subline of the human ovarian cancer cell line IGROV-1, *Cancer Chemotherapy and Pharmacology 41*, 186-192.
66. Kröning, R., Katz, D., Lichtenstein, A. K., and Nagami, G. T. (1999) Differential effects of cisplatin in proximal and distal renal tubule epithelial cell lines, *Br J Cancer 79*, 293–299.
67. Smith, I. E., and Talbot, D. C. (1992) Cisplatin and its analogues in the treatment of advanced breast cancer: A review, *Br J Cancer 65*, 787-793.
68. McGuire, W. L., Horwitz, K. B., Pearson, O. H., and Segaloff, A. (1977) Current status of estrogen and progesterone receptors in breast cancer, *Cancer 39*, 2934-2947.
69. Brooks, S. C., Locke, E. R., and Soule, H. D. (1973) Estrogen receptor in a human cell line (MCF-7) from breast carcinoma, *Journal of Biological Chemistry 248*, 6251-6253.
70. Glascock, R. F., and Hoekstra, W. G. (1959) Selective accumulation of tritium-labelled hexoestrol by the reproductive organs of immature female goats and sheep. , *Biochem. J. 72*, 673-682.

71. Folca, P. J., Glascock, R. F., and Irvine, W. T. (1961) Studies with tritium-labelled hexœstrol in advanced breast cancer: Comparison of tissue accumulation of hexœstrol with response to bilateral adrenalectomy and oophorectomy, *The Lancet 278*, 796-798.
72. Grant, E., and Niculescu-Duvăz, I. (1965) Potential anticancer agents. I. Urethane-type nitrogen mustards of some synthetic estrogens, *Canadian Journal of Chemistry 43*, 1227-1230.
73. Nogrady, T., Vagi, K. M., and Adamkiewicz, V. W. (1962) N-mustard derivatives of estrogens, *Canadian Journal of Chemistry 40*, 2126-2129.
74. Katzenellenbogen, J. A., McElvany, K. D., Senderoff, S. G., Carlson, K. E., Landvatter, S. W., Welch, M. J., and Group, L. A. M. R. (1982) 16α-[77Br]Bromo-11β-methoxyestradiol-17β: A gamma-emitting estrogen imaging agent with high uptake and retention by target organs, *Journal of Nuclear Medicine 23*, 411-419.
75. Lippman, M. E. (1982) Evoluation of hormone-receptor systems, *Journal of Cellular Biochemistry 19*, 109-185.
76. Bloomer, W. D. (1982) Evoluation of hormone-receptor systems, *Journal of Cellular Biochemistry 19*, 109-185.
77. Katzenellenbogen, B. S. (1982) Evoluation of hormone-receptor systems, *Journal of Cellular Biochemistry 19*, 109-185.
78. Katzenellenbogen, J., and Katzenellenbogen, B. (1982) Considerations in the design and evaluation of cytotoxic estrogens, *Breast Cancer Research and Treatment 2*, 347-353.
79. Wappes, B., Jennerwein, M., Von Angerer, E., Schoenenberger, H., Engel, J., Berger, M., and Wrobel, K. H. (1984) Dichloro[1,2-bis(4-hydroxyphenyl)ethylenediamine]platinum(II) complexes: An approach to develop compounds with a specific effect on the hormone-dependent mammary carcinoma, *Journal of Medicinal Chemistry 27*, 1280-1286.
80. Karl, J., Gust, R., Spruss, T., Schneider, M. R., Schoenenberger, H., Engel, J., Wrobel, K. H., Lux, F., and Haeberlin, S. T. (1988) Ring-substituted [1,2-bis(4-hydroxyphenyl)ethylenediamine]dichloroplatinum(II) complexes: Compounds with a selective effect on the hormone-dependent mammary carcinoma, *Journal of Medicinal Chemistry 31*, 72-83.
81. Reile, H., Bernhardt, G., Koch, M., Schönenberger, H., Hollstein, M., and Lux, F. (1992) Chemosensitivity of human MCF-7 breast cancer cells to diastereoisomeric diaqua(1,2-diphenylethylenediamine) platinum(II) sulfates and specific platinum accumulation, *Cancer Chemotherapy and Pharmacology 30*, 113-122.
82. Jennerwein, M., Wappes, B., Gust, R., Schönenberge, H., Engel, J., Seeber, S., and Osieka, R. (1988) Influence of ring substituents on the antitumor effect of dichloro(1,2-diphenylethylenediamine)platinum(II) complexes, *Journal of Cancer Research and Clinical Oncology 114*, 347-358.
83. Reile, H., Spruß, T., Müller, R., Gust, R., Bernhardt, G., Schönenberger, H., and Engel, J. (1990) Tumor inhibiting [1,2-bis(fluorophenyl)ethylenediamine]platinum(II) complexes, III1): Evaluation of the mammary tumor inhibiting properties, *Archiv der Pharmazie 323*, 301-306.
84. vom Orde, H. D., Reile, H., Müller, R., Gust, R., Bernhardt, G., Spruß, T., Schönenberger, H., Burgemeister, T., and Mannschreck, A. (1990) Tumor-inhibiting [1,2-bis(fluorophenyl)ethylenediamine]platinum(II) complexes, *Journal of Cancer Research and Clinical Oncology 116*, 434-438.

85. Kapp, T. (2006) Untersuchungen zur Optimierung der biologischen aktivität von antitumoralen platin(II)-wirkstoffen mittels einbindung in polynukleare komplexe sowie in makromolekulare träger, In *Fachbereich FB Biologie, Chemie, Pharmazie*, Freie Universität Berlin Berlin
86. Reile, H., Müller, R., Gust, R., Laske, R., Krischke, W., Bernhardt, G., Spruß, T., Jennerwein, M., Engel, J., Seeber, S., Osieka, R., and Schönenberger, H. (1990) Tumor inhibiting [1,2-bis(fluorophenyl)ethylenediamine]platinum(II) complexes part II: Biological evaluation - in vitro studies on the P 388 D1 leukemia cell line, *Archiv der Pharmazie 323*, 133-140.
87. Reile, H., Spruß, T., Bernhardt, G., Müller, R., Gust, R., and Schönenberger, H. (1991) Tumor inhibiting [1,2-bis(fluorophenyl)ethylenediamine]platinum(II) complexes. Part IV: Biological evaluation - in vivo studies on the P 388 D1 leukemia cell line., *Archiv der Pharmazie 324*, 405-409.
88. Gust, R., and Schönenberger, H. (1995) Third generation antitumor platinum(II) complexes of the [1-(fluoro/difluorophenyl)-2-phenylethylenediamine]platinum(II) type, *Archiv der Pharmazie 328*, 595-603.
89. Gust, R., Krauser, R., Schmid, B., and Schönenberger, H. (1996) Breast cancer inhibiting diastereomeric diacetato[1,2-bis(4-fluorophenyl)ethylenediamine]platinum(II) derivatives: Synthesis and studies on the relationship between reactivity and antitumor activity, *Inorganica Chimica Acta 250*, 203-218.
90. Gust, R., Schnurr, B., Krauser, R., Bernhardt, G., Koch, M., Schmid, B., Hummel, E., and Schönenberger, H. (1998) Stability and cellular studies of [*rac*-1,2-bis(4-fluorophenyl)- ethylenediamine][cyclobutane-1,1-dicarboxylato]platinum(II), a novel, highly active carboplatin derivative, *Journal of Cancer Research and Clinical Oncology 124*, 585-597.
91. Dullin, A. (2006) Variation von neutralligand und abgangsgruppe zur Optimierung von [1,2-bis(4-fluorphenyl)ethylendiamin]platin(II)-komplexen. Untersuchungen pharmakologischer eigenschaften, stabilität, reaktivität und antitumoraktivität, In *Fachbereich Biologie, Chemie, Pharmazie*, Freie Universität Berlin Berlin.
92. Beretta, G. L., Righetti, S. C., Lombardi, L., Zunino, F., and Perego, P. (2002) Electron microscopy analysis of early localization of cisplatin in ovarian carcinoma cells, *Ultrastructural Pathology 26*, 331-334.
93. Khan, M. U. A., and Sadler, P. J. (1978) Distribution of a platinum anti-tumour drug in HeLa cells by analytical electron microscopy, *Chemico-Biological Interactions 21*, 227-232.
94. Hall, M., Dillon, C., Zhang, M., Beale, P., Cai, Z., Lai, B., Stampfl, A. J., and Hambley, T. (2003) The cellular distribution and oxidation state of platinum(II) and platinum(IV) antitumour complexes in cancer cells, *Journal of Biological Inorganic Chemistry 8*, 726-732.
95. Kalayda, G., Jansen, B. J., Molenaar, C., Wielaard, P., Tanke, H., and Reedijk, J. (2004) Dinuclear platinum complexes with *N,N'*-bis(aminoalkyl)-1,4-diaminoanthraquinones as linking ligands. Part II. Cellular processing in A2780 cisplatin-resistant human ovarian carcinoma cells: New insights into the mechanism of resistance, *Journal of Biological Inorganic Chemistry 9*, 414-422.
96. Kalayda, G. V., Jansen, B. A. J., Wielaard, P., Tanke, H. J., and Reedijk, J. (2005) Dinuclear platinum anticancer complexes with fluorescent *N,N'*-

bis(aminoalkyl)-1,4-diaminoanthraquinones: Cellular processing in two cisplatin-resistant cell lines reflects the differences in their resistance profiles, *Journal of Biological Inorganic Chemistry 10*, 305-315.

97. Kalayda, G. V., Zhang, G., Abraham, T., Tanke, H. J., and Reedijk, J. (2005) Application of fluorescence microscopy for investigation of cellular distribution of dinuclear platinum anticancer drugs, *Journal of Medicinal Chemistry 48*, 5191-5202.
98. Alderden, R. A., Mellor, H. R., Modok, S., Hambley, T. W., and Callaghan, R. (2006) Cytotoxic efficacy of an anthraquinone linked platinum anticancer drug, *Biochemical Pharmacology 71*, 1136-1145.
99. Liang, X.-J., Shen, D.-W., Chen, K. G., Wincovitch, S. M., Garfield, S. H., and Gottesman, M. M. (2005) Trafficking and localization of platinum complexes in cisplatin-resistant cell lines monitored by fluorescence-labeled platinum, *Journal of Cellular Physiology 202*, 635-641.
100. Molenaar, C., Teuben, J.-M., Heetebrij, R. J., Tanke, H. J., and Reedijk, J. (2000) New insights in the cellular processing of platinum antitumor compounds, using fluorophore-labeled platinum complexes and digital fluorescence microscopy, *Journal of Biological Inorganic Chemistry 5*, 655-665.
101. Milacic, R., Cemazar, M., and Sersa, G. (1997) Determination of platinum in tumour tissues after cisplatin therapy by electrothermal atomic absorption spectrometry, *Journal of Pharmaceutical and Biomedical Analysis 16*, 343-348.
102. Brouwers, E. E. M., Tibben, M. M., Joerger, M., van Tellingen, O., Rosing, H., Schellens, J. H. M., and Beijnen, J. H. (2005) Determination of oxaliplatin in human plasma and plasma ultrafiltrate by graphite-furnace atomic-absorption spectrometry, *Analytical and Bioanalytical Chemistry 382*, 1484-1490.
103. Vouillamoz-Lorenz, S., Bauer, J., Lejeune, F., and Decosterd, L. A. (2001) Validation of an AAS method for the determination of platinum in biological fluids from patients receiving the oral platinum derivative JM216, *Journal of Pharmaceutical and Biomedical Analysis 25*, 465-475.
104. Sharma, R. P., and Edwards, I. R. (1983) Microanalysis of platinum in biological media by graphite furnace atomic absorption spectroscopy, *Therapeutic Drug Monitoring 5*, 367-370.
105. Lindauer, E., and Holler, E. (1996) Cellular distribution and cellular reactivity of platinum(II) complexes, *Biochemical Pharmacology 52*, 7-14.
106. Kapp, T., Dullin, A., and Gust, R. (2006) Mono- and polynuclear [alkylamine]platinum(II) complexes of [1,2-bis(4-fluorophenyl)ethylenediamine]platinum(II): Synthesis and investigations on cytotoxicity, cellular distribution, and DNA and protein binding, *Journal of Medicinal Chemistry 49*, 1182-1190.
107. Abraham, M. H., Chadha, H. S., Whiting, G. S., and Mitchell, R. C. (1994) Hydrogen bonding. 32. An analysis of water-octanol and water-alkane partitioning and the delta log P parameter of seiler, *Journal of Pharmaceutical Sciences 83*, 1085-1100.
108. Coats, J. R., Metcalf, R. L., Lu, P. Y., Brown, D. D., Williams, J. F., and Hansen, L. G. (1976) Model ecosystem evaluation of the environmental impacts of the veterinary drugs phenothiazine, sulfamethazine, clopidol, and diethylstilbestrol, *Environ Health Perspect 18*.

109. Leo, A., Hansch, C., and Elkins, D. (1971) Partition coefficients and their uses, *Chemical Reviews 71*, 525-616.
110. Platts, J. A., Hibbs, D. E., Hambley, T. W., and Hall, M. D. (2000) Calculation of the hydrophobicity of platinum drugs, *Journal of Medicinal Chemistry 44*, 472-474.
111. Screnci, D., McKeage, M. J., Galettis, P., Hambley, T. W., Palmer, B. D., and Baguley, B. C. (2000) Relationships between hydrophobicity, reactivity, accumulation and peripheral nerve toxicity of a series of platinum drugs, *Br J Cancer 82*, 966-972.
112. Hall, M. D., Amjadi, S., Zhang, M., Beale, P. J., and Hambley, T. W. (2004) The mechanism of action of platinum(IV) complexes in ovarian cancer cell lines, *Journal of Inorganic Biochemistry 98*, 1614-1624.
113. Berners-Price, S. J., Frenkiel, T. A., Frey, U., Ranford, J. D., and Sadler, P. J. (1992) Hydrolysis products of cisplatin: pKa determinations via[1H, 15N] NMR spectroscopy, *Journal of the Chemical Society, Chemical Communications*, 789-791.
114. Appleton, T. G., Hall, J. R., Ralph, S. F., and Thompson, C. S. M. (1989) NMR study of acid-base equilibria and other reactions of ammineplatinum complexes with aqua and hydroxo ligands, *Inorganic Chemistry 28*, 1989-1993.
115. Miller, S. E., and House, D. A. (1991) The hydrolysis products of cis-diamminedichloroplatinum(II) 5. The anation kinetics of cis-Pt(X)(NH3)2(OH2)+ (X=Cl, OH) with glycine, monohydrogen malonate and chloride, *Inorganica Chimica Acta 187*, 125-132.
116. Robillard, M. S., Galanski, M., Zimmermann, W., Keppler, B. K., and Reedijk, J. (2002) (aminoethanol)dichloroplatinum(II) complexes: Influence of the hydroxyethyl moiety on 5'-GMP and DNA binding, intramolecular stability, the partition coefficient and anticancer activity, *Journal of Inorganic Biochemistry 88*, 254-259.
117. Martelli, L., Di Mario, F., Botti, P., Ragazzi, E., Martelli, M., and Kelland, L. (2007) Accumulation, platinum-DNA adduct formation and cytotoxicity of cisplatin, oxaliplatin and satraplatin in sensitive and resistant human osteosarcoma cell lines, characterized by p53 wild-type status, *Biochemical Pharmacology 74*, 20-27.
118. Albert, A. (1973) *Selective toxicity : The physico-chemical basis of therapy / adrien albert*, Chapman and Hall [distributed in the U.S. by Halsted Press, New York, London :.
119. Loh, S. Y., Mistry, P., Kelland, L. R., Abel, G., and Harrap, K. R. (1992) Reduced drug accumulation as a major mechanism of acquired resistance to cisplatin in a human ovarian carcinoma cell line: Circumvention studies using novel platinum (II) and (IV) ammine/amine complexes, *Br J Cancer 66*, 1109-1115.
120. Borenfreund, E., and Puerner, J. A. Toxicity determined in vitro by morphological alterations and neutral red absorption, *Toxicology Letters 24*, 119-124.
121. Mosmann, T. (1983) Rapid colorimetric assay for cellular growth and survival: Application to proliferation and cytotoxicity assays, *Journal of Immunological Methods 65*, 55-63.

122. Denizot, F., and Lang, R. (1986) Rapid colorimetric assay for cell growth and survival: Modifications to the tetrazolium dye procedure giving improved sensitivity and reliability, *Journal of Immunological Methods 89*, 271-277.
123. Saotome, K., Morita, H., and Umeda, M. (1989) Cytotoxicity test with simplified crystal violet staining method using microtitre plates and its application to injection drugs, *Toxicology in Vitro 3*, 317-321.
124. Ferguson, R. J., McMaster, J. H., and Weinert Jr, C. R. (1975) Assay of cell-mediated cytotoxicity by tritiated thymidine labeled tumor cells, *Journal of Immunological Methods 7*, 347-357.
125. Clark, J. B., and Webb, R. B. (1955) The site of action of the crystal violet nuclear stain, *Biotechnic & Histochemistry 30*, 89-92.
126. Carmichael, J., DeGraff, W. G., Gazdar, A. F., Minna, J. D., and Mitchell, J. B. (1987) Evaluation of a tetrazolium-based semiautomated colorimetric assay: Assessment of chemosensitivity testing, *Cancer Research 47*, 936-942.
127. Graham, J. M., Rickwood (1997) Subcellular fractionation: A practical approach, *Oxford University Press*.
128. Ford, T., Graham, J., and Rickwood, D. (1994) Iodixanol: A nonionic iso-osmotic centrifugation medium for the formation of self-generated gradients, *Analytical Biochemistry 220*, 360-366.
129. Morand, J. N., and Kent, C. (1986) A one-step technique for the subcellular fractionation of total cell homogenates, *Analytical Biochemistry 159*, 157-162.
130. Bradford, M. M. (1976) A rapid and sensitive method for the quantitation of microgram quantities of protein utilizing the principle of protein-dye binding, *Analytical Biochemistry 72*, 248-254.
131. Zor, T., and Selinger, Z. (1996) Linearization of the bradford protein assay increases its sensitivity: Theoretical and experimental studies, *Analytical Biochemistry 236*, 302-308.
132. Bosmann, H. B., Hagopian, A., and Eylar, E. H. (1968) Cellular membranes: The isolation and characterization of the plasma and smooth membranes of HeLa cells, *Archives of Biochemistry and Biophysics 128*, 51-69.
133. Li, Q., Harraz, M. M., Zhou, W., Zhang, L. N., Ding, W., Zhang, Y., Eggleston, T., Yeaman, C., Banfi, B., and Engelhardt, J. F. (2006) Nox2 and Rac1 regulate H2O2-dependent recruitment of TRAF6 to endosomal interleukin-1 receptor complexes, *Mol. Cell. Biol. 26*, 140-154.
134. Salvi, M., Battaglia, V., Brunati, A. M., La Rocca, N., Tibaldi, E., Pietrangeli, P., Marcocci, L., Mondovì, B., Rossi, C. A., and Toninello, A. (2007) Catalase takes part in rat liver mitochondria oxidative stress defense, *Journal of Biological Chemistry 282*, 24407-24415.
135. Graham, J. M. (2001) *Purification of a crude mitochondrial fraction by density-gradient centrifugation*, John Wiley & Sons, Inc.
136. Antonenkov, V. D., Sormunen, R. T., and Hiltunen, J. K. (2004) The behavior of peroxisomes in vitro: Mammalian peroxisomes are osmotically sensitive particles, *American Journal of Physiology - Cell Physiology 287*, C1623-C1635.
137. Miller, L. (1979) A detergent-citric acid technique for isolating nuclear and cytoplasmic fractions containing undegraded RNA from cells of xenopus laevis, *Analytical Biochemistry 100*, 166-173.
138. Knowler, J. T., Moses, H. L., and Spelsberg, T. C. (1973) Comparison and characterization of nuclear isolation procedures as applied to chick oviduct, *The Journal of Cell Biology 59*, 685-695.

139. Blobel, G., and Potter, V. R. (1966) Nuclei from rat liver: Isolation method that combines purity with high yield, *Science 154*, 1662-1665.
140. Gurr, M. I., Finean, J. B., and Hawthorne, J. N. (1963) The phospholipids of liver-cell fractions : I. The phospholipid composition of the liver-cell nucleus, *Biochimica et Biophysica Acta (BBA) - Specialized Section on Lipids and Related Subjects 70*, 406-416.
141. Busch, H., and Daskal, Y. (1977) Chapter 1 methods for isolation of nuclei and nucleoli, In *Methods in cell biology* (Gary Stein, J. S., and Lewis, J. K., Eds.), pp 1-43, Academic Press.
142. Rosenberger, U., Shakibaei, M., Weise, C., Franke, P., and Buchner, K. (1995) Citric acid extracts a specific set of proteins from isolated cell nuclei, *Journal of Cellular Biochemistry 59*, 177-185.
143. Riley, D. E., Keller, J. M., and Byers, B. (1975) Isolation and characterization of nuclear ghosts from cultured HeLa cells, *Biochemistry 14*, 3005-3013.
144. Atkinson, P. H. (1974) Chapter 8 HeLa cell plasma membranes, In *Methods in cell biology* (David, M. P., Ed.), pp 157-188, Academic Press.
145. Atkinson, P. H., and Summers, D. F. (1971) Purification and properties of HeLa cell plasma membranes, *Journal of Biological Chemistry 246*, 5162-5175.
146. Costantino-Ceccarini, E., Novikoff, P., Atkinson, P., and Novikoff, A. (1978) Further characterization of HeLa S3 plasma membrane ghosts, *The Journal of Cell Biology 77*, 448-463.
147. Boone, C. W., Ford, L. E., Bond, H. E., Stuart, D. C., and Lorenz, D. (1969) Isolation of plasma membrane fragments from HeLa cells, *The Journal of Cell Biology 41*, 378-392.
148. Hoelzl Wallach, D. F., and Ullrey, D. (1964) Studies on the surface and cytoplasmic membranes of ehrlich ascites carcinoma cells: II. Alkali-cation-activated adenosine triphosphate hydrolysis in a microsomal membrane fraction, *Biochimica et Biophysica Acta (BBA) - Specialized Section on Biophysical Subjects 88*, 620-629.
149. Cariani, L., Thomas, L., Brito, J., and del Castillo, J. R. (2004) Bismuth citrate in the quantification of inorganic phosphate and its utility in the determination of membrane-bound phosphatases, *Analytical Biochemistry 324*, 79-83.
150. Bimboim, H. C., and Doly, J. (1979) A rapid alkaline extraction procedure for screening recombinant plasmid DNA, *Nucleic Acids Research 7*, 1513-1523.
151. Tamura, K., and Aotsuka, T. (1988) Rapid isolation method of animal mitochondrial DNA by the alkaline lysis procedure, *Biochemical Genetics 26*, 815-819.
152. Yang, Z., Schumaker, L. M., Egorin, M. J., Zuhowski, E. G., Guo, Z., and Cullen, K. J. (2006) Cisplatin preferentially binds mitochondrial DNA and voltage-dependent anion channel protein in the mitochondrial membrane of head and neck squamous cell carcinoma: Possible role in apoptosis, *Clinical Cancer Research 12*, 5817-5825.
153. Higuchi, Y., and Linn, S. (1995) Purification of all forms of HeLa cell mitochondrial DNA and assessment of damage to it caused by hydrogen peroxide treatment of mitochondria or cells, *Journal of Biological Chemistry 270*, 7950-7956.
154. Sambrook, J. (2001) *Molecular cloning : A laboratory manual / joseph sambrook, david w. Russell*, Cold Spring Harbor Laboratory, Cold Spring Harbor, N.Y. :.

155. Magalhaes, P. J., Andreu, A. L., and Schon, E. A. (1998) Evidence for the presence of 5S rRNA in mammalian mitochondria, *Molecular Biology of the Cell 9*, 2375-2382.
156. Glasel, J. A. (1995) Validity of nucleic acid purities monitored by A260/A280 absorbance ratios, *Biotechniques 18*, 62-63.
157. Laws, G. M., and Adams, S. P. (1996) Measurement of 8-OHdG in DNA by HPLC/ECD: The importance of DNA purity, *Biotechniques 20*, 36-38.
158. Jadot, M., Colmant, C., Wattiaux-De Coninck, S., Wattiaux, R. (1984) Intralysosomal hydrolysis of glycyl-L-phenylalanine 2-naphthylamide, *Biochemical Journal 219*, 965-970.
159. Reeves, J. P. (1979) Accumulation of amino acids by lysosomes incubated with amino acid methyl esters, *Journal of Biological Chemistry 254*, 8914-8921.
160. Berg, O. T., Strømhaug, E., Løvdal, T., Seglen, O., Berg, T. (1994) Use of glycyl-L-phenylalanine 2-naphthylamide, a lysosome-disrupting cathepsin C substrate, to distinguish between lysosomes and prelysosomal endocytic vacuoles, *Biochemical Journal 300*, 229-236.
161. Michihara, A., Toda, K., Kubo, T., Fujiwara, Y., Akasaki, K., and Tsuji, H. (2005) Disruptive effect of chloroquine on lysosomes in cultured rat hepatocytes, *Biological & Pharmaceutical Bulletin 28*, 947-951.
162. Akasaki, K., Michihara, A., Mibuka, K., Fujiwara, Y., and Tsuji, H. (1995) Biosynthetic transport of a major lysosomal membrane glycoprotein, Lamp-1: Convergence of biosynthetic and endocytic pathways occurs at three distinctive points, *Experimental Cell Research 220*, 464-473.
163. Furuno, K., Ishikawa, T., Akasaki, K., Yano, S., Tanaka, Y., Yamaguchi, Y., Tsuji, H., Himeno, M., and Kato, K. (1989) Morphological localization of a major lysosomal membrane glycoprotein in the endocytic membrane system, *Journal of Biochemistry 106*, 708-716.
164. Feldherr, C. M., and Akin, D. (1990) The permeability of the nuclear envelope in dividing and nondividing cell cultures, *The Journal of Cell Biology 111*, 1-8.
165. Keminer, O., and Peters, R. (1999) Permeability of single nuclear pores, *Biophysical journal 77*, 217-228.
166. Sharma, R. P., and Edwards, I. R. (1983) Cis-platinum: Subcellular distribution and binding to cytosolic ligands, *Biochemical Pharmacology 32*, 2665-2669.
167. Zayed, A., Shoeib, T., Taylor, S. E., Jones, G. D. D., Thomas, A. L., Wood, J. P., Reid, H. J., and Sharp, B. L. Determination of Pt-DNA adducts and the sub-cellular distribution of Pt in human cancer cell lines and the leukocytes of cancer patients, following mono- or combination treatments, by inductively-coupled plasma mass spectrometry, *International Journal of Mass Spectrometry In Press, Corrected Proof*.
168. Qian, W., Nishikawa, M., Haque, A. M., Hirose, M., Mashimo, M., Sato, E., and Inoue, M. (2005) Mitochondrial density determines the cellular sensitivity to cisplatin-induced cell death, *American Journal of Physiology - Cell Physiology 289*, C1466-C1475.
169. Clayton, D. A., Doda, J. N., and Friedberg, E. C. (1974) The absence of a pyrimidine dimer repair mechanism in mammalian mitochondria, *Proceedings of the National Academy of Sciences 71*, 2777-2781.
170. Olivero, O. A., Chang, P. K., Lopez-Larraza, D. M., Cristina Semino-Mora, M., and Poirier, M. C. (1997) Preferential formation and decreased removal of

cisplatin-DNA adducts in chinese hamster ovary cell mitochondrial DNA as compared to nuclear DNA, *Mutation Research/Genetic Toxicology and Environmental Mutagenesis 391*, 79-86.
171. van Boom, S. S. G. E., Chen, B. W., Teuben, J. M., and Reedijk, J. (1999) Platinum−thioether bonds can be reverted by guanine−N7 bonds in Pt(dien)2+ model adducts, *Inorganic Chemistry 38*, 1450-1455.
172. Peleg-Shulman, T., and Gibson, D. (2001) Cisplatin−protein adducts are efficiently removed by glutathione but not by 5‘-guanosine monophosphate, *Journal of the American Chemical Society 123*, 3171-3172.
173. Giurgiovich, A. J., Diwan, B. A., Olivero, O. A., Anderson, L. M., Rice, J. M., and Poirier, M. C. (1997) Elevated mitochondrial cisplatin-DNA adduct levels in rat tissues after transplacental cisplatin exposure, *Carcinogenesis 18*, 93-96.
174. Olivero, O. A., Semino, C., Kassim, A., Lopez-Larraza, D. M., and Poirier, M. C. (1995) Preferential binding of cisplatin to mitochondrial DNA of chinese hamster ovary cells, *Mutation Research Letters 346*, 221-230.
175. Steinman, R. M., and Cohn, Z. A. (1972) The interaction of soluble horseradish peroxidase with mouse peritoneal macrophages in vitro, *The Journal of Cell Biology 55*, 186-204.
176. Claiborne, A., and Fridovich, I. (1979) Chemical and enzymic intermediates in the peroxidation of o-dianisidine by horseradish peroxidase. 1. Spectral properties of the products of dianisidine oxidation, *Biochemistry 18*, 2324-2329.
177. Darbyshire, B. (1975) The results of freezing and dehydration of horseradish peroxidase, *Cryobiology 12*, 276-281.
178. Catanzaro, P. J., and Graham, R. C. (1974) Normal peritoneal lymphocytes: A population with increased capacity for endocytosis, *The American journal of pathology 77*, 23-40.
179. Steinman, R. M., Silver, J. M., and Cohn, Z. A. (1974) Pinocytosis in fibroblasts, *The Journal of Cell Biology 63*, 949-969.
180. Porstmann, B., Porstmann, T., Gaede, D., Nugel, E., and Egger, E. (1981) Temperature dependent rise in activity of horseradish peroxidase caused by non-ionic detergents and its use in enzyme-immunoassay, *Clinica Chimica Acta 109*, 175-181.
181. Gallati, H., and Pracht, I. (1985) Peroxidase aus Meerrettich: Kinetische Studien und Optimierung der Peroxidase-aktivitätsbestimmung mit den Substraten H2O2 und 3,3',5,5'-tetramethylbenzidin, *Clinical Chemistry and Laboratory Medicine 23*, 453-460.
182. Eremin, A. N., Budnikova, L. P., Sviridov, O. V., and Metelitsa, D. I. (2002) Stabilization of diluted aqueous solutions of horseradish peroxidase, *Applied Biochemistry and Microbiology 38*, 151-158.
183. Steinman, R. M., Brodie, S. E., and Cohn, Z. A. (1976) Membrane flow during pinocytosis. A stereologic analysis, *The Journal of Cell Biology 68*, 665-687.
184. Storrie, B., Sachdeva, M., and Viers, V. S. (1984) Chinese hamster ovary cell lysosomes retain pinocytized horseradish peroxidase and in situ-radioiodinated proteins, *Mol. Cell. Biol. 4*, 296-301.
185. Steinman, R. M., Mellman, I. S., Muller, W. A., and Cohn, Z. A. (1983) Endocytosis and the recycling of plasma membrane, *The Journal of Cell Biology 96*, 1-27.
186. Schröter, C. J., Braun, M., Englert, J., Beck, H., Schmid, H., and Kalbacher, H. (1999) A rapid method to separate endosomes from lysosomal contents using

differential centrifugation and hypotonic lysis of lysosomes, *Journal of Immunological Methods 227*, 161-168.
187. Kapp, T., Müller, S., and Gust, R. (2006) Dinuclear alkylamine platinum(II) complexes of [1,2-bis(4-fluorophenyl)ethylenediamine]platinum(II): Influence of endocytosis and copper and organic cation transport systems on cellular uptake, *ChemMedChem 1*, 560-564.
188. Zaro, J. L., Rajapaksa, T. E., Okamoto, C. T., and Shen, W.-C. (2006) Membrane transduction of oligoarginine in HeLa cells is not mediated by macropinocytosis, *Molecular Pharmaceutics 3*, 181-186.
189. Rejman, J., Bragonzi, A., and Conese, M. (2005) Role of clathrin- and caveolae-mediated endocytosis in gene transfer mediated by lipo- and polyplexes, *Mol Ther 12*, 468-474.
190. Singh, R. D., Puri, V., Valiyaveettil, J. T., Marks, D. L., Bittman, R., and Pagano, R. E. (2003) Selective caveolin-1-dependent endocytosis of glycosphingolipids, *Mol. Biol. Cell 14*, 3254-3265.
191. Lewis, W. (1931) Pinocytosis, *Bulletin of the Johns Hopkins Hospital 49*.
192. Lewis, W. (1937) Pinocytosis by malignant cells, *American Journal of Cancer 29*, 666-679.
193. Hewlett, L., Prescott, A., and Watts, C. (1994) The coated pit and macropinocytic pathways serve distinct endosome populations, *The Journal of Cell Biology 124*, 689-703.
194. Sallusto, F., Cella, M., Danieli, C., and Lanzavecchia, A. (1995) Dendritic cells use macropinocytosis and the mannose receptor to concentrate macromolecules in the major histocompatibility complex class II compartment: Downregulation by cytokines and bacterial products, *The Journal of Experimental Medicine 182*, 389-400.
195. West, M. A., Prescott, A. R., Eskelinen, E.-L., Ridley, A. J., and Watts, C. (2000) Rac is required for constitutive macropinocytosis by dendritic cells but does not control its downregulation, *Current biology : CB 10*, 839-848.
196. Wrenn, J. T., and Wessells, N. K. (1970) Cytochalasin B: Effects upon microfilaments involved in morphogenesis of estrogen-induced glands of oviduct, *Proceedings of the National Academy of Sciences 66*, 904-908.
197. Carter, S. B. (1967) Effects of cytochalasins on mammalian cells, *Nature 213*, 261-264.
198. Brown, S., and Spudich, J. (1979) Cytochalasin inhibits the rate of elongation of actin filament fragments, *The Journal of Cell Biology 83*, 657-662.
199. Flanagan, M. D., and Lin, S. (1980) Cytochalasins block actin filament elongation by binding to high affinity sites associated with F-actin, *Journal of Biological Chemistry 255*, 835-838.
200. Ayscough, K. R., Stryker, J., Pokala, N., Sanders, M., Crews, P., and Drubin, D. G. (1997) High rates of actin filament turnover in budding yeast and roles for actin in establishment and maintenance of cell polarity revealed using the actin inhibitor latrunculin-A, *The Journal of Cell Biology 137*, 399-416.
201. Koivusalo, M., Welch, C., Hayashi, H., Scott, C. C., Kim, M., Alexander, T., Touret, N., Hahn, K. M., and Grinstein, S. (2010) Amiloride inhibits macropinocytosis by lowering submembranous pH and preventing Rac1 and Cdc42 signaling, *The Journal of Cell Biology 188*, 547-563.
202. Stoorvogel, W., Oorschot, V., and Geuze, H. J. (1996) A novel class of clathrin-coated vesicles budding from endosomes, *The Journal of Cell Biology 132*, 21-33.

203. Hussain, K. M., Leong, K. L. J., Ng, M. M.-L., and Chu, J. J. H. (2011) The essential role of clathrin-mediated endocytosis in the infectious entry of human enterovirus 71, *Journal of Biological Chemistry 286*, 309-321.
204. Meier, O., Boucke, K., Hammer, S. V., Keller, S., Stidwill, R. P., Hemmi, S., and Greber, U. F. (2002) Adenovirus triggers macropinocytosis and endosomal leakage together with its clathrin-mediated uptake, *The Journal of Cell Biology 158*, 1119-1131.
205. Brodsky, F. M., Chen, C.-Y., Knuehl, C., Towler, M. C., and Wakeham, D. E. (2001) Biological basket weaving: Formation and function of clathrin-coated vesicles, *Annual Review of Cell and Developmental Biology 17*, 517-568.
206. Hopkins, C. R. (1985) The appearance and internalization of transferrin receptors at the margins of spreading human tumor cells, *Cell 40*, 199-208.
207. Hopkins, C. R., and Trowbridge, I. S. (1983) Internalization and processing of transferrin and the transferrin receptor in human carcinoma A431 cells, *The Journal of Cell Biology 97*, 508-521.
208. Miller, K., Shipman, M., Trowbridge, I. S., and Hopkins, C. R. (1991) Transferrin receptors promote the formation of clathrin lattices, *Cell 65*, 621-632.
209. Anderson, R. G., Goldstein, J. L., and Brown, M. S. (1976) Localization of low density lipoprotein receptors on plasma membrane of normal human fibroblasts and their absence in cells from a familial hypercholesterolemia homozygote, *Proceedings of the National Academy of Sciences 73*, 2434-2438.
210. Pearse, B. M. F. (1975) Coated vesicles from pig brain: Purification and biochemical characterization, *Journal of Molecular Biology 97*, 93-98.
211. Wang, L. H., Rothberg, K. G., and Anderson, R. G. (1993) Mis-assembly of clathrin lattices on endosomes reveals a regulatory switch for coated pit formation, *The Journal of Cell Biology 123*, 1107-1117.
212. Henley, J. R., Krueger, E. W. A., Oswald, B. J., and McNiven, M. A. (1998) Dynamin-mediated internalization of caveolae, *The Journal of Cell Biology 141*, 85-99.
213. Le, P. U., Guay, G., Altschuler, Y., and Nabi, I. R. (2002) Caveolin-1 is a negative regulator of caveolae-mediated endocytosis to the endoplasmic reticulum, *Journal of Biological Chemistry 277*, 3371-3379.
214. Anderson, R. G. W. (1998) The caveolae membrane system, *Annual Review of Biochemistry 67*, 199-225.
215. Rothberg, K. G., Heuser, J. E., Donzell, W. C., Ying, Y.-S., Glenney, J. R., and Anderson, R. G. W. (1992) Caveolin, a protein component of caveolae membrane coats, *Cell 68*, 673-682.
216. Smart, E. J., Ying, Y. S., Mineo, C., and Anderson, R. G. (1995) A detergent-free method for purifying caveolae membrane from tissue culture cells, *Proceedings of the National Academy of Sciences 92*, 10104-10108.
217. Sargiacomo, M., Sudol, M., Tang, Z., and Lisanti, M. (1993) Signal transducing molecules and glycosyl-phosphatidylinositol-linked proteins form a caveolin-rich insoluble complex in MDCK cells, *The Journal of Cell Biology 122*, 789-807.
218. Kamen, B. A., and Capdevila, A. (1986) Receptor-mediated folate accumulation is regulated by the cellular folate content, *Proceedings of the National Academy of Sciences 83*, 5983-5987.
219. Kamen, B. A., Johnson, C. A., Wang, M. T., and Anderson, R. G. (1989) Regulation of the cytoplasmic accumulation of 5-methyltetrahydrofolate in

MA104 cells is independent of folate receptor regulation, *The Journal of Clinical Investigation 84*, 1379-1386.
220. Kamen, B. A., Smith, A. K., and Anderson, R. G. (1991) The folate receptor works in tandem with a probenecid-sensitive carrier in MA104 cells in vitro, *The Journal of Clinical Investigation 87*, 1442-1449.
221. Kamen, B. A., Wang, M. T., Streckfuss, A. J., Peryea, X., and Anderson, R. G. (1988) Delivery of folates to the cytoplasm of MA104 cells is mediated by a surface membrane receptor that recycles, *Journal of Biological Chemistry 263*, 13602-13609.
222. Lacey, S. W., Sanders, J. M., Rothberg, K. G., Anderson, R. G., and Kamen, B. A. (1989) Complementary DNA for the folate binding protein correctly predicts anchoring to the membrane by glycosyl-phosphatidylinositol, *The Journal of Clinical Investigation 84*, 715-720.
223. Rothberg, K. G., Ying, Y. S., Kamen, B. A., and Anderson, R. G. (1990) Cholesterol controls the clustering of the glycophospholipid-anchored membrane receptor for 5-methyltetrahydrofolate, *The Journal of Cell Biology 111*, 2931-2938.
224. Rothberg, K. G., Ying, Y. S., Kolhouse, J. F., Kamen, B. A., and Anderson, R. G. (1990) The glycophospholipid-linked folate receptor internalizes folate without entering the clathrin-coated pit endocytic pathway, *The Journal of Cell Biology 110*, 637-649.
225. Coutinho, A., and Prieto, M. (2003) Cooperative partition model of nystatin interaction with phospholipid vesicles, *Biophysical journal 84*, 3061-3078.
226. Castanho, M. A., Coutinho, A., and Prieto, M. J. (1992) Absorption and fluorescence spectra of polyene antibiotics in the presence of cholesterol, *Journal of Biological Chemistry 267*, 204-209.
227. Anderson, H. A., Hiltbold, E. M., and Roche, P. A. (2000) Concentration of MHC class II molecules in lipid rafts facilitates antigen presentation, *Nat Immunol 1*, 156-162.
228. Monis, G. F., Schultz, C., Ren, R., Eberhard, J., Costello, C., Connors, L., Skinner, M., and Trinkaus-Randall, V. (2006) Role of endocytic inhibitory drugs on internalization of amyloidogenic light chains by cardiac fibroblasts, *The American journal of pathology 169*, 1939-1952.
229. Khalil, I. A., Kogure, K., Futaki, S., and Harashima, H. (2006) High density of octaarginine stimulates macropinocytosis leading to efficient intracellular trafficking for gene expression, *Journal of Biological Chemistry 281*, 3544-3551.
230. Norbury, C. C., Hewlett, L. J., Prescott, A. R., Shastri, N., and Watts, C. (1995) Class I MHC presentation of exogenous soluble antigen via macropinocytosis in bone marrow macrophages, *Immunity 3*, 783-791.
231. Racoosin, E. L., and Swanson, J. A. (1993) Macropinosome maturation and fusion with tubular lysosomes in macrophages, *The Journal of Cell Biology 121*, 1011-1020.
232. Lagana, A., Vadnais, J., Le, P. U., Nguyen, T. N., Laprade, R., Nabi, I. R., and Noel, J. (2000) Regulation of the formation of tumor cell pseudopodia by the Na(+)/H(+) exchanger NHE1, *Journal of Cell Science 113*, 3649-3662.
233. Li, Y., Zhang, J., and Zhang, B. (2009) Atomic force microscopy study on chlorpromazine-induced morphological changes of living HeLa cells in vitro, *Scanning 31*, 259-265.

234. Leake, P. A., and Snyder, R. L. (1987) Uptake of horseradish peroxidase from perilymph by cochlear hair cells, *Hearing Research 25*, 153-171.
235. Strange, K., Willingham, M. C., Handler, J. S., and Harris, H. W. (1988) Apical membrane endocytosis via coated pits is stimulated by removal of antidiuretic hormone from isolated, perfused rabbit cortical collecting tubule, *Journal of Membrane Biology 103*, 17-28.
236. Goldenthal, K. L., Pastan, I., and Willingham, M. C. (1985) Serial section analysis of clathrin-coated pits in rat liver sinusoidal endothelial cells, *Experimental Cell Research 161*, 342-352.
237. Sandvig, K., Pust, S., Skotland, T., and van Deurs, B. (2011) Clathrin-independent endocytosis: Mechanisms and function, *Current Opinion in Cell Biology 23*, 413-420.
238. Glebov, O. O., Bright, N. A., and Nichols, B. J. (2006) Flotillin-1 defines a clathrin-independent endocytic pathway in mammalian cells, *Nat Cell Biol 8*, 46-54.
239. Payne, C. K., Jones, S. A., Chen, C., and Zhuang, X. (2007) Internalization and trafficking of cell surface proteoglycans and proteoglycan-binding ligands, *Traffic 8*, 389-401.
240. Kishimoto, S., Kawazoe, Y., Ikeno, M., Saitoh, M., Nakano, Y., Nishi, Y., Fukushima, S., and Takeuchi, Y. (2006) Role of Na^+/K^+-ATPase α1 subunit in the intracellular accumulation of cisplatin, *Cancer Chemotherapy and Pharmacology 57*, 84-90.
241. Mellish, K. J., and Kelland, L. R. (1994) Mechanisms of acquired resistance to the orally active platinum-based anticancer drug bis-acetato-ammine-dichloro-cyclohexylamine platinum (IV) (JM216) in two human ovarian carcinoma cell lines, *Cancer Research 54*, 6194-6200.
242. Perego, P., Romanelli, S., Carenini, N., Magnani, I., Leone, R., Bonetti, A., Paolicchi, A., and Zunino, F. (1998) Ovarian cancer cisplatin-resistant cell lines: Multiple changes including collateral sensitivity to taxol, *Annals of Oncology 9*, 423-430.
243. Zou, J., Yang, X. G., Li, R. C., Lu, J. F., and Wang, K. (1997) The chirality selectivity in the uptake of platinum (II) complexes with 1,2-cyclohexanediamine isomers as carrier ligand by human erythrocytes, *BioMetals 10*, 37-43.
244. Weakley, B., S, (Ed.) (1981) *A beginner's handbook in biological transmission electron microscopy*, Second ed., Churchill Livingstone.
245. Horne, R. W., and Pasquali Ronchetti, I. (1974) A negative staining--carbon film technique for studying viruses in the electron microscope: I. Preparative procedures for examining icasahedral and filamentous viruses, *Journal of Ultrastructure Research 47*, 361-383.
246. Robin Harris, J. (1991) Negative staining-carbon film technique: New cellular and molecular applications, *Journal of Electron Microscopy Technique 18*, 269-276.
247. Bruggeller, P., and Mayer, E. (1980) Complete vitrification in pure liquid water and dilute aqueous solutions, *Nature 288*, 569-571.
248. Taylor, K. A., and Glaeser, R. M. (1974) Electron diffraction of frozen, hydrated protein crystals, *Science 186*, 1036-1037.
249. Adrian, M., Dubochet, J., Lepault, J., and McDowall, A. W. (1984) Cryo-electron microscopy of viruses, *Nature 308*, 32-36.

250. Ayache, J., Beaunier, L., Boumendil, J., Ehret, G., and Laub, D. (2010) In *Sample preparation handbook for transmission electron microscopy*, Springer New York.
251. Burger, K. N. J., Staffhorst, R. W. H. M., de Vijlder, H. C., Velinova, M. J., Bomans, P. H., Frederik, P. M., and de Kruijff, B. (2002) Nanocapsules: Lipid-coated aggregates of cisplatin with high cytotoxicity, *Nat Med 8*, 81-84.
252. Prezbindowski, K. S., Sun, F. F., and Crane, F. L. (1968) Characterization of microsomal membranes by negative staining technique, *Experimental Cell Research 50*, 241-256.
253. Fawcett, D. W. (1966) *The cell, an atlas of fine structure*, W.B. Saunders Company, Boston, Massachusetts.
254. Beier, K., and Fahimi, H. D. (1992) Application of automatic image analysis for quantitative morphological studies of peroxisomes in rat liver in conjunction with cytochemical staining with 3-3′-diaminobenzidine and immunocytochemistry, *Microscopy Research and Technique 21*, 271-282.
255. Dudkina, N. V., Kouřil, R., Bultema, J. B., and Boekema, E. J. (2010) Imaging of organelles by electron microscopy reveals protein–protein interactions in mitochondria and chloroplasts, *FEBS letters 584*, 2510-2515.
256. Nicastro, D., Frangakis, A. S., Typke, D., and Baumeister, W. (2000) Cryo-electron tomography of neurospora mitochondria, *Journal of Structural Biology 129*, 48-56.
257. Gruska, M., Medalia, O., Baumeister, W., and Leis, A. (2008) Electron tomography of vitreous sections from cultured mammalian cells, *Journal of Structural Biology 161*, 384-392.
258. Debney, E. W. (1952) The polarographic determination of phosphate, *Journal of Experimental Botany 3*, 47-51.
259. Chrétien, D., Kenney, J. M., Fuller, S. D., and Wade, R. H. (1996) Determination of microtubule polarity by cryo-electron microscopy, *Structure (London, England : 1993) 4*, 1031-1040.
260. Grassucci, R. A., Taylor, D. J., and Frank, J. (2007) Preparation of macromolecular complexes for cryo-electron microscopy, *Nat. Protocols 2*, 3239-3246.
261. Posakony, J., England, J., and Attardi, G. (1977) Mitochondrial growth and division during the cell cycle in HeLa cells, *The Journal of Cell Biology 74*, 468-491.
262. Berkenstam, A., Ahlberg, J., and Glaumann, H. (1986) Lysosomal uptake of isolated cell organelles microinjected into HeLa cells, *Experimental Cell Research 163*, 301-308.
263. Epstein, M. A. (1961) Some unusual features of fine structure observed in HeLa cells, *The Journal of Biophysical and Biochemical Cytology 10*, 153-162.
264. Amchenkova, A. A., Bakeeva, L. E., Chentsov, Y. S., Skulachev, V. P., and Zorov, D. B. (1988) Coupling membranes as energy-transmitting cables. I. Filamentous mitochondria in fibroblasts and mitochondrial clusters in cardiomyocytes, *The Journal of Cell Biology 107*, 481-495.
265. Collins, T. J., Berridge, M. J., Lipp, P., and Bootman, M. D. (2002) Mitochondria are morphologically and functionally heterogeneous within cells, *EMBO J 21*, 1616-1627.

266. Legros, F., Lombes, A., Frachon, P., and Rojo, M. (2002) Mitochondrial fusion in human cells is efficient, requires the inner membrane potential, and is mediated by mitofusins, *Molecular Biology of the Cell 13*, 4343-4354.
267. Benard, J., and Rossignol, R. (2008) Ultrastructure of the mitochondrion and its bearing on function and bioenergetics, *Antioxidants and Redox Signalling 10*, 1313-1342.
268. Stoeckenius, W. (1963) Some observations on negatively stained mitochondria, *The Journal of Cell Biology 17*, 443-454.
269. Fahimi, H. D. (1968) Cytochemical localization of peroxidase activity in rat hepatic microbodies (peroxisomes), *Journal of Histochemistry & Cytochemistry 16*, 547-550.
270. Holtzman, E. (1989) *Lysosomes*, Plenum Press, New York and London.
271. Yamada, H., Hayashi, H., and Natori, Y. (1984) A simple procedure for the isolation of highly purified lysosomes from normal rat liver, *Journal of Biochemistry 95*, 1155-1160.
272. Holtzman, E., and Dominitz, R. (1968) Cytochemical studies of lysosomes, Golgi apparatus and endoplasmic reticulum in secretion and protein uptake by adrenal medulla cells of the rat, *Journal of Histochemistry & Cytochemistry 16*, 320-336.
273. Cheng, Y., Boll, W., Kirchhausen, T., Harrison, S. C., and Walz, T. (2007) Cryo-electron tomography of clathrin-coated vesicles: Structural implications for coat assembly, *Journal of Molecular Biology 365*, 892-899.
274. Lebbink, M. N., Jiménez, N., Vocking, K., Hekking, L. H., Verkleij, A. J., and Post, J. A. (2010) Spiral coating of the endothelial caveolar membranes as revealed by electron tomography and template matching, *Traffic 11*, 138-150.
275. Vandlen, R. L., Sarcione, S. L., and Telakowski, C. A. (1981) Purification and characterization of plasma membrane fractions from cultured pituitary cells, *Biochimica et Biophysica Acta (BBA) - Biomembranes 649*, 595-607.
276. Ray, T. K. (1970) A modified method for the isolation of the plasma membrane from rat liver, *Biochimica et Biophysica Acta (BBA) - Biomembranes 196*, 1-9.
277. Kartner, N., Alon, N., Swift, M., Buchwald, M., and Riordan, J. R. (1977) Isolation of plasma membranes from human skin fibroblasts, *Journal of Membrane Biology 36*, 191-211.
278. Zam, Z. S., Cerda, J., and Polack, F. M. (1980) Isolation of the plasma membrane from corneal endothelial cells, *Investigative Ophthalmology & Visual Science 19*, 648-652.
279. Evans, W. H. (1970) Fractionation of liver plasma membranes prepared by zonal centrifugation, *Biochem J. 116*, 833–842.
280. Gluschankof, P., Mondor, I., Gelderblom, H. R., and Sattentau, Q. J. (1997) Cell membrane vesicles are a major contaminant of gradient-enriched human immunodeficiency virus type-1 preparations, *Virology 230*, 125-133.
281. Graham, J. M. (1993) Isolation of mitochondria, mitochondrial membranes, lysosomes, peroxisomes, and Golgi membranes from rat liver, In *Biomembrane protocols* (Graham, J. M., and Higgins, J. A., Eds.), pp 29-40, Humana Press.
282. Palade, G. E., and Siekevitz, P. (1956) Liver microsomes: An integrated morphological and biochemical study, *The Journal of Biophysical and Biochemical Cytology 2*, 171-200.

283. Adelman, M. R., Blobel, G., and Sabatini, D. D. (1973) An improved cell fractionation procedure for the preparation of rat liver membrane-bound ribosomes, *The Journal of Cell Biology 56*, 191-205.
284. Bergstrand, A., and Dallner, G. (1969) Isolation of rough and smooth microsomes from rat liver by means of a commercially available centrifuge, *Analytical Biochemistry 29*, 351-356.
285. Lewis, J. A., and Tata, J. R. (1973) A rapidly sedimenting fraction of rat liver endoplasmic reticulum, *Journal of Cell Science 13*, 447-459.
286. Rolleston, F. S. (1972) The binding of ribosomal subunits to endoplasmic reticulum membranes, *Biochem. J. 129*, 721-731.
287. Attardi, B., Cravioto, B., and Attardi, G. (1969) Membrane-bound ribosomes in HeLa cells : I. Their proportion to total cell ribosomes and their association with messenger RNA, *Journal of Molecular Biology 44*, 47-50.
288. Bennett, J., and Hallinan, T. (1968) The attachment of ribosomes to the endoplasmic reticulum of liver, *Life Sciences 7*, 553-560.
289. Harano, T., and Omura, T. (1978) Biogenesis of endoplasmic reticulum membrane in rat liver cells, *Journal of Biochemistry 84*, 213-223.
290. Sabatini, D. D., Tashiro, Y., and Palade, G. E. (1966) On the attachment of ribosomes to microsomal membranes, *Journal of Molecular Biology 19*, 503-524, IN508-IN509.
291. Verschoor, A., Srivastava, S., Grassucci, R., and Frank, J. (1996) Native 3D structure of eukaryotic 80S ribosome: Morphological homology with E. Coli 70S ribosome, *The Journal of Cell Biology 133*, 495-505.
292. Yan, X.-D., Li, M., Yuan, Y., Mao, N., and Pan, L.-Y. (2007) Biological comparison of ovarian cancer resistant cell lines to cisplatin and taxol by two different administrations, *Oncology Reports 17*, 1163-1169.
293. McLaughlin, K., Stephens, I., McMahon, N., and Brown, R. (1991) Single step selection of cis-diamminedichloroplatinum(II) resistant mutants from a human ovarian carcinoma cell line, *Cancer Research 51*, 2242-2245.
294. Mese, H., Sasaki, A., Alcalde, R. E., Nakayama, S., and Matsumura, T. (1998) Establishment and characterization of cisplatin-resistant human epidermoid carcinoma cell line, A431 cell, *Chemotherapy 44*, 414-420.
295. Brown, R., Clugston, C., Edlin, A., Vasey, P., Kaye, S. B., Burns, P., and Vojtěšek, B. (1993) Increased accumulation of p53 protein in cisplatin-resistant ovarian cell lines, *International Journal of Cancer 55*, 678-684.
296. Shen, D. W., Akiyama, S., Schoenlein, P., Pastan, I., and Gottesman, M. M. (1995) Characterisation of high-level cisplatin-resistant cell lines established from a human hepatoma cell line and human KB adenocarcinoma cells: Cross-resistance and protein changes, *Br J Cancer 71*, 676-683.
297. Holford, J., Beale, P. J., Boxall, F. E., Sharp, S. Y., and Kelland, L. R. (2000) Mechanisms of drug resistance to the platinum complex ZD0473 in ovarian cancer cell lines, *European Journal of Cancer 36*, 1984-1990.
298. Tozawa, K., Oshima, T., Kobayashi, T., Yamamoto, N., Hayashi, C., Matsumoto, T., and Miwa, H. (2008) Oxaliplatin in treatment of the cisplatin-resistant MKN45 cell line of gastric cancer, *Anticancer Research 28*, 2087-2092.
299. Beretta, G. L., Benedetti, V., Cossa, G., Assaraf, Y. G. A., Bram, E., Gatti, L., Corna, E., Carenini, N., Colangelo, D., Howell, S. B., Zunino, F., and Perego, P. (2010) Increased levels and defective glycosylation of MRPs in ovarian

carcinoma cells resistant to oxaliplatin, *Biochemical Pharmacology 79*, 1108-1117.
300. Jones, M., Siracky, J., Kelland, L. R., and Harrap, K. R. (1993) Acquisition of platinum drug resistance and platinum cross resistance patterns in a panel of human ovarian carcinoma xenografts, *Br J Cancer 67*, 24-29.
301. Negoro, K., Yamano, Y., Nakashima, D., Saito, K., Nakatani, K., Shiiba, M., Bukawa, H., Yokoe, H., Uzawa, K., Wada, T., Tanzawa, H., and Fujita, S. (2009) Cross-resistance of platinum derivatives in H-1R, a cisplatin-resistant cell line, *Oncology Reports 21* 443-449.
302. Eckstein, N., Servan, K., Girard, L., Cai, D., von Jonquieres, G., Jaehde, U., Kassack, M. U., Gazdar, A. F., Minna, J. D., and Royer, H.-D. (2008) Epidermal growth factor receptor pathway analysis identifies amphiregulin as a key factor for cisplatin resistance of human breast cancer cells, *Journal of Biological Chemistry 283*, 739-750.
303. Song, I.-S., Savaraj, N., Siddik, Z. H., Liu, P., Wei, Y., Wu, C. J., and Kuo, M. T. (2004) Role of human copper transporter Ctr1 in the transport of platinum-based antitumor agents in cisplatin-sensitive and cisplatin-resistant cells, *Molecular Cancer Therapeutics 3*, 1543-1549.
304. Perego, P., Caserini, C., Gatti, L., Carenini, N., Romanelli, S., Supino, R., Colangelo, D., Viano, I., Leone, R., Spinelli, S., Pezzoni, G., Manzotti, C., Farrell, N., and Zunino, F. (1999) A novel trinuclear platinum complex overcomes cisplatin resistance in an osteosarcoma cell system, *Molecular Pharmacology 55*, 528-534.
305. Zhang, P., Zhang, Z., Zhou, X., Qiu, W., Chen, F., and Chen, W. (2006) Identification of genes associated with cisplatin resistance in human oral squamous cell carcinoma cell line, *BMC Cancer 6*, 224.
306. Chauhan, S. S., Liang, X. J., Su, A. W., Pai-Panandiker, A., Shen, D. W., Hanover, J. A., and Gottesman, M. M. (2003) Reduced endocytosis and altered lysosome function in cisplatin-resistant cell lines, *Br J Cancer 88*, 1327-1334.
307. Gottesman, M. M., Hall, M. D., Liang, X.-J., and Shen, D.-W. (2009) Resistance to cisplatin results from multiple mechanisms in cancer cells, In *Platinum and other heavy metal compounds in cancer chemotherapy* (Bonetti, A., Leone, R., Muggia, F. M., and Howell, S. B., Eds.), pp 83-88, Humana Press.
308. Lukyanova, N. Y., Rusetskya, N. V., Tregubova, N. A., and Chekhun, V. F. (2009) Molecular profile and cell cycle in MCF-7 cells resistant to cisplatin and doxorubicin, *Experimental Oncology 31*, 87-91.
309. Jansen, B. J., Wielaard, P., Kalayda, G., Ferrari, M., Molenaar, C., Tanke, H., Brouwer, J., and Reedijk, J. (2004) Dinuclear platinum complexes with *N,N'*-bis(aminoalkyl)-1,4-diaminoanthraquinones as linking ligands. Part I. Synthesis, cytotoxicity, and cellular studies in A2780 human ovarian carcinoma cells, *Journal of Biological Inorganic Chemistry 9*, 403-413.
310. Safaei, R., Katano, K., Larson, B. J., Samimi, G., Holzer, A. K., Naerdemann, W., Tomioka, M., Goodman, M., and Howell, S. B. (2005) Intracellular localization and trafficking of fluorescein-labeled cisplatin in human ovarian carcinoma cells, *Clinical Cancer Research 11*, 756-767.
311. Moretto, P., Ortega, R., Llabador, Y., Simonoff, M., and Bénard, J. (1995) Nuclear microanalysis of platinum and trace elements in cisplatin-resistant human ovarian adenocarcinoma cells, *Nuclear Instruments and Methods in*

Physics Research Section B: Beam Interactions with Materials and Atoms 104, 292-298.
312. Collins, T. J. (2007) ImageJ for microscopy, *Biotechniques 43*, 25-30.